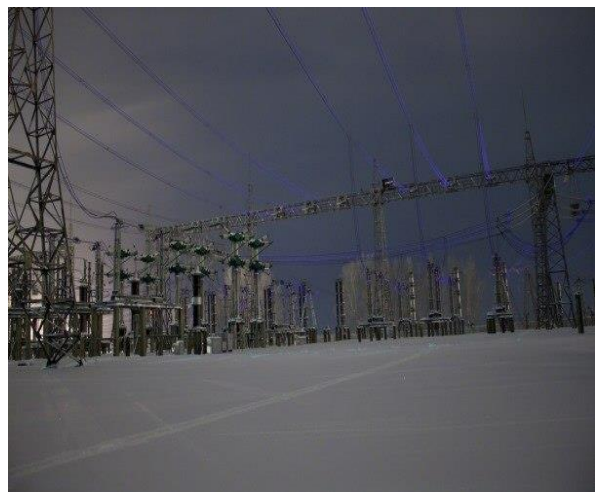


HIGH VOLTAGE ENGINEERING



Dr. Alexey V. Mytnikov



UDK 621.3.027.3(075.8)

BBK 31.24я73

M99

Author: A.V. Mytnikov

M99 High Voltage Engineering: – Tomsk: TPU, 2012. – **160 c.**

ISBN 0-00000-000-0

In the textbook basic fundamentals of high voltage engineering are given: processes of charge particles generation, moving and recombination under influence of strong electric fields, main forms and kinds of electrical discharges in gases, breakdown mechanisms of condensed dielectric media, techniques of high voltage generation and measurement, phenomena of over-voltages and protection measures from them, new trends in actual part of modern high voltage technology.

The textbook is appropriated for foreign students who study bachelor electric engineering course.

UDK 621.3.027.3(075.8)

BBK 31.24я73

Reviewers

Doctor of technical sciences, leading scientist of high current electron beams laboratory, Institute of high current electronics, Russian Academy of Science
E.N. Abdullin

Doctor of technical sciences, Professor of Electric energy systems department, Power engineering institute, Tomsk polytechnical university
V.A. Lavrinovich

© Tomsk polytechnical university, 2012

© Mytnikov A.V., 2012

© Design. Publishing of Tomsk polytechnical university, 2012

Preface

This textbook has been written for the foreign students who come to study Bachelor's course in Electrical Engineering of Tomsk Polytechnical University. The author has an experience of course "High Voltage Engineering" teaching for students who study on English language only, both from non-English (France, China, Czech Republic, Vietnam) and English-speaking countries (India, Jamaica).

There are a lot of different textbooks on this subject of famous professors (Adolf Schwab, Walter Zaengl, Dieter Kind, Vasilij Ushakov, C. Wadhwa and others). But most of them have too big volume and appropriate more for master and post graduate students. General course "High Voltage Engineering" is given in our Power Engineering Institute include lectures and practice course. An analysis of student's requirements, their basic fundamental knowledge level, correlation between auditorium lectures, laboratory workshop and self-studying work volume make me prepare the textbook.

Chapter 1 deals with the fundamental phenomena in gaseous media at the applying of electric field. Numerical enter control results show that basic fundamentals of gases should be explained more detailed. This chapter contains main kinds of ionization, emission and recombination processes. Here is description of main forms and kinds of electrical discharges in gases.

Chapter 2 discusses main mechanisms of breakdown in condensed dielectric materials. Reasons and ways of plasma channel formation are discussed here.

Chapter 3 tells about the techniques of generation of high direct and alternative current voltages and high impulse voltages. Methods of measurement of high voltages are discussed in this chapter also.

Chapter 4 deals with overvoltages. Lightning phenomena, switching overvoltages, insulation coordination problem are reported. Protection devices which allow providing reliable work of industrial high voltage equipment are shown and described.

Chapter 5 devoted to new trends in some parts of modern high voltage engineering. New approaches to power transformer diagnostics are covered and discussed. High current synthetic scheme for circuit breaker phenomena investigation and testing is shown. This chapter deals with new information which is in special scientific papers only. These are advanced scientific directions which are developed in High voltage laboratory of Power engineering institute of Tomsk polytechnical university.

Tomsk, Summer–Autumn 2012

Dr. Alexey V. Mytnikov

Introduction

High voltage engineering has very wide range of application in many areas of modern industry. High voltage engineering occupies an important place in power engineering development all over the World. Problem of stable work supply of any electric energy system is solved by means of high voltage technology using: reliable external and internal insulation performance, timely and high quality diagnostic of all high voltage equipment range, overvoltages restriction and reliable protection, high voltage equipment testing, advanced high voltage equipment development and many others.

High voltage is used in electro–physical installations for pulsed power purposes: charge particle accelerators, power lasers, plasma sources and thermonuclear reactors. High voltage is widely used in technological processes such as: electroseparation, electrofiltering, pulsed magnetic field treatment, plasmachemistry, nanostructure material synthesis with new properties.

In this connection, a studying of High Voltage Engineering course is necessary for every high qualified specialist in electrical engineering.

CHAPTER 1. ELECTROPHYSICAL PROCESSES IN GASES

1.1. Basic fundamentals of kinetic gas theory

All gases are good dielectric materials. Basic electro–physical processes of charges appearing are considered in gases. Before proceeding to discuss breakdown in gases a brief review of the fundamental principles of kinetic theory of gases, which are pertinent to the study of gaseous ionization and breakdown, will be presented. The review will include the classical gas laws, followed by the ionization and decay processes which lead to conduction of current through a gas and ultimately to a complete breakdown or spark formation.

To begin a consideration of charge carriers generation and electrical discharges processes, it is necessary to overview main basic fundamentals of inner gas structure. There are kinetic gas theory laws, distribution of velocities, free paths distribution of molecules and electrons, collision–energy transfer, types of collisions and etc. In the absence of electric or magnetic fields charged particles in weakly ionized gases participate in molecular collisions. Their motions follow closely the classical kinetic gas theory. The oldest gas law established experimentally by Boyle and Mariotte states that for a given amount of enclosed gas at a constant temperature the product of pressure (p) and volume (V) is constant or:

$$pV = C = \text{const} \quad (1.1)$$

In the same system, if the pressure is kept constant, then the volumes V and V_0 are related to their absolute temperatures T and T_0 (in K) by Gay–Lussac’s law:

$$\frac{V}{V_0} = \frac{T}{T_0} \quad (1.2)$$

When temperatures are expressed in degrees Celsius, equation (1.2) becomes:

$$\frac{V}{V_0} = \frac{273 + \theta}{273} \quad (1.3)$$

— Equation (1.3) suggests that as we approach $\theta = 273^\circ\text{C}$ the volume of gas shrinks to zero. In reality, all gases liquefy before reaching this value.

According to equation (1.2) the constant C in equation (1.1) is related to

a given temperature T_0 for the volume V_0 :

$$pV_0 = C_0 \quad (1.4)$$

Substituting V_0 from equation (1.2) gives:

$$— \quad \frac{p}{V} = \left(\frac{C_0}{T_0} \right) T \quad (1.5)$$

The ratio C_0/T_0 is called the universal gas constant and is denoted by R . Equation (1.5) then becomes:

$$pV = RT = C \quad (1.6)$$

Numerically R is equal to $8.314 \text{ joules}/^\circ\text{K mol}$. If we take n as the number of moles, i.e. the mass m of the gas divided by its mol-mass, then for the general case equation (1.1) takes the form:

$$pV = nC = nRT \quad (1.7)$$

Equation (1.7) then describes the state of an ideal gas, since we assumed that R is a constant independent of the nature of the gas. Equation (1.7) may be written in terms of gas density N in volume V could contain about N_1 gas molecules. Putting $N = N_A$ where $N_A = 6.02 \times 10^{23}$ molecules/mole, N_A is known as the Avogadro's number. Then equation (1.7) becomes:

$$pV = \frac{N_1}{N_A} RT = N_1 kT \text{ or } p = NkT \quad (1.8)$$

The constant $k = R/N_A$ is the universal Boltzmann's constant ($= 1.3804 \div 10^{-23} \text{ joules}/^\circ\text{K}$) and N is the number of molecules in the gas.

If two gases with initial volumes V_1 and V_2 are combined at the same temperature and pressure, then the new volume will be given by

$$V = V_1 + V_2 + V_3 = \dots + V_N \quad (1.9)$$

Combining equations (1.7) and (1.9) gives:

$$V = \frac{n_1 RT}{p} + \frac{n_2 RT}{p} + \dots + \frac{n_n RT}{p}$$

rearranging

$$n = \frac{n_1 RT}{V} + \frac{n_2 RT}{V} + \dots + \frac{n_n RT}{V}$$

or

$$p = p_1 + p_2 + \dots + p_n \quad (1.10)$$

where p_1, p_2, \dots, p_n denote the partial pressures of gases 1, 2, ... , n . Equation (1.10) is generally referred to as the law of partial pressures. Equations (1.1) to (1.10) can be derived directly from the kinetic theory of gases developed by Maxwell in the middle of the nineteenth century. A brief derivation will be presented.

The fundamental principals for the kinetic theory of gas is derived with the following assumed conditions:

1. Gas consists of molecules of the same mass which are assumed spheres.
2. Molecules are in continuous random motion.
3. Collisions are elastic – simple mechanical.
4. Mean distance between molecules is much greater than their diameter.
5. Forces between molecules and the walls of the container are negligible [1].

Consider a cubical container of side $l=l$ m as shown in Fig. 1.1 with N_l molecules, each of mass m and velocity u . Let us resolve the velocity into components u_x, u_y, u_z , where $u^2 = u_x^2 + u_y^2 + u_z^2$. Suppose a molecule of mass m is moving in the x -direction with velocity u_x . As it strikes the wall of container plane YZ it rebounds with the velocity $-u_x$. The change in momentum, therefore, is: $\Delta m = mu_x - (-mu_x) = 2mu_x$. For the cube of side l the number of collisions per second with the right-hand wall is $\frac{u_x}{2l}$, therefore $\Delta m/\text{sec}/\text{molecule} = \frac{2mu_x u_x}{2l} = \frac{mu_x^2}{l}$, but the same molecule will experience the same change in momentum at the opposite wall. Hence $\Delta m/\text{sec}/\text{molecule}$ in the x -direction is $\frac{2mu_x^2}{l}$. For the three-dimensional cube with total change in momentum per second per molecule (which is the force) we obtain the force per particle as:

$$F = \frac{2m}{l} (u_x^2 + u_y^2 + u_z^2) = \frac{2mu^2}{l} \quad (1.11)$$

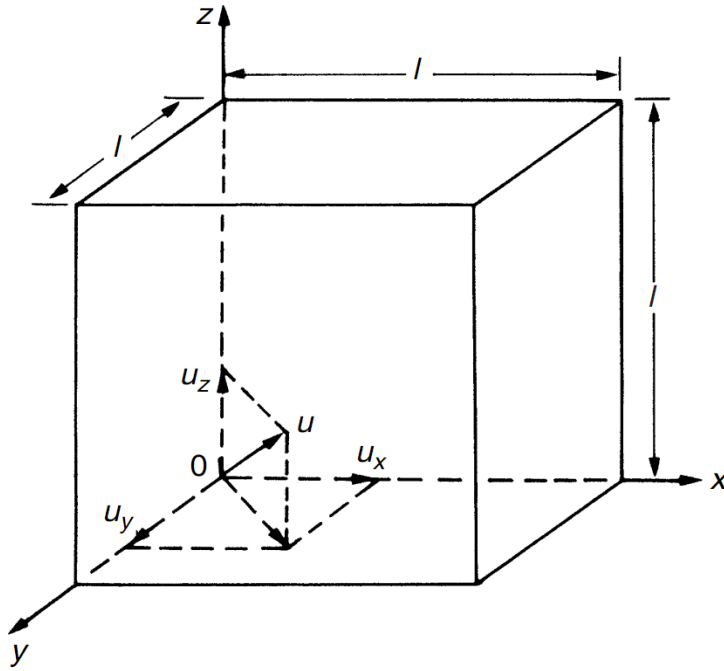


Figure 1.1 Resolution of molecular forces

As kinetic energy for a particle is $W = \frac{mv^2}{2}$, therefore $F = 4 \frac{W}{l}$. For N_1 particles the energy due to different velocities u of particles will become the mean energy, and therefore $4 \frac{N_1 \bar{W}}{l}$. Force leads to pressure p , taking into account the total area of the cube ($A = 6l^2$), it could be written:

$$p = \frac{F}{A} = \frac{4N_1 \bar{W}}{6l \cdot l^2} = \frac{2}{3} \frac{N \bar{W}}{l^3} \quad (1.12)$$

Comparing equations (1.8) and (1.12) and taking into account that $l^3 = V = \text{volume}$ leads to: $pV = \frac{2}{3} N_1 \bar{W}$.

Comparing equation (1.12) with equation (1.1) we note that these equations are identical for constant temperature. Using equation (1.8) gives: $pV = \frac{2}{3} \frac{N_1}{V} \bar{W} = \frac{2}{3} N \bar{W} = NkT$, which leads to the expression for mean energy per molecule:

$$\bar{W} = \frac{3}{2} kT \quad (1.13)$$

Important question is velocity distribution of molecules. It has been shown using probability consideration that the distribution of molecular velocities depends on both the temperature and the molecular weight of the gas. The mathematical analysis shows the most probable velocity is neither the average nor the velocity of all the molecules. The velocity u of gas molecules or particles has a statistical distribution and follows the Boltzmann – Maxwell distribution given by the expression:

$$f(u)du = \frac{dN_u}{N} = \frac{4}{\sqrt{\pi}} \left(\frac{u}{u_p} \right)^2 \left[e^{-\left(\frac{u}{u_p}\right)^2} \right] \frac{du}{u_p} \quad (1.14)$$

where u_p is most probable velocity and $\frac{dN_u}{N}$ the relative number of particles whose instantaneous velocities lie in the range $\frac{u}{u_p}$ and $\frac{(u + du)}{u_p}$.

$$\text{Let } f\left(\frac{u}{u_p}\right) = \frac{\frac{dN_u}{N}}{\frac{du}{u_p}} \text{ and } u_r = \frac{u}{u_p} \text{ (relative velocity).}$$

Introducing this dimensionless variable into equation (1.14) gives the function representing velocity distribution

$$f(u_r) = \frac{4}{\sqrt{\pi}} u_r^2 e^{-u_r^2} \quad \text{with} \quad \frac{dN_u}{N} = f(u_r) du_r. \quad (1.14a)$$

The distribution function corresponding to equation (1.14a) is shown in Fig. 1.2. It should be noted that the function is asymmetrical about the most probable velocity u_p . A greater number of particles has a velocity higher than u_p . The average velocity \bar{u} is obtained from integrating u_r from 0 to ∞ .

$$\bar{u}_r = \int_{u_r=0}^{\infty} u_r f(u_r) du_r = \frac{4}{\sqrt{\pi}} \int_0^{\infty} u_r^3 e^{-u_r^2} du_r = \frac{2}{\sqrt{\pi}} \text{ or}$$

$$\bar{u} = \bar{u}_r u_p = 1.128 u_p \quad (1.15)$$

The reference measuring system (r.m.s.) [2] or effective value of velocity is obtained by squaring u_r and obtaining the average square value

$$(\mathbf{u}_r)_{eff}^2 = \int_{u_r=0}^{\infty} u_r^2 f(u_r) du_r = \frac{4}{\sqrt{\pi}} \int_0^{\infty} u_r^4 e^{-u_r^2} du_r = \frac{3}{2} \quad (1.16)$$

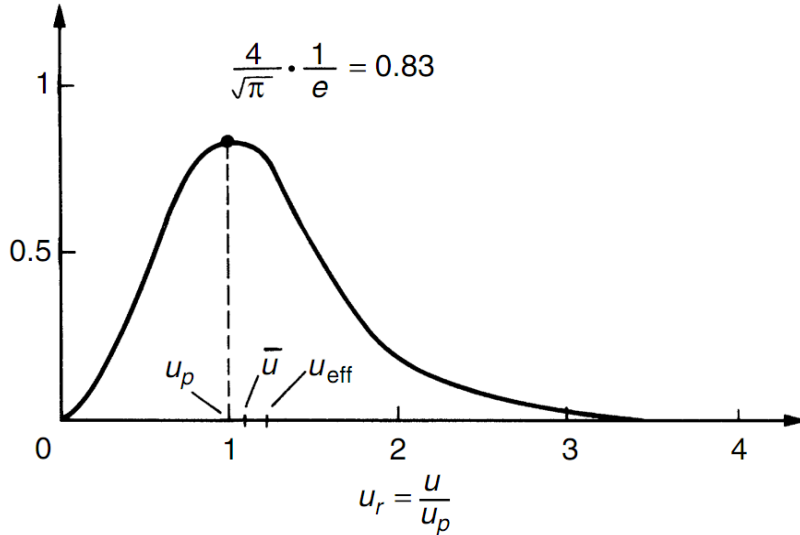


Figure 1.2. Distribution of velocities:
 u_p - most probable, \bar{u} - average, u_{eff} - effective

The mean kinetic energy of the particle given by equation (1.13) relates its effective velocity to the temperature ($\frac{1}{2}mv_{eff}^2 = \frac{3}{2}kT$) and we obtain:

$$u_{eff} = \sqrt{\frac{3kT}{m}}; u = \sqrt{\frac{8kT}{\pi m}}; u_p = \sqrt{\frac{2kT}{m}} \quad (1.17)$$

Hence the respective velocities remain in the ratio $u_p : u : u_{eff} = 1 : 1.128 : 1.124$.

It should be noted that the foregoing considerations apply only when the molecules or particles remain in thermal equilibrium, and in the absence of particle acceleration by external fields, diffusion, etc. If the gas contains electrons or ions or other atoms that are at the same temperature, the average particle energy of such mixture is $= \frac{3}{2}kT$.

The values of the mean molecular velocities calculated for 20°C and 760 Torr for several of the common gases are included in Table 1.1 [3].

Table 1.1 Mean molecular velocities at 20°C and 760 Torr

Gas	Electron	H ₂	O ₂	N ₂	Air	CO ₂	H ₂ O (vapour)	SF ₆
\bar{u} (m/sec)	100×10^3	1760	441	470	465	375	556	199

The free path λ is defined as the distance molecules or particles travel between collisions. The free path is a random quantity and as we will see its mean value depends upon the concentration of particles or the density of the gas. To derive the mean free path $\bar{\lambda}$ assume an assembly of stationary molecules of radius r_1 , and a moving layer of smaller particles of radius r_2 as particles move, their density will decrease as shown in Fig. 1.3. As the smaller particles move, their density will decrease due to scattering caused by collisions with gas molecules. If we assume that the moving particles and molecules behave as solid spheres, then a collision will occur every time the centres of two particles come within a distance $r_1 + r_2$. The area for collision presented by a molecule is then $\pi(r_1 + r_2)^2$ and in a unit volume it is $N\pi(r_1 + r_2)^2$. This is often called the *effective area* for interception where N = number of particles per unit volume of gas. If we consider a layer of thickness dx , distant x from the origin (Fig. 1.3) and $n(x)$ the number of particles that survived the distance x , then the decrease in the moving particles due to scattering in layer dx is:

$$dn = -n(x)N\pi(r_1 + r_2)^2 dx.$$

Assuming the number of particles entering (at $x=0$) is n_0 , integration gives:

$$n(x) = N_0 e^{-N(r_1+r_2)^2 x} \quad (1.18)$$

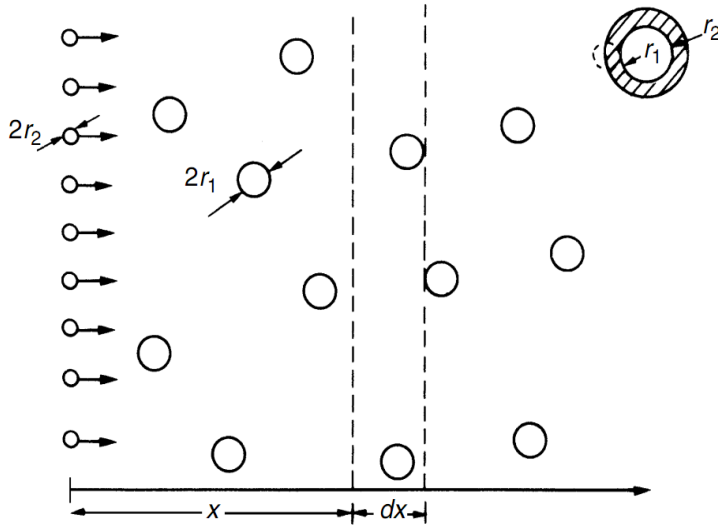


Figure 1.3 Model for determining free paths

The probability of free path of length x is equal to the probability of collisions between x and $x + dx$. The mean free path is $\bar{\lambda} = x$ obtained as follows. Differentiating equation (1.18) we obtain:

$$f(x) = \frac{dN}{n_0} = N\pi(r_1 + r_2)^2 e^{-N\pi(r_1 + r_2)^2 x} dx.$$

For mean free path:

$$x = \bar{\lambda} = \int_{x=0}^{\infty} xf(x)dx = N\pi(r_1 + r_2)^2 \int_{x=0}^{\infty} xe^{-N\pi(r_1 + r_2)^2 x} dx = \frac{1}{N\pi(r_1 + r_2)^2} \quad (1.19)$$

The denominator in equation (1.19) has the dimensions of area and the value $\pi(r_1 + r_2)^2$ is usually called the cross-section for interception or simply collision cross-section and is denoted by σ :

$$\sigma = \frac{1}{N\bar{\lambda}} \quad (1.20)$$

We will see later that the collisions between the incoming particles and the stationary molecules may lead to processes such as ionization, excitation, attachment and many others. If we put in equation (1.20) $Q = N\sigma$, then Q will represent the effective cross-section presented by molecules or particles in unit volume of gas for all collisions for density of N molecules per volume. If, for example, only a fraction P_i of collisions between the incoming parti-

cles and the gas particles leads to ionization then P_i is the **probability of ionization**. Thus if only ionizing collisions are counted, the molecules present an effective area of only $P_i Q = Q_i$; Q_i is the **effective cross-section for ionization**. Similarly for other processes, excitation Q_e , photoionization Q_{ph} , attachment Q_a , etc., including elastic collisions can be taken into account:

$$Q = Q_{elastic} + Q_i + Q_e + Q_{ph} + Q_a + \dots \quad (1.21)$$

Atomic cross-sections (σ) for different processes vary over a wide range. For ionization they can rise to some $2 \times 10^{-16} \text{ cm}^2$, but for collisions resulting in nuclear reactions they may be 10^{-24} cm^2 or less. In deriving the expression (1.19) it was assumed that the struck molecules were stationary, i.e. the molecules of gas type 2 had no thermal velocity. In reality this is not true. It can be shown that the expression giving the collisional cross-section must be still multiplied by a factor

$$\eta = \sqrt{1 + \frac{m_1}{m_2}}$$

with m_1 and m_2 the mass of each gas component. In a gas mixture the collisional cross-section of particles of type 1 of gas (m_1, r_1, N_1) becomes equal to the sum of all collisional cross-sections of the other particles of types of gas $m_2, m_3, \dots, r_2, r_3, \dots, N_2, N_3, \dots$. Thus the mean free path of particles of type 1 is:

$$\lambda_1 = \frac{1}{\pi \sum_{i=1}^n N_i (r_1 + r_i)^2 \sqrt{1 + \frac{m}{m_i}}} \quad (1.22)$$

For an atom in its own gas $r_1 = r_2 = r, u_1 = u_2$. Then:

$$\bar{\lambda}_a = \frac{1}{4\sqrt{2}\pi r^2 N} \quad (1.23)$$

For an electron in a gas $r_1 \ll r_2$ and $m_1 \ll m_2$ equation (1.22) gives:

$$\bar{\lambda}_e = \frac{1}{\pi r_2^2 N} \quad \text{or} \quad \bar{\lambda}_e = 4\sqrt{2}\bar{\lambda}_a = 5.66\bar{\lambda}_a \quad (1.24)$$

Table 1.2 shows examples of mean free path (gas) for gases of different molecular weight [4].

Table 1.2 Mean free paths measured at 15°C and 760 Torr

Type of gas	H ₂	O ₂	N ₂	CO ₂	H ₂ O	Dimensions
λ	11.77	6.79	6.28	4.19	4.18	10 ⁻⁸ m
Molecular weight	2.016	32.00	28.020	44.00	18.00	

From equation (1.8), it follows that the mean free path is directly proportional to temperature and inversely as the gas pressure:

$$\lambda(p, T) = \lambda_0 \frac{p_0 T}{p T_0} \quad (1.25)$$

Considering a typical practical case with values for average velocities of gas $u \approx 500m/sec$ and the mean free path $\bar{\lambda} \approx 10^{-7}m$ we obtain the number of collisions per second:

$$v = \frac{u}{\bar{\lambda}} = 5 \times 10^9 \frac{1}{sec} \approx 5 \text{ collisions / nsec.}$$

The average time between two collisions:

$$\Delta t = \frac{1}{v} = \frac{1}{5 \times 10^9} = 0.2 \text{ nsec.}$$

In the earlier section it was shown that molecular collisions are random events and these determine free paths. Hence, free path is a random quantity and will have a distribution about a mean value. For the system in Fig. 1.3 the mean free path is given by equation (1.19).

$$\bar{\lambda} = \frac{1}{N\pi(r_1 + r_2)^2},$$

N being the gas density and r_1 and r_2 the radii of the two types of particles. The distribution function of free paths is obtained from equation (1.18):

$$\int_{n_0}^n dn = - \int_{x=0}^x \ln \frac{dx}{\bar{\lambda}} \quad \text{or} \quad n(x) = n_0 e^{-x/\bar{\lambda}} \quad (1.26)$$

where $n(x)$ = number of molecules reaching a distance x without collisions, dn = number of molecules colliding thereafter within a distance dx , n_0 = total number of molecules at $x = 0$. Equation (1.26) is plotted in Fig. 1.4.

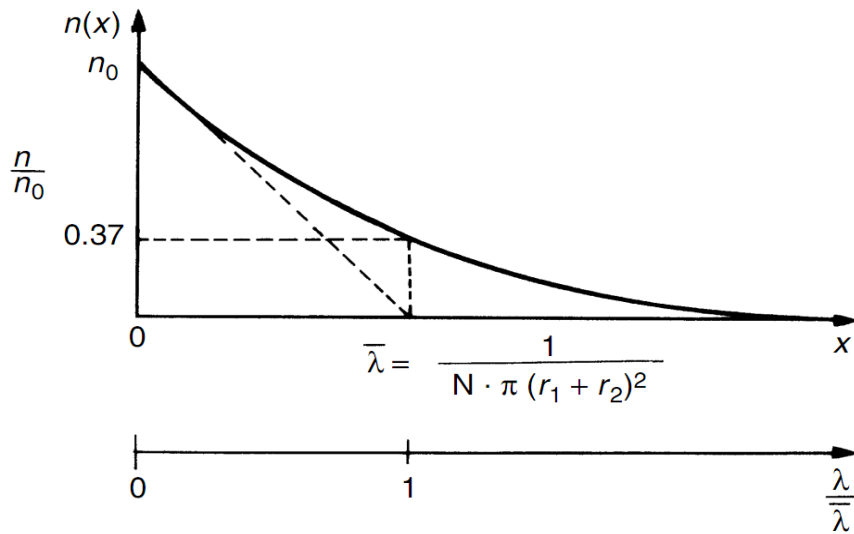


Figure 1.4 Distribution of free paths

It is seen that the percentage of molecules that survive collisions are *only 36 per cent*. The exponent in equation (1.26) may also be written in terms of collision cross-sections defined by equation (1.20), to represent absorption or decay of particles along the path x or

$$n = n_0 e^{-N\sigma x} \quad (1.27)$$

where σ may include photo-absorption, attachment, etc.

Next important term of gas theory is **collision-energy transfer**. The collisions between gas particles are of two types: *a) elastic* or simple **mechanical collisions** in which the energy exchange is always kinetic, and *b) inelastic* in which some of the kinetic energy of the colliding particles is transferred into potential energy of the struck particle or vice versa [3,4]. Examples of the second type of collisions include excitation, ionization, attachment, etc., which will be discussed later. To derive an expression for energy transfer between two colliding particles, let us consider first the case of an elastic collision between two particles of masses m and M . Assume that before collision the particle of large mass M was at rest and the velocity of the smaller particle was u_0 in the direction shown in Fig. 1.5.

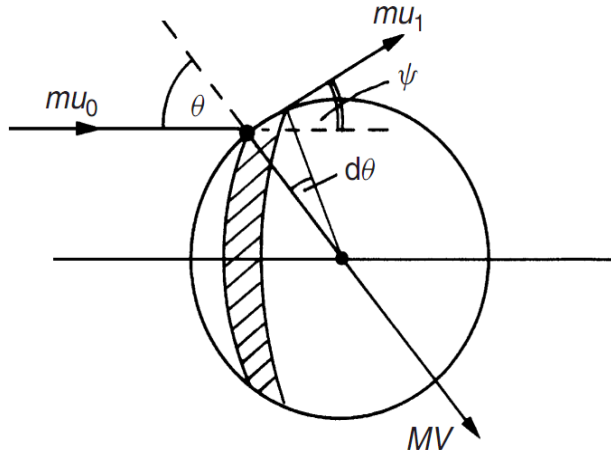


Figure 1.5 Energy transfer during elastic collision

After collision let the corresponding velocities be u_1 and V , the latter along line of centres as shown. θ is the incidence angle and ψ is the scattering angle. The fractional energy loss by the incoming particle during a collision at an angle θ is then given by:

$$\Delta(\theta) = \left(\frac{u_0^2 - u_1^2}{u_0^2} \right) \quad (1.28)$$

Since the collision is assumed to be kinetic, the equations for conservation of momentum and energy are:

$$mu_0 - mu_1 \cos \psi = MV \cos \theta \quad (1.29)$$

$$mu_1 \sin \psi = MV \sin \theta \quad (1.30)$$

$$\frac{1}{2} mu_0^2 - \frac{1}{2} mu_1^2 = \frac{1}{2} MV^2 \quad (1.31)$$

Squaring equations (1.29) and (1.30) and adding and combining with equation (1.31) we obtain:

$$V = \frac{2mu_0 \cos \theta}{M + m} \quad (1.32)$$

Rearranging equation (1.31) and combining with equation (1.28) gives:

$$\Delta \theta = \frac{MV^2}{mu_0^2} = \frac{4mM \cos^2 \theta}{(m + M)^2} \quad (1.33)$$

To obtain the mean fractional energy loss per collision, let $P(\theta)$ be the probability of a collision at an angle of incidence between θ and $d\theta$. The total area presented for collision is $\pi(r_1 + r_2)^2$. The probability of a collision

taking place between θ and $d\theta$ is the ratio of the projected area (Fig. 1.5) to the whole area or:

$$P(\theta)d\theta = \left\{ \frac{2\pi(r_1 + r_2)\sin\theta\cos\theta d\theta}{\pi(r_1 + r_2)} \right\} = \sin 2\theta d\theta \left\{ \begin{array}{l} \text{for } 0 \leq \theta \\ \text{for } \pi/2 \leq \theta \leq \pi \end{array} \right\}.$$

The mean fractional loss of energy per collision allowing for collisions at all angles is:

$$\Delta\bar{\theta} = \frac{\int_0^{\pi/2} P(\theta)\Delta\theta d\theta}{\int_0^{\pi/2} P(\theta)d\theta} \quad (1.34)$$

Using equations (1.33) and (1.34), we obtain:

$$\Delta\bar{\theta} = \frac{2mM}{(m+M)^2} \quad (1.35)$$

If we consider the case when the incoming particle is an ion of the same mass as the struck particle, then $m=M$ and equation (1.35) gives $\Delta\bar{\theta} = 1/2$ which indicates a high rate of energy loss in each elastic collision. On the other hand, if the incoming particle is an electron, then $m \ll M$ and equation (1.35) gives $\Delta\bar{\theta} = \frac{2m}{M}$. The average fraction of energy lost by an electron in an elastic collision is therefore very small. For example, if we consider the case of electrons colliding with *He* gas atoms, the average fractional energy loss per collision $\bar{\theta}$ is 2.7×10^{-4} and in argon it is 2.7×10^{-5} . Thus electrons will not readily lose energy in elastic collisions whereas ions will. Let us now consider the case when part of the kinetic energy of the incoming particle is converted into potential energy of the struck particle. Then applying the laws of energy and momentum conservation we obtain:

$$\frac{1}{2}mu_0^2 = \frac{1}{2}mu_1^2 + \frac{1}{2}MV^2 + W_p \quad (1.36)$$

$$mu_0 = mu_1 + MV \quad (1.37)$$

where W_p is the increase in potential energy of the particle of mass M initially at rest. Substituting equation (1.37) into equation (1.36) and rearranging we obtain:

$$W_p = \frac{1}{2} \left[m(u_0^2 - u_1^2) - \frac{m^2}{M} (u_0 - u_1)^2 \right]. \quad (1.38)$$

For the conditions of constant kinetic energy of the incoming particles, differentiation of equation (1.38) with respect to u_1 gives the maximum of energy transfer when:

$$\frac{dW_{p\max}}{du} = 0 \quad \text{or} \quad \frac{u_1}{u_0} = \frac{m}{m+M} \quad (1.39)$$

Equation (1.39) shows that the potential energy gained from the incident particle reaches a maximum value when the ratio of its final to initial velocity equals the ratio of its mass to the sum of masses of the individual particles. When the colliding particles are identical, the maximum kinetic to potential energy transfer occurs when $u_1 = u_0/2$. On the other hand, if the colliding particle is an electron of mass $m \ll M$ the maximum energy transfer corresponds to $u_1 = (m/M)u_0$ which means that the new velocity u_1 becomes only a small fraction of the original velocity. For the case when the target particle was initially at rest, the maximum amount of potential energy gained will be given by the expression obtained by inserting the value of velocity u_1 from equation (1.39) into equation (1.38) or:

$$W_{p\max} = \frac{M}{m+M} \frac{mu_0^2}{2}. \quad (1.40)$$

For an electron $m \ll M$, equation (1.40) becomes:

$$W_{p\max} \approx \frac{1}{2} \frac{mu_0^2}{2} \quad (1.41)$$

or almost all its kinetic energy is converted into potential energy. Thus we will see later that electrons are good ionizers of gas, while ions are not. To cause ionization the incoming electrons must have a kinetic energy of at least $\frac{1}{2}mu_0^2 \geq eV_i$, where V_i is the ionization potential of the atom or molecule.

1.2 Charge particles generation, movement and recombination

1.2.1 Ionization processes

Breakdown channel in gases is formed as result of different ionization processes in volume of anode–cathode gap (*volume ionization*) and metal electrode surface (*surface ionization*). Main volume ionization processes are: *impact ionization, step ionization, photoionization, ionization by interaction of metastables with atoms, thermal ionization, field ionization*. At normal temperature and pressure gases are excellent insulators. The conduction in air at low field is in the region $10^{16} - 10^{17} \text{ A/cm}^2$. This current results from cosmic radiations and radioactive substances present in earth and the atmosphere. At higher fields charged particles may gain sufficient energy between collisions to cause ionization on impact with neutral molecules. It was shown in above that electrons on average lose little energy in elastic collisions and readily build up their kinetic energy which may be supplied by an external source, e.g. an applied field. On the other hand, during inelastic collisions a large fraction of their kinetic energy is transferred into potential energy, causing, for example, ionization of the struck molecule. Ionization by electron impact is for higher field strength the most important process leading to breakdown of gases. The effectiveness of ionization by electron impact depends upon the energy that an electron can gain along the mean free path in the direction of the field.

If $\bar{\lambda}_e$ is the mean free path in the field direction of strength E then the average energy gained over a distance $\bar{\lambda}$ is $\Delta W = eE\bar{\lambda}_e$. This quantity is proportional to E/p since $\bar{\lambda}_e$ is proportional to $1/p$. To cause ionization on impact (*impact ionization*) the energy ΔW must be at least equal to the ionization energy of the neutral atom or molecule (eV_i). Electrons with lower energy than eV_i may excite particles and the excited particles on collisions with electrons of low energy may become ionized (*step ionization*). Furthermore, not all electrons having gained energy $\Delta W \geq eV_i$ upon collision will cause ionization. This simple model is not applicable for quantitative calculations, because *ionization* by collision, as are all other processes in gas discharges, *is a probability phenomenon*, and is generally expressed in terms of cross-section for ionization defined as the product $P_i\sigma = \sigma_i$ where P_i is the probability of ionization on impact and σ is the molecular or atomic cross-sectional area for interception defined earlier. The cross-section σ_i is measured using mono-energetic electron beams of different energy. The variation of ionization cross-sections for H_2 , O_2 and N_2 with electron energy is shown in Fig. 1.6. It is seen that the cross-section is strongly dependent upon the

electron energy. At energies below ionization potential the collision may lead to excitation of the

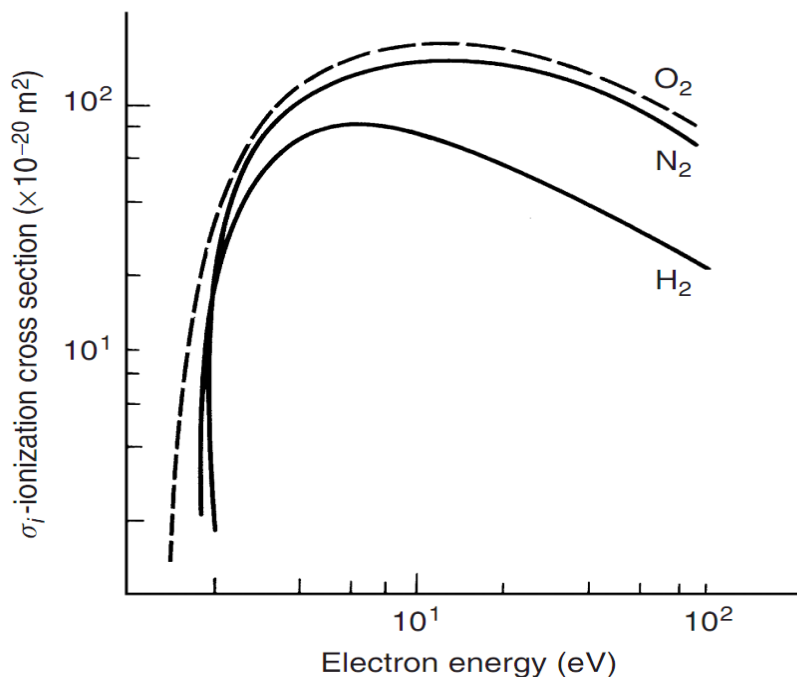


Figure 1.6 Variation of ionization cross-sections for O_2 , N_2 , H_2 with electron energy

struck atom or molecule which on collision with another slow moving electron may become ionized. This process becomes significant only when densities of electrons are high. Very fast moving electrons may pass near an atom without ejecting an electron from it. For every gas there exists an optimum electron energy range which gives a maximum ionization probability.

In the absence of electric field the rate of electron and positive ion generation in an ordinary gas is counterbalanced by decay processes and a state of equilibrium exists. This state of equilibrium will be upset upon the application of a sufficiently high field. The variation of the gas current measured between two parallel plate electrodes was first studied as a function of the applied voltage by Townsend [5]. Townsend found that the current at first increased proportionately with the applied voltage and then remained nearly constant at a value i_0 which corresponded to the background current (saturation current), or if the cathode was irradiated with a u.v. light, i_0 gave the emitted photocurrent. At still higher voltage the current increased above the value i_0 at an exponential rate. The general pattern of the current – voltage relationship is shown schematically in Fig. 1.7.

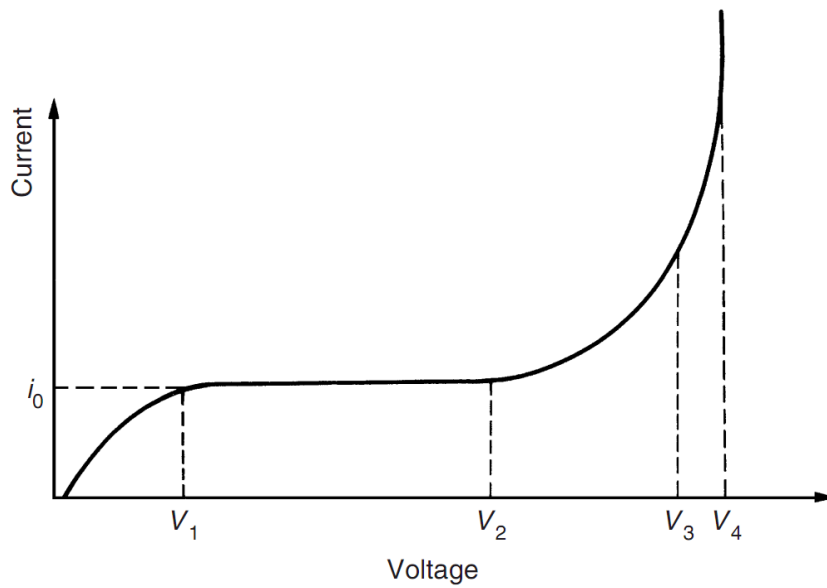


Figure 1.7 Current – voltage relationship in prespark region

The increase in current beyond V_2 Townsend ascribed to ionization of the gas by electron collision. As the field increases, electrons leaving the cathode are accelerated more and more between collisions until they gain enough energy to cause ionization on collision with gas molecules or atoms. To explain this current increase Townsend introduced a quantity α , known as Townsend's first ionization coefficient, defined as the number of electrons produced by an electron per unit length of path in the direction of the field. Thus if we assume that n is the number of electrons at a distance x from the cathode in field direction (Fig. 1.8) the increase in electrons dn in additional

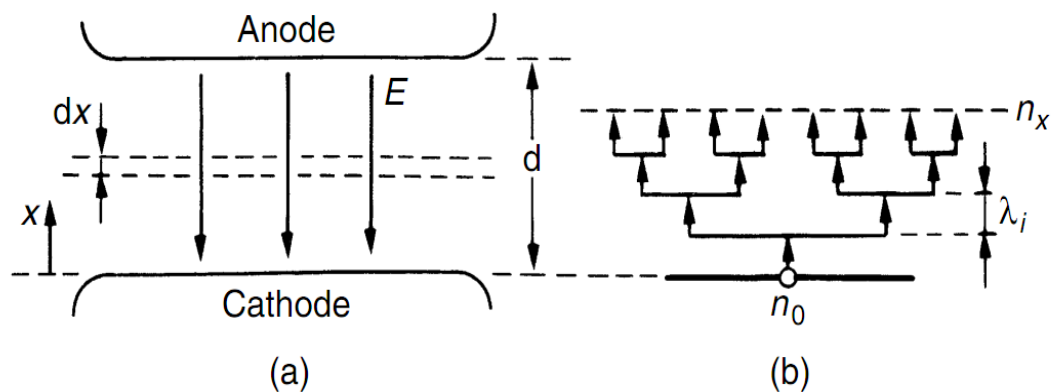


Figure 1.8 Schematic representation of electron multiplication:
a – gap arrangement, b – electron avalanche

distance dx is given by:

$$dn = \alpha n dx.$$

Integration over the distance (d) from cathode to anode gives:

$$n = n_0 e^{\alpha d} \quad (1.42)$$

where n_0 is the number of primary electrons generated at the cathode. In terms of current, with I_0 the current leaving the cathode, equation (1.42) becomes:

$$I = I_0 e^{\alpha d} \quad (1.43)$$

The term $e^{\alpha d}$ in equation (1.42) is called the **electron avalanche** and it represents the number of electrons produced by one electron in travelling from cathode to anode. The electron multiplication within the avalanche is shown diagrammatically in Fig. 1.8. The increase of current (avalanche growth) shown in the diagram (Fig. 1.8(b)) would be $I = I e^k$, with k = number of ionizing steps ($k = \frac{x}{\lambda_i}$). The transition for infinitely small values of dx ($\lim_{\lambda_x} \lambda_x \rightarrow dx$) leads to the expression $e^{\alpha x}$.

The quantity α , although a basic quantity describing the rate of ionization by electron collision, cannot be readily calculated from the measured cross-section for ionization. The latter is determined for mono-energetic electrons and calculation of α from value of σ_i is only possible when the electron energy distribution in the gas is known. For "swarm" conditions Raether derived a relationship between α and σ_i , which is of the form:

$$\frac{\alpha}{N} = \frac{1}{u_e} \int_0^{\infty} v \sigma_i(v) f(v) dv.$$

With N the concentration, molecules/atoms, $f(v)$ the distribution of velocities of electrons, and u_e the drift velocity of electrons in the field direction. A simple derivation is possible for simple gases (non-attaching) using the Clausius distribution of free paths (Fig. 1.4) and applying it to electrons.

We have seen that at a constant temperature for a given gas the energy distribution ΔW depends only on the value E/p . Also for a given energy distribution the probability of an ionization occurring will depend on the gas density or pressure. Therefore, we can write:

$$\alpha = pf\left(\frac{E}{p}\right) \text{ or } \frac{\alpha}{p} = f\left(\frac{E}{p}\right) \quad (1.44)$$

Equation (1.44) describes a general dependence of α/p upon E/p which has been confirmed experimentally. A derivation of expression for this dependence is possible for simple gases, using the Clausius distribution (equation (1.27)) for free paths applied to electrons. This means that we assume that this distribution will not be altered by the additional velocity of electrons in field direction. Then all electrons which acquire energy $\Delta W \geq eV_i$, where V_i is the ionization potential, will ionize the gas. These electrons have travelled a distance x , and using equation (1.27) the fraction of electrons with paths exceeding a given value x is:

$$f'(x) = e^{-x/\lambda}$$

The number of successful collisions – the ionization coefficient α – clearly related to this distribution, and is certainly directly proportional to the decay of collisions in the intervals between x and $x + dx$, or:

$$\alpha = -\frac{df'(x)}{dx} = \frac{1}{\lambda} e^{-x/\lambda} \quad (1.45)$$

where $\lambda_i = x$ is ionizing free path. The above treatment assumes $\lambda_e = \bar{\lambda}$, i.e. the velocity distribution is not altered by the additional velocity of electrons in the field direction. In reality there is a serious difference between $\bar{\lambda}$ and λ_e as shown below on Fig.1.9.

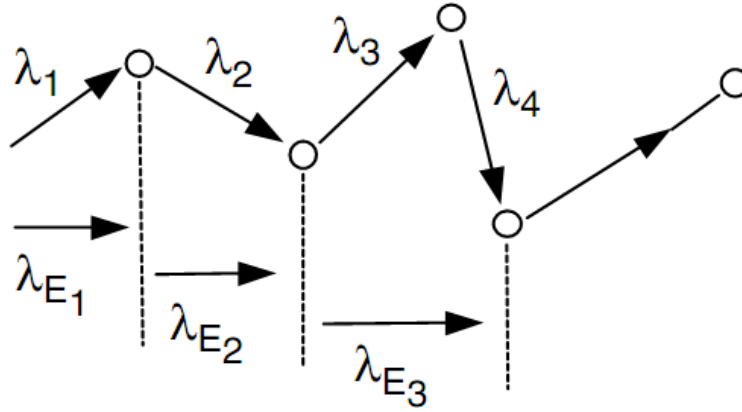


Figure 1.9 Schematic representation of a difference between field direction and real free paths

Introducing from equation (1.8) N , for a gas pressure p the mean free path becomes:

$$\bar{\lambda} = \frac{kT}{p\sigma_i}$$

So, taking into account (1.44) and abovementioned determination of E/p , we can conclude:

$$\frac{\alpha}{p} = \frac{\sigma_i}{kT} \exp\left(-\left(\frac{\sigma_i}{kT}\right)\left[\frac{V_i}{E/p}\right]\right) = A_{(r)} \exp\left[-\frac{B_{(r)}}{E/p}\right] \quad (1.46)$$

where

$$A_{(r)} = \frac{\sigma_i}{kT}; \quad B_{(r)} = \frac{V_i\sigma_i}{kT}. \quad (1.47)$$

Constant values of A and B , equation (1.47) determines the ionization process within certain ranges of E/p . Therefore, for various gases the constants A and B have been determined experimentally and can be found in the literature. Some of these experimental values for several of the more common gases are listed in Table 1.3.

Table 1.3 Ionization constants A and B ($T=20\text{ C}$)

Gas	A ion pairs $\text{cm}^{-1}\text{ Torr}^{-1}$	B V cm^{-1} Torr^{-1}	E/p range $\text{V cm}^{-1}\text{ Torr}^{-1}$	V_i volts
H ₂	5	130	150–600	15.4
N ₂	12	342	100–600	15.5
air	15	365	100–800	–
CO ₂	20	466	500–1000	12.6
He	3	34	20–150	24.5
Hg	20	370	200–600	–

The constants A and B in equation (1.47), as derived from kinetic theory, rarely agree with the experimentally determined values. The reasons of this disagreement lie in the assumptions made in our derivations. We assumed that every electron whose energy exceeds eV_i will automatically lead to ionization. In reality the probability of ionization for electrons with energy just above the ionization threshold is small and it rises slowly to a maximum value of about 0.5 at 4 to 6 times the ionization energy. Beyond that it decreases. We have also assumed that the mean free path is independent of electron energy which is not necessarily true. A rigorous treatment would require taking account of the dependence of the ionization cross-section upon the electron energy.

Using the experimental values for the constants A and B for N_2 and H_2 in equation (1.47), the graphical relationship between the parameters α/p and E/p has been plotted in Fig. 1.10. The values have been corrected to $T=0^\circ\text{C}$. It should be noted that theoretically α/p begins at zero value of E/p , which follows from distribution of free path which have values for 0 to ∞ .

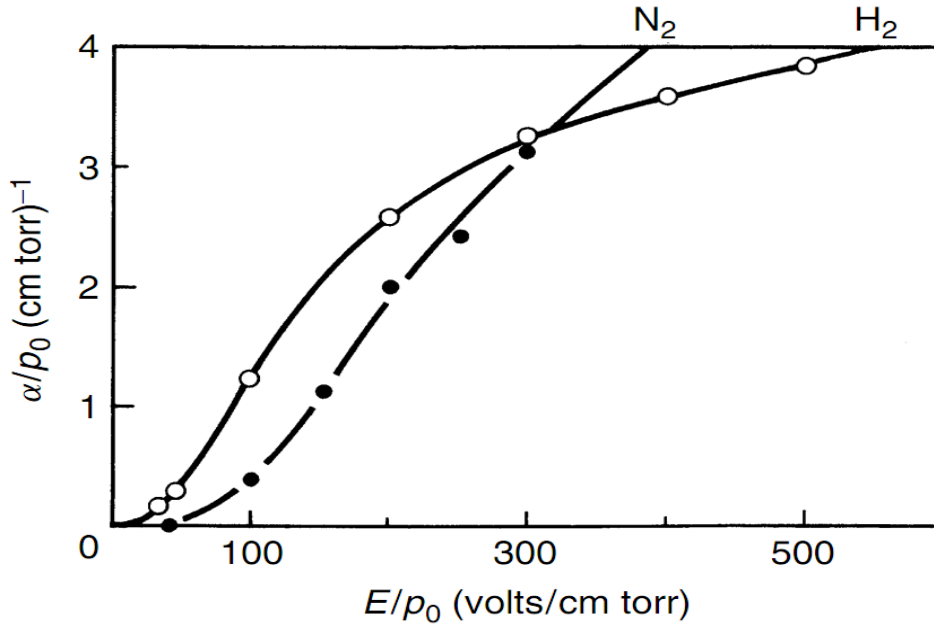


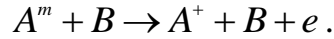
Figure 1.10 Dependence of α/p on E/p in N_2 and H_2 reduced to 0 C

Electrons of lower energy than the ionization energy eV_i may on collision excite the gas atoms to higher states. The reaction may be symbolically represented as $A + e + K \text{ energy} \rightarrow A^* + e; A^* \rightarrow A + hv; A^*$; represents the atom in an excited state. On recovering from the excited state in some $10^{-7} - 10^{-10}$ sec, the atom radiates a quantum of energy of photon hv which in turn may ionize another atom whose ionization potential energy is equal to or less than the photon energy. The process is known as **photoionization** and may be represented as $A + hv \rightarrow A^+ + e$, where A represents a neutral atom or molecule in the gas and hv the photon energy. Expression $hv \geq eV_i$ is photoionization condition. It is necessary to say, that only very short wavelength light quanta can cause photoionization of gas. For example, the shortest wavelength radiated from a u.v. light with quartz envelope is 145 nm , which corresponds to $eV_i = 8.5 \text{ eV}$, lower than the ionization potential of most gases. The probability of photon ionizing a gas or molecule is maximum when $hv - eV_i$ is small enough and is in the range $(0.1 - 1 \text{ eV})$.

Photoionization is a secondary ionization process and may be acting in the Townsend breakdown mechanism and is essential in the streamer breakdown mechanism and in some corona discharges. If the photon energy is less than eV_i it may still be absorbed by the atom and raise the atom to a higher energy level. This process is known as **photoexcitation**. **The photoexcitation is a reason of strong enough fluorescence of all electrical discharges.**

In certain elements the lifetime in some of the excited electronic states

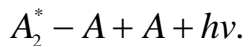
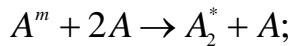
extends to seconds. These states are known as metastable states and the atoms in these states are simply referred to as metastables represented by A^m . Metastables have a relatively high potential energy and are therefore able to ionize neutral particles. If V^m , the energy of a metastable A^m , exceeds V_i , the ionization of another atom B , then on collision ionization may result according to the reaction



For V^m of an atom $A^m < V_i$ of an atom B the reaction may lead to the exciting of the atom B which may be represented by $A^m + B \rightarrow A + B^*$.

Another possibility for ionization by metastables is when $2V^m$ for A^m is greater than V_i for A . Then the reaction may proceed as $A^m + A^m \rightarrow A^+ + A + e + K.E.$, where $K.E.$ is kinetic energy. This last reaction is important only when the density of metastables is high.

Another reaction may follow as:



The photon released in the last reaction is of too low energy to cause ionization in pure gas, but it may release electrons from the cathode.

Ionization by metastable interactions comes into operation long after excitation, and it has been shown that these reactions are responsible for long time lags observed in some gases. It is effective in gas mixtures.

The term ***thermal ionization***, in general, applies to the ionizing actions of molecular collisions, radiation and electron collisions occurring in gases at high temperature. If a gas is heated to sufficiently high temperature many of the gas atoms or molecules acquire sufficiently high velocity to cause ionization on collision with other atoms or molecules. Thermal ionization is the principal source of ionization in flames and high-pressure arcs.

In analysing the process of thermal ionization, the recombination between positive ions and electrons must be taken into account. Under thermodynamic equilibrium conditions the rate of new ion formation must be equal to the rate of recombination. Using this assumption *Saha* (Indian physicist) derived an expression for the degree of ionization in terms of the gas pressure and absolute temperature as follows:

$$\frac{\theta^2}{1-\theta^2} = \frac{1}{p} \frac{(2\pi m_e)^{3/2}}{h} (kT)^{5/2} \exp\left(-\frac{W_i}{kT}\right)$$

or

$$(1.48)$$

$$\frac{\theta^2}{1-\theta^2} = \frac{2.4 \times 10^{-4}}{p} T^{5/2} \exp\left(-\frac{W_i}{kT}\right)$$

where p is the pressure in *torr*, W_i the ionization energy of the gas, k Boltzmann's constant, the ratio of n_i/n , and n_i the number of ionized particles of total n particles. The strong dependence of on temperature in equation (1.48) shows that the degree of ionization is negligible at room temperature. On substitution of values W_i , kT , p and T in equation (1.48) we find that thermal ionization becomes significant for temperatures above 3000 K.

1.2.2 Recombination processes

Whenever there are positively and negatively charged particles present, recombination takes place. The potential energy and the relative kinetic energy of the recombining electron – ion is released as quantum of radiation. At high pressures, ion – ion recombination takes place. The rate of recombination in either case is directly proportional to the concentration of both positive ions and negative ions. For equal concentrations of positive ions n_+ and negative ions n_- the rate of recombination is written as:

$$\frac{dn_+}{dt} = \frac{dn_-}{dt} = -\beta n_+ n_- \quad (1.49)$$

where β is a constant known as the **recombination rate coefficient**.

Since $n_+ \approx n_- = n_i$ and we assume that at initial time moment $t=0$, $n_i = n_{i0}$ and at time moment t : $n_i = n_i(t)$, then equation (1.49) can be written as:

$$\frac{dn_i}{dt} = -\beta n_i^2$$

Integration gives:

$$\int_{n_{i0}}^{n_i} \frac{dn_i}{n_i^2} = -\beta \int_0^t dt \quad \text{or} \quad n_i(t) = \frac{n_{i0}}{1 + n_{i0}\beta t} \quad (1.50)$$

The half-time duration, during which time the concentration of ions has decreased to half its original value, is given by expression:

$$t_n = \frac{1}{n_{i0}\beta} \quad (1.51)$$

The variation of the recombination rate coefficient β with pressure in air is shown in Fig. 1.11.

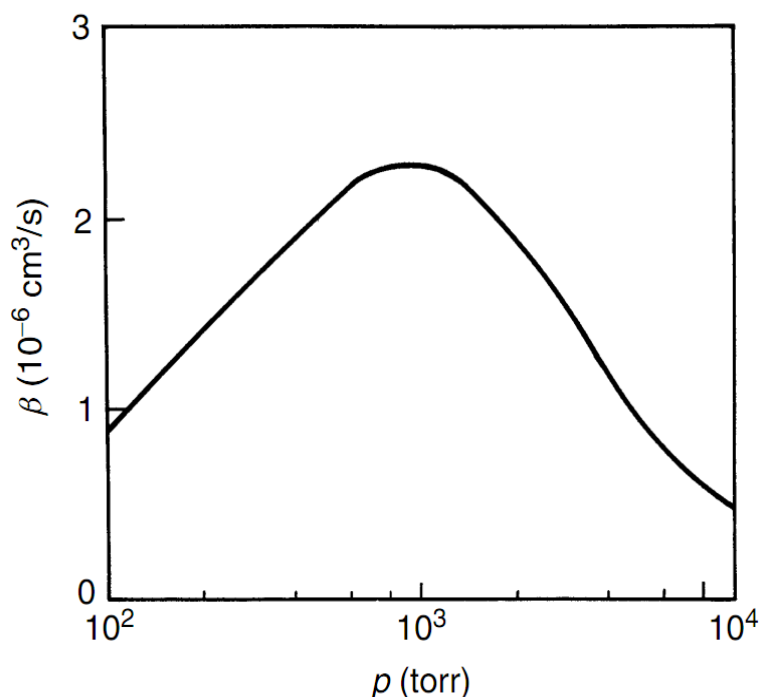


Figure 1.11 Recombination coefficient in air at 20 C

One of important recombination process is deionization by **attachment**. A base of this process is **negative ion formation**. Certain atoms or molecules in their gaseous state can readily acquire a free electron to form a stable negative ion. Gases, whether atomic or molecular, that have this tendency are those that are lacking one or two electrons in their outer shell and are known as electronegative gases. Examples include the halogens (*F*, *Cl*, *Br*, *I* and *At*) with one electron missing in their outer shell, *O*, *S*, *Se* with two electrons deficient in the outer shell.

For a negative ion to remain stable for some time, the total energy must be lower than that of an atom in the ground state. The change in energy that occurs when an electron is added to a gaseous atom or molecule is called the electron affinity of the atom and is designated by W_a . This energy is released as a quantum or kinetic energy upon attachment.

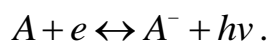
Table 1.4 shows electron affinities of some elements.

Table 1.4 Electron affinities of some elements

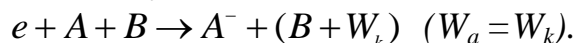
<i>Element</i>	<i>Ion formed</i>	W_a (kJ/mole)
H	H ⁻	-72
O	O ⁻	-135
F	F ⁻	-330
Cl	Cl ⁻	-350
Br	Br ⁻	-325
I	I ⁻	-295

There are several processes of negative ion formation:

a) The simplest mechanism is one in which the excess energy upon attachment is released as quantum known a **radiative attachment**. This process is reversible, that is the captured electron can be released by absorption of a photon known as photodetachment. Symbolically the process is represented as:



b) The excess energy upon attachment can be acquired as kinetic energy of a third body upon collision and is known as a third body collision attachment, represented symbolically as:



c) A third process is known as dissociative attachment which is predominant in molecular gases. Here the excess energy is used to separate the molecule into a neutral particle and an atomic negative ion, symbolically expressed as:



d) In process (c) in the intermediate stage the molecular ion is at a higher potential level and upon collision with a different particle this excitation energy may be lost to the colliding particle as potential and/or kinetic energy. The two stages of the process here are:

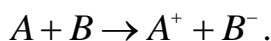


Other processes of negative ion formation include splitting of a mole-

cule into positive and negative ions upon impact of an electron without attaching the electron:



and a charge transfer following heavy particle collision, yielding an ion pair according to:



All the above electron attachment processes are reversible, leading to electron detachment. The process of electron attachment may be expressed by cross-section for negative ion formation σ_A in an analogous way to ionization by electron impact. Typical examples of the variation of attachment cross-section with electron energy for processes (b) and (c) measured in SF_6 and CO_2 are shown in Figs 1.12 and 1.13 respectively.

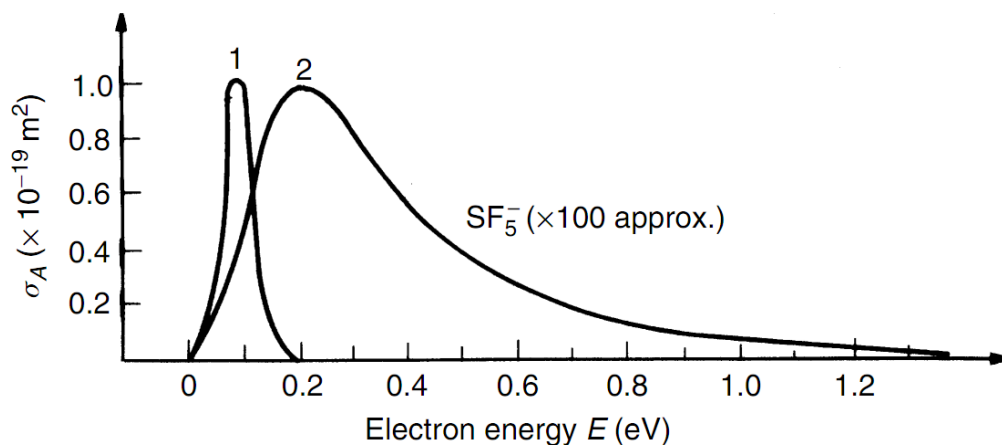


Figure 1.12 Variation of attachment cross-section with electron energy in SF_6 .

1 - Radiative attachment, 2 - Dissociative attachment

Cumulatively the process of electron attachment describing the removal of electrons by attachment from ionized gas by any of the above processes may be expressed by a relation analogous to the expression (1.43) which defines electron multiplication in a gas. If η is the attachment coefficient defined by analogy with the first Townsend ionization coefficient α , as the number of attachments produced in a path of a single electron travelling a distance of l cm in the direction of field, then the loss of electron current in a distance dx due to this cause is:

$$dI = -\eta I dx$$

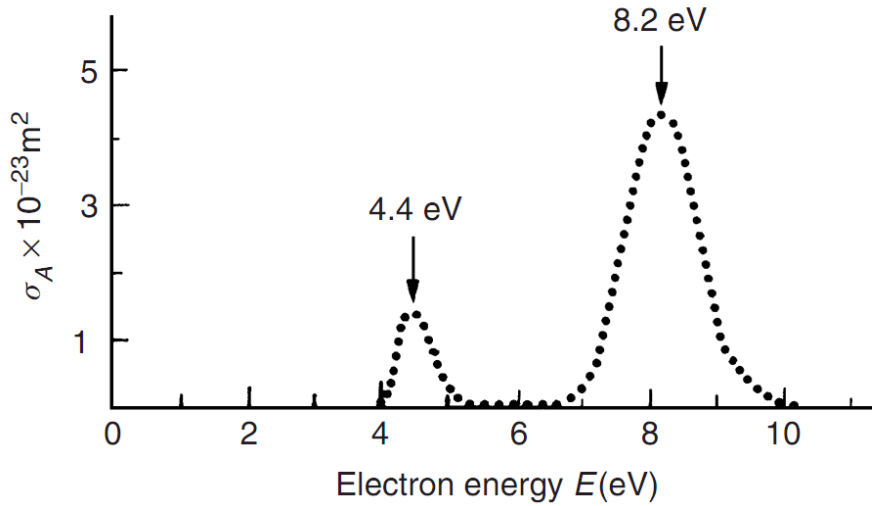


Figure 1.13 Variation of electron attachment cross-section with electron energy in CO_2 (both peaks are for O^-)
or for a gap of length d with electron current I_0 starting at cathode:

$$I = I_0 e^{-\alpha x} \quad (1.52)$$

If the processes of electron multiplication by electron, collision and electron loss by attachment are considered to operate simultaneously, then neglecting other processes the number of electrons produced by collision in distance dx is:

$$dn_i = n \alpha dx$$

where x is the distance from the cathode. At the same time the number of electrons lost in dx by attachment is:

$$dn_A = -n \eta dx$$

so that the number of electrons still free is:

$$dn = dn_i + dn_A = n(\alpha - \eta) dx.$$

Integration from $x=0$ to x with n_0 electrons starting from the cathode gives the number of electrons at any point in the gap as:

$$n = n_0 e^{(\alpha - \eta)x} \quad (1.53)$$

The steady state current under such conditions will have two components, one resulting from the flow of electrons and the other from negative

ions. To determine the total current we must find the negative ion current component. We note that the increase in negative ions in distance dx is:

$$dn_- = n\eta dx = n_0\eta e^{(\alpha-\eta)x} dx.$$

Integration of this equation from 0 to x gives:

$$n_- = \frac{\eta_0\eta}{\alpha - \eta} [e^{(\alpha-\eta)x} - 1].$$

The total current equals the sum of the two components or:

$$\frac{n + n_-}{n_0} = \frac{\alpha}{\alpha - \eta} e^{(\alpha-\eta)d} - \frac{\eta}{\alpha - \eta} \quad (1.54)$$

and the expression for current becomes:

$$I = I_0 \left[\frac{\alpha}{\alpha - \mu} e^{(\alpha-\eta)d} - \frac{\eta}{\alpha - \eta} \right]. \quad (1.55)$$

In the absence of attachment when η is zero the expression (1.55) reduces to the form $i = i_0 e^{\alpha d}$ and the $\log i - d$ plot of equation (1.55) gives a straight line, with α representing the slope. When the value of η is appreciable, there may be a decrease in currents, especially at large values of d , such that the $\log i$ against d curve drops below the straight line relation. The departure from linearity in plotting $\log i$ against d gives a measure of the attachment coefficient. The results obtained by this method by Geballe and Harrison for ionization α and attachment η in oxygen and in air are included in Table 1.5. It is convenient to represent the observed ionization coefficient by a single coefficient $\alpha = \alpha - \eta$ defined as the effective ionization coefficient.

As electron attachment reduces electron amplification in a gas, gases with a high attachment coefficient such as *sulphur hexafluoride* or Freon have much higher dielectric strength than air or nitrogen. The measured data for ionization and attachment coefficients for SF_6 are included in Table 1.6. These gases are very technically important and are widely used as insulating medium in compact high voltage apparatus including totally enclosed substations and high voltage cables [5].

Table 1.5. Geballe and Harrison's values for α/p and η/p in oxygen and air

E/p V/cm. torr	Oxygen			Air		
	α/p	η/p	$\alpha/p - \eta/p$	α/p	η/p	$\alpha/p - \eta/p$
25.0	0.0215	0.0945	-0.0730	0.00120	0.00495	-0.00375
27.5	0.0293	0.0900	-0.0607	0.00205	0.00473	-0.00268
30.0	0.0400	0.0851	-0.0451	0.00340	0.00460	-0.00120
32.5	0.0532	0.0795	-0.0263	0.00560	0.00460	+0.00100
35.0	0.0697	0.0735	-0.0038	0.00880	0.00475	+0.00405
37.5	0.0862	0.0685	+0.0177	0.0130	0.00497	+0.0080
40.0	0.107	0.0645	+0.043	0.0190	0.00530	+0.0137
42.5	0.128	0.0605	+0.068	0.0260	0.00575	+0.0203
45.0	0.152	0.0570	+0.095	0.0340	0.00635	+0.0277
47.5	0.179	0.0535	+0.126	0.0460	0.00700	+0.0390
50.0	0.206	0.052	+0.154	0.057	0.00780	+0.049
52.5	0.234	0.049	+0.185	0.070	0.00870	+0.061
55.0	0.263	0.047	+0.216	0.087	0.00967	+0.077
57.5	0.292	0.045	+0.247	0.102	0.0108	+0.091
60.0	0.323	0.043	+0.280	0.120	0.0119	+0.108
62.5	0.355	0.0415	+0.314	0.140	-	-
65.0	0.383	0.040	+0.343	0.170	-	-
70.0	0.450	-	-	-	-	-
72.5	0.480	-	-	-	-	-
75.0	0.518	-	-	-	-	-

1.2.3 Charged particle movement in electric field

In the presence of an electric field charged particles in a gas will experience a force causing them to drift with a velocity that varies directly with the field and inversely with the density of the gas through which it moves. The drift velocity component in the field direction of unit strength is defined as the *mobility* (K) or symbolically:

$$K = \frac{u}{E} \left(\frac{m^2}{V \times \text{sec}} \right),$$

where u is the average drift velocity in field direction and E is the electric field strength. The mobility K is mainly a characteristic of the gas through which the ion moves and is independent of E/p over a wide range of E/p so long as the velocity gained by the ion from the field is considerably less than the average thermal velocity of the gas through which the ion moves. To derive an expression for mobility of ions in a gas under an influence of electric field in the region of low values of E/p we assume that the ions are in thermal equilibrium with the gas molecules. Their drift velocity is small compared to the thermal velocity.

Table 1.6 Experimental values of the ionization and attachment coefficients in SF₆ (temperature = 20 C)

E/p_{20} V/cm. torr	p torr	$\bar{\alpha}/p \times 10^3$ cm^{-1} torr ⁻¹	α/p cm^{-1} torr ⁻¹	η/p cm^{-1} torr ⁻¹	$\gamma \times 10^7$
115.0	5.2	-90	1.05	1.14	
125.0	5.2	200	1.32	1.12	
135.0	5.2	480	1.52	1.04	
145.0	5.2	760	1.73	0.97	
154.0	5.2	1000			
155.0	5.2	1050			
165.0	5.2	1300			
175.0	5.2	1550			
185.0	5.2	1850			
200.0	5.2	2250			
115.0	19.5	90	1.04	1.13	
120.0	19.5	50	1.18	1.13	
125.0	19.5	200	1.30	1.10	
135.0	19.5	505			1
116.0	50.2	-25			
118.0	50.2	8	1.15	1.14	
120.0	50.2	60	1.18	1.12	
122.0	50.2	115			
125.0	50.2	225			
126.0	50.2	240			3
116.0	99.1	-38			
118.0	99.1	10			
119.0	99.1	33			
120.0	99.1	56			
122.0	99.1	120			
115.0	202.0	75			
117.0	202.0	-16			
118.0	202.0	4			
119.0	202.0	29			
119.25	202.0	36			60
122.0	202.0	110			6
117.0	402.4	-30			
118.0	402.4	5			
118.5	402.4	16			75

It is good famous from general physics course, that in electric field a charge particle begin to possess by drift velocity u . It can be determined as:

$$u = \frac{eE}{2m}\tau,$$

where τ is time during of one particle moves a distance $s = \frac{eE}{2m}\tau$. So, for drift velocity we can write:

$$u = \frac{eE}{2m}\tau = \left(\frac{e\tau}{2m}\right)E = \left(\frac{e\bar{\lambda}_i}{2m\bar{c}}\right)E,$$

and as result for mobility we have:

$$K = \frac{u}{E} = \frac{e\bar{\lambda}_i}{2m\bar{c}} \quad (1.56)$$

where $\bar{\lambda}_i$ and \bar{c} are mean free path and mean thermal velocity of ion respectively.

Table 1.7 gives some experimentally determined mobilities for negative and positive ions.

Table 1.7 Mobility of singly charged gaseous ions at 0 C and 760 Hg

<i>Gas</i>	K^-	K^+	<i>Gas</i>	K^-	K^+
Air (dry)	2.1	1.36	H ₂ (very pure)	7900.0	
Air (very pure)	2.5	1.8	HCl	0.95	1.1
A	1.7	1.37	H ₂ S	0.56	0.62
A (very pure)	206.0	1.31	He	6.3	5.09
Cl ₂	0.74	0.74	He (very pure)	500.0	5.09
CCl ₄	0.31	0.30	N ₂	1.84	1.27
C ₂ H ₂	0.83	0.78	N ₂ (very pure)	145.0	1.28
C ₂ H ₅ Cl	0.38	0.36	NH ₃	0.66	0.56
C ₂ H ₅ OH	0.37	0.36	N ₂ O	0.90	0.82
CO	1.14	1.10	Ne		9.9
CO ₂	0.98	0.84	O ₂	1.80	1.31
H ₂	8.15	5.9	SO ₂	0.41	0.41

The presence of impurities is found to have a profound effect on the measured mobility. The effect is particularly large in the case of negative ions when measured in non-attaching gases such as helium or hydrogen for which the electrons are free if the gases are extremely pure. The ion and elec-

tron mobilities can be used for the determination of conductivity or resistivity of an ionized gas. In the simplest case when the concentrations of positive ions and electrons are equal $n_+ = n_e = n$. Then total current density is:

$$j = j_i + j_e = n(u_i + u_e)e$$

where u_i and u_e are the drift velocities of the ions and electrons respectively.

In terms of mobilities, the current density (j) and conductivity (σ) become:

$$j = neE(K_i + K_e)$$

$$\sigma = \frac{j}{E} = ne(K_e + K_i) \quad (1.57)$$

Since, $K_e \gg K_i$, the conductivity is given by the expression:

$$\sigma = neK_e \quad (1.58)$$

In electrical discharges whenever there is a non-uniform concentration of ions there will be movement of ions from regions of higher concentration to regions of lower concentration. The process by which equilibrium is achieved is called diffusion. This process will cause a deionizing effect in the regions of higher concentrations and an ionizing effect in regions of lower concentrations. The presence of walls confining a given volume augments the deionizing effect as the ions reaching the walls will lose their charge. The flow of particles along the ion concentration gradient constitutes a drift velocity similar to that of charged particles in an electric field. Both diffusion and mobility result in mass motion described by drift velocity caused in one case by the net effect of unbalanced collision forces (ion concentration gradient) and in the other case by the electric field. If we consider a container with gas in which the concentration varies in the x -direction, then taking a layer of unit area and thickness dx placed perpendicularly to the direction x , the number of particles crossing this area is proportional to the ion concentration gradient dn/dx . The flow of particles or flux in the x -direction is:

$$\Gamma = -D \frac{dn}{dx} \quad (1.59)$$

The negative sign indicates that n increases and the rate of flow Γ must decrease in the direction of flow. The constant D is known as the diffusion coefficient. From kinetic theory it can be shown that $D = u \cdot \bar{\lambda}/3$. With u being the mean thermal velocity, the rate of change of concentration in the layer dx is:

$$\frac{d}{dt}(ndx) = \Gamma - \left(\Gamma + \frac{d\Gamma}{dx} dx \right) \quad (1.60)$$

$$\frac{dn}{dt} = D \frac{d^2 n}{dx^2}.$$

For the three-dimensional case equation (1.60) becomes:

$$\frac{\partial n}{\partial t} = D \nabla^2 n, \quad (1.61)$$

which is the general equation for diffusion.

In most transport phenomena, both diffusion and mobility will be acting together. It is therefore important to establish a relation between the diffusion coefficient and mobility. To determine this connection it is necessary to recall material from paragraph 1.1.

$$\frac{D}{K} = \frac{P_i}{eN} = \frac{kTn_i}{en_i} = \frac{kT}{e} \left(n_i = \frac{p_i}{kT} \right) \quad (1.62)$$

In general the mobilities of negatively charged ions are higher than those of positive ones (Table 1.7) and consequently the negative ions will diffuse more rapidly. If the concentration of the diffusing particles is significant, the differential rate of diffusion will cause charge separation which will give rise to an electric field. The action of the field is such that it will tend to augment the drift velocity of the positive ions and retard that of negative ions, and the charge separation reaches a state of equilibrium in which the positive and negative ions diffuse with the same velocity. This process is known as *ambipolar diffusion*. The average velocity of the diffusing ions may be obtained by considering the ion motion to be governed by the combined action of diffusion and mobility in the induced field E . Then the velocity of the positive ions is given by:

$$u^+ = -\frac{D^+ dn^+}{n^+ dx} + K^+ E. \quad (1.63)$$

Similarly the velocity of negative ions is:

$$u^- = -\frac{D^- dn^-}{n^- dx} - K^- E. \quad (1.64)$$

Eliminating E between equations (1.63) and (1.64), and assuming that $n^+ = n^- = n$,

$$\frac{dn^+}{dx} = \frac{dn^-}{dx} = \frac{dn}{dx} \quad \text{and} \quad u^+ = u^- = u.$$

The average velocity of the ions then becomes:

$$u = -\frac{D^+K^- + D^-K^+}{n(K^+ + K^-)} \frac{dn}{dx} \quad (1.65)$$

And the ambipolar diffusion coefficient for mixed ions may be written as:

$$u = -\frac{D^+K^- + D^-K^+}{K^+ + K^-} \quad (1.66)$$

Finally, the electric field E between the space charges can be obtained by eliminating u from equations (1.62) and (1.63), giving:

$$E = -\frac{D^- - D^+}{K^- + K^+} \frac{1}{n} \frac{dn}{dx} \quad (1.67)$$

Diffusion processes are of particular importance in such discharge phenomena as streamer formation and spark channels.

1.2.4 Emission processes

Electrodes, in particular the cathode, play a very important role in gas discharges by supplying electrons for the initiation, for sustaining and for the completion of a discharge. Under normal conditions electrons are prevented from leaving the solid electrode by the electrostatic forces between the electrons and the ions in the lattice. The energy required to remove an electron from a Fermi level is known as the work function W_a and is a characteristic of a given material. There are several ways in which the required energy may be supplied to release the electrons from metal surface. Photons incident upon the cathode surface whose energy exceeds the work function $h\nu > W_a$ may eject electrons from the surface. For most metals the critical frequency ν_0 lies in the u.v. range. When the photon energy exceeds the work function, the excess energy may be transferred to electron kinetic energy according to the Einstein relation:

$$\frac{1}{2}mu_e^2 = h\nu = h\nu_0 \quad (1.68)$$

where m is the electron mass, u_e its velocity and $h\nu_0$ is the critical energy required to remove the electron from the surface and $h\nu_0 = W_a$ the work function. This process is called a **photoelectric emission**. Table 1.8 gives the work functions for several elements. The work function is sensitive to contamination which is indicated by the spread in the measured values shown in Table 1.8.

Table 1.8 Work function for typical cathode elements

Element	Ag	Al	Cu	Fe	W
W_a (eV)	4.74	2.98–4.43	4.07–4.7	3.91–4.6	4.35–4.6

The spread is particularly large in the case of aluminium and metals which readily oxidize. In the presence of a thin oxide film, it has been shown by Malter that positive ions may gather at the oxide layer without being neutralized, giving rise to a high field strength leading to augmented secondary emission. The effect is known as the Malter effect.

Electrons may be emitted from metal surfaces by bombardment of positive ions or metastable atoms. To cause a secondary emission of an electron the impinging ion must release two electrons, one of which is utilized to neutralize the ion charge. The minimum energy required for a positive ion electron emission is twice the work function $W_k + W_p > 2W_A$ since the ion is neutralized by one electron and the other electron is ejected. W_K and W_p are the respective kinetic and potential energies of the incident ion. The electron emission by positive ions is the principal secondary process in the Townsend spark discharge mechanism.

Neutral excited (metastable) atoms or molecules incident upon the electrode surface are also capable of ejecting electrons from the surface.

In metals at room temperature the conduction electrons will not have sufficient thermal energy to leave the surface. If we consider the electrons as a gas at room temperature, then their average thermal energy is:

$$\frac{mu_e^2}{2} = \frac{3}{2}kT = 3.8 \times 10^{-2} eV,$$

which is much lower than the work function (Table 1.8). If, however, the metal temperature is increased to some 1500 – 2500 K, the electrons will receive energy from the violent thermal lattice vibrations sufficient to cross the surface barrier and leave the metal. The emission current is related to the temperature of the emitter by the Richardson relation for thermionically emitted saturation current density:

$$J_s = \frac{4\pi me k^2}{h^3} T^2 \exp\left(-\frac{W_A}{kT}\right) A/m^2 \quad (1.69)$$

where e and m are the electronic charge and mass respectively, h is Planck's constant, k Boltzmann's constant, T the absolute temperature and W_A surface work function.

Putting $A = \frac{4\pi m e k^2}{h^3}$ the above expression become:

$$J_s = AT^2 \exp\left(-\frac{W_A}{kT}\right), \quad (1.70)$$

which shows that the saturation current density increases with decreasing work function and increasing temperature. This is main equation of **thermo-electron emission**.

Electrons may be drawn out of a metal surface by very high electrostatic fields. It will be shown that a strong electric field at the surface of a metal may modify the potential barrier at the metal surface to such an extent that electrons in the upper level close to the Fermi level will have a definite probability of passing through the barrier. The effect is known as "**tunnel effect**". The fields required to produce emission currents of a few microamperes are of the order of $10^7 - 10^8$ V/cm. Such fields are observed at fine wires, sharp points and submicroscopic irregularities with an average applied voltage quite low (2 – 5 kV). These fields are much higher than the breakdown stress even in compressed gases.

To derive an expression for the emission current let us consider an electron as it leaves the surface in the direction x as shown in Fig. 1.14. Its electric field can be approximated as that between a point charge and the equipotential planar surface. The field lines here are identical to those existing when an image charge of $+e$ is thought to exist at a normal distance of x on the other side of the equipotential metal surface. Applying Coulomb's law, the force on the electron in the x -direction is given by:

$$F(x) = \frac{-e^2}{4\pi\epsilon_0(2x)^2} = \frac{-e^2}{16\pi\epsilon_0 x^2}.$$

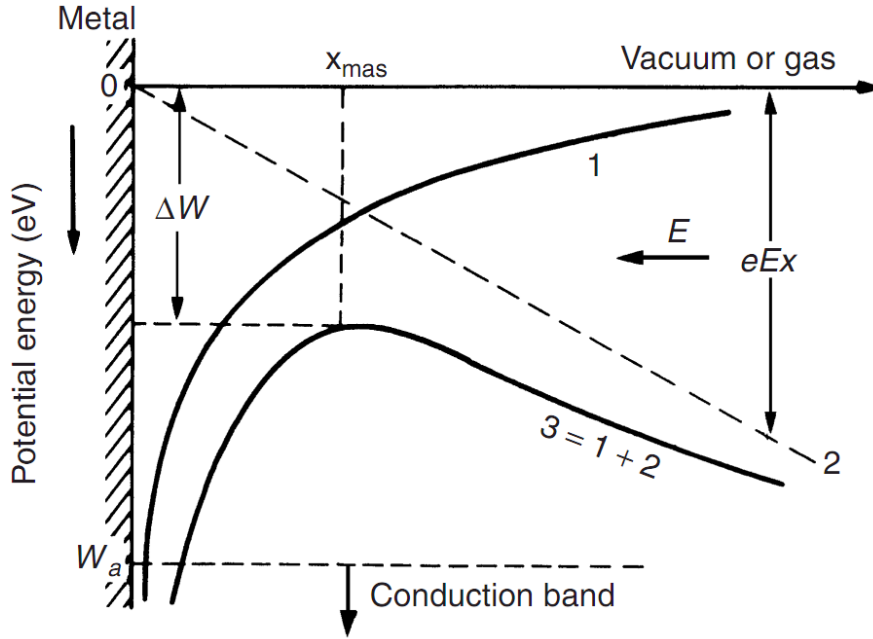


Figure 1.14 Changing of the potential barrier by external electric field.
 1. Energy with no field. 2. Energy due to field. 3. Resultant energy.

The effect shown on Fig.1.14 has been explained by Fowler and Nordheim who derived an expression for field emission on the basis of wave mechanics. These authors have shown that a few electrons in a metal will have an energy slightly above the Fermi level and thus will have a greater probability to penetrate the potential barrier “*tunnel effect*”. The **Fowler – Nordheim equation** has the form:

$$j_{FE} = CE^2 \exp\left(\frac{D}{E}\right) \quad (1.71)$$

where C and D are constants involving atomic constants. Equation (1.70) shows that field emission is independent of temperature, but this is valid only at low temperatures. At higher temperatures both thermionic and field emission will occur simultaneously.

A number of electrons, which are produced at the cathode by positive ion bombardment, is called γ .

The case where the **secondary emission** arises **from photon impact** at the cathode may be expressed by the equation:

$$I = I_0 \times \frac{\alpha e^{\beta d}}{\alpha - \theta \eta g e^{(\alpha - \mu)d}} \quad (1.72)$$

where θ is the number of photons produced by an electron in advancing 1 cm in the direction of the field, μ is the average absorption coefficient for photons in the gas, g is a geometrical factor representing the fraction of photons that reach the cathode, and η is the fraction of the photons producing electrons at the cathode capable of leaving the surface. In practice both positive ions and photons may be active at the same time in producing electrons at the cathode. Furthermore, metastable atoms may contribute to the secondary emission at the cathode. Which of the particular secondary mechanisms is predominant depends largely upon the experimental conditions in question. Llewellyn Jones and Davies have studied the influence of cathode surface layers on the breakdown characteristic of air and on the corresponding values of γ . Their data are included in Table 1.9 which shows a wide variation in the minimum breakdown voltage V_m and the accompanying variation in the values of γ .

Table 1.9 Breakdown voltage V_m , E/p and γ as function of cathode material

Gas	Cathode	V_m (volts)	E/p $\left(\frac{V}{\text{cm.torr}}\right)$	γ
Air contaminated with Hg vapour	Copper amalgam	460	720	0.004
	Mercury film on aluminium	390	885	0.014
	Mercury film on nickel	390	885	0.014
	Mercury film on staybrite steel	390	585	0.006
Air	Oxidized aluminium	416	905	0.01
	Oxidized nickel	421	957	0.01
Hydrogen (electrode treated by glow discharge)	Aluminium	243	200	0.1
	Aluminium deposited on nickel	212	200	0.15
	Nickel	289	180	0.075
	Nickel deposited on aluminium	390	245	0.015
	Commercial aluminium	225	200	0.125
	Aluminium on staybrite steel	205	210	0.15
	Staybrite steel	274	190	0.075
Steel deposited on aluminium	282	190	0.075	

1.3 Forms of electrical discharge

As the voltage between electrodes in a gas with small or negligible electron attachment increases, the electrode current at the anode increases in accordance with equation:

$$I = I_0 \frac{e^{\alpha d}}{1 - \gamma(e^{\alpha d} - 1)} \quad (1.73)$$

Taking into account this equation and all above discussed ionization and emission processes, we can write *main condition of self-sustaining discharge*:

$$\gamma(e^{\alpha d} - 1) \geq 1 \quad (1.74)$$

This expression means that the ionization produced by successive avalanches is cumulative. The discharge is then self-sustaining and grows more rapidly the more expression (1.74) exceeds unity. Growth of electron is arisen very rapidly, due to exponential law. Such mechanism of discharge processing is called *electron avalanche*. So, this phenomenon is named "*avalanche discharge*" or *Townsend mechanism of discharge*. Townsend is English physicist, who described this discharge form for the first time [6].

The growth of charge carriers in an avalanche in a uniform field $E_0 = V_0/d$ is described by the exponent $e^{\alpha d}$. This is valid only as long as the electrical field of the space charges of electrons and ions can be neglected compared to the external field E_0 . In his studies of the effect of space charge of an avalanche on its own growth, Raether observed that when the charge concentration was higher than 10^6 but lower than 10^8 the growth of an avalanche was weakened and disappeared [7,8].

When the ion concentration exceeded 10^8 the avalanche current was followed by a steep rise in current and breakdown of the gap followed. Both the under-exponential growth at the lower concentration and rapid growth in the presence of the high concentration have been attributed to the modification of the originally uniform field E_0 by the space charge field. Figure 1.15 shows diagrammatically the electric field around an avalanche as it progresses along the gap and the resulting modification to the original field E_0 . For simplicity the space charge at the head of the avalanche is assumed concentrated within a spherical volume, with the negative charge ahead because of the higher electron mobility. The field is enhanced in front of the head of the avalanche with field lines from the anode terminating at the head. Further back in the avalanche, the field between the electrons and the ions left behind reduced the applied field E_0 . Still further back the field between the cathode and the positive ions is enhanced again.

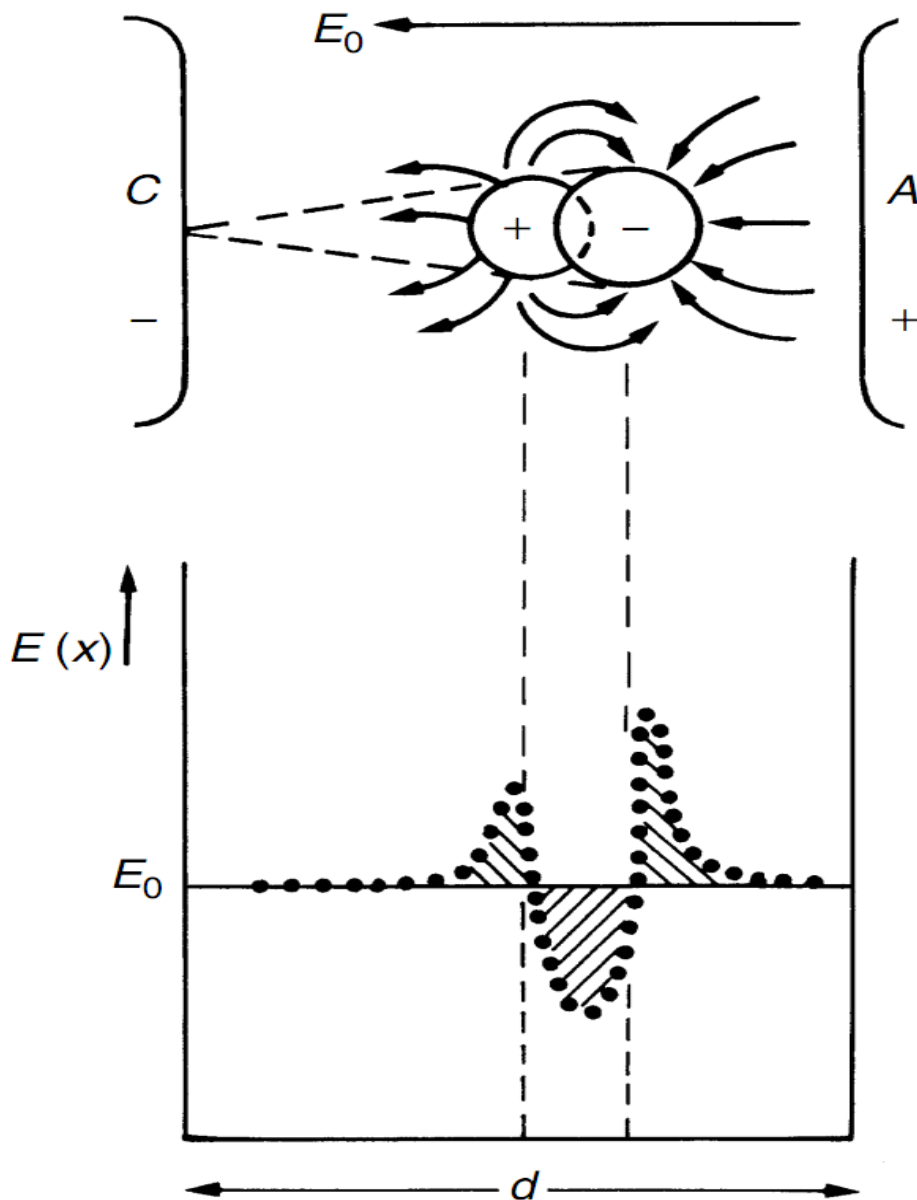


Figure 1.15 Scheme of field distortion in a gap caused by Space charge of an electron avalanche

The field distortion becomes noticeable with a carrier number $n > 10^6$. For instance, in nitrogen with $d = 2 \text{ cm}$, $p = 760 \text{ Torr}$, $\alpha \approx 7$, $E/p \approx 40 \text{ V/Torr} \cdot \text{cm}$, the field distortion is about 1%.

In the Townsend avalanche mechanism the gap current grows as a result of ionization by electron impact in the gas and electron emission at the cathode by positive ion impact. According to this theory, formative time lag of the avalanche should be at best equal to the electron transit time. When

common quantity of electron in avalanche reaches 10^8 ($\alpha d \approx 18 \div 20$), physical mechanism of discharge is critically changed. Self electrical field of avalanche is too large that begins to screen external field. Discharge can't exist so as no possibility to take energy for electrons and continue charge generation process. In this conditions discharge changes the form. Avalanche transforms to another form which is called "**streamer**" or "**kanal**" **mechanism of electrical discharge**. In this mechanism for discharge formation the secondary mechanism results from photoionization of gas molecules and is independent of the electrodes.

In the models developed by German scientists Raether and Meek it has been proposed that when the avalanche in the gap reaches a certain critical size the combined space charge field and externally applied field lead to intense ionization and excitation of the gas particles in front of the avalanche head [9,10]. Instantaneous recombination between positive ions and electrons releases photons which in turn generate secondary electrons by the photoionization process. These electrons under the influence of the electric field in the gap develop into secondary avalanches as shown in Fig. 1.16 and 1.17. Since photons travel with the velocity of light, the process leads to a rapid development of conduction channel across the gap. On the basis of his experimental observations and some simple assumptions Raether developed an empirical expression for the streamer spark criterion of the form:

$$\alpha x_c = 17.7 + \ln x_c + \ln \frac{E_r}{E} \quad (1.75)$$

where E_r is space charge field strength directed radially at the head of avalanche as shown on Fig. 1.17, E is externally applied field strength, x_c is the avalanche length in field direction [11].

The resultant field strength in front of the avalanche is thus $E + E_r$ while in the positive ion region just behind the head the field is reduced to a value $E - E_r$. It is also evident that the space charge increases with the avalanche length $e^{\alpha x}$. The condition for the transition from avalanche to streamer assumes that space charge field E_r approaches the externally applied field.

The minimum breakdown value for a uniform field gap by streamer mechanism is obtained on the assumption that the transition from avalanche to streamer occurs when the avalanche has just crossed the gap d .

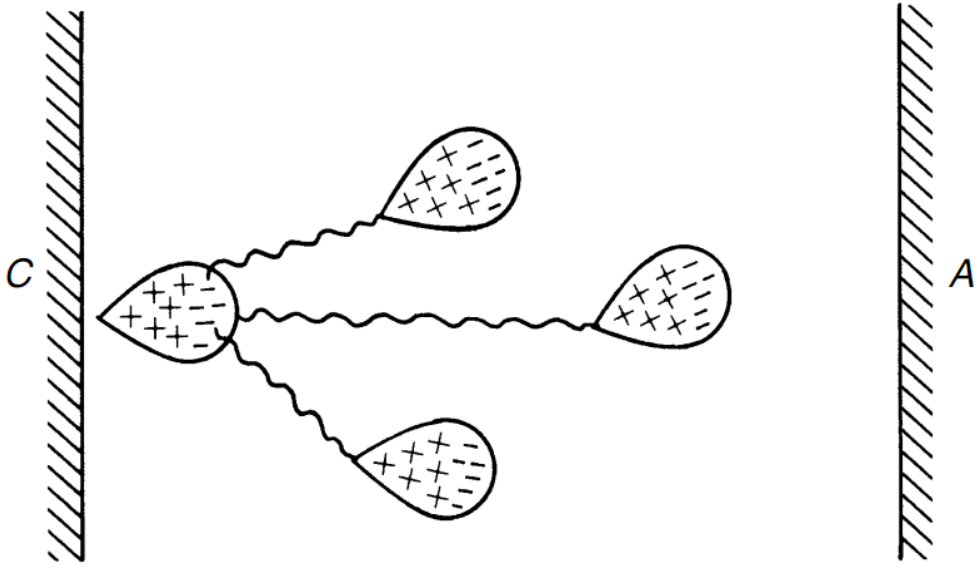


Figure 1.16 Secondary avalanche formation by photoelectrons

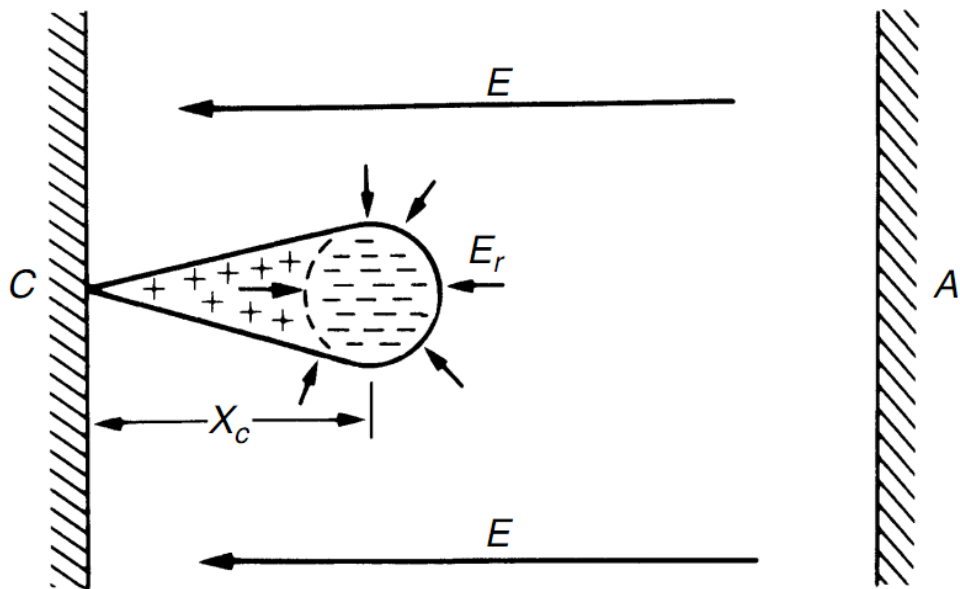


Figure 1.17 Space charge field around avalanche head

Connection between electric field strength and ionization process is given by Meek (German physicist and electric discharge specialist) equation [12-14]:

$$\alpha d + \ln \frac{\alpha}{p} = 14.5 + \ln \frac{E}{p} + \frac{1}{2} \ln \frac{d}{p} \quad (1.76)$$

This equation is solved by trial and error using the experimentally determined relation between α/p and E/p . Values of α/p corresponding to E/p at a given pressure are chosen until the equation is satisfied.

Table 1.10 compares Meek's calculated and the measured values of breakdown voltage V_B for air according to equation (1.76). At *small d*, the calculated values V_B are higher than the measured ones. The reverse is true at large *d*. In general, however, the deviation between theory and experiment should be regarded as not very large, in view of the various simplifying assumptions made by Meek, especially those in order to determine the charge density and the tip radius of the avalanche.

Table 1.10 Comparison of calculated and measured breakdown voltage values (V_B) for air according to Meek's model

<i>Gap length</i> <i>cm</i>	<i>E/p</i> <i>V/cm</i> <i>torr</i>	<i>αd</i>	<i>V_b</i> <i>calculated</i> <i>kV</i>	<i>V_b</i> <i>measured</i> <i>kV</i>
0.1	68.4	15.7	5.19	4.6
0.5	48.1	17.7	18.25	17.1
1.0	42.4	18.6	32.20	31.6
2.5	37	19.7	70.50	73
10	32.8	21.5	249	265
20	31.2	22.4	474	510

Besides avalanche and streamer form of discharge, one more one exists. This is **leader form**. Main conditions of this discharge form existence are non-uniform electric field and long enough gap length. Criteria of streamer-leader transition is high temperature in discharge channel area (3 000 – 5 000 K). This discharge mechanism is discussed more detailed when lightning is described.

So, every kind of electrical discharge can exist in one of three form described above. Discharge channel formation means that gap loses electrical strength totally. This phenomenon has other name – **breakdown** of gaseous gap [3, 14–17].

An analytical expression for breakdown voltage for uniform field gaps as a function of gap length and gas pressure can be derived from the threshold equation (1.74) by expressing the ionization coefficient α/p as a function of field strength and gas pressure. Taking into account parameter E/p , ionization coefficient and our discussion about self-sustain discharge condition, analysis leads to simple and important electrical discharge law in gases: for uniform electric field where $V_B=Ed$, breakdown voltage of a uniform field gap is a unique function of the product of pressure and the electrode separation for a particular gas and electrode material:

$$V_B = F(p \times d) \quad (1.77)$$

Equation (1.77) is known as **Paschen's law**, and was established experimentally *in 1889* by famous German physicist **Friedrich Paschen**. Equation (1.77) does not imply that the discharge voltage increases linearly with the product pd , although it is found in practice to be nearly linear over certain regions. The relation between the sparking voltage and the product pd takes the form shown in Fig. 1.18 (solid curve). The breakdown voltage goes through a minimum value V_{Bmin} at a particular value of the product pd_{min} .

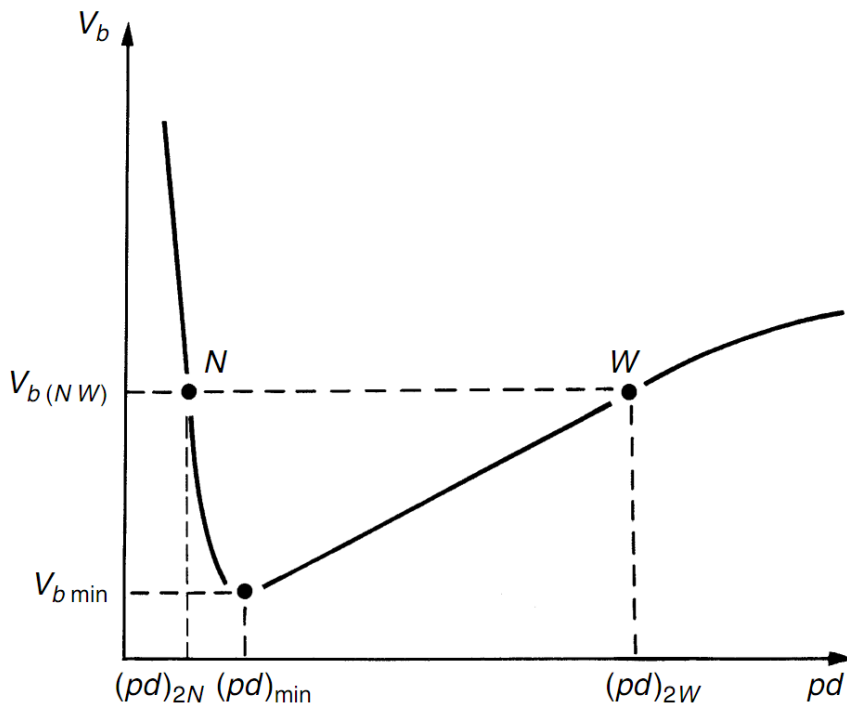


Figure 1.18 Dependence of breakdown voltage as function of pressure \times gap distance (Paschen's law)

In practice, the sparking constants (V_{bmin} and pd_{min}) are measured values, and some of these are shown in Table 1.12. It should be noted, however, that these values are sometimes strongly dependent upon the cathode material and electrode conditions.

Table 1.11 Minimum discharge constants for various gases

<i>Gas</i>	$(pd)_{min}$ <i>torr cm</i>	V_{bmin} <i>volts</i>
Air	0.55	352
Nitrogen	0.65	240
Hydrogen	1.05	230
Oxygen	0.7	450
Sulphur hexafluoride	0.26	507
Carbon dioxide	0.57	420
Neon	4.0	245
Helium	4.0	155

1.4. Discharge in non-uniform electric fields. Main discharge processes.

In uniform fields at the normal atmosphere conditions breakdown voltage is determined by Paschen's law. *Electrical strength of atmosphere air* is constant value in this case and equal approximately 30 kV/cm . In non-uniform fields like such geometrical configurations as point – plate, sharp end – plate, cylindrical surface with sharp edge – plate and others, breakdown voltage is much lower that in uniform field. Below reasons of that are explained.

Figure 1.19 illustrates the case of a strongly divergent field in a positive point – plane gap. For the special case of a coaxial cylindrical geometry in air, an empirical relation based on many measurements of the critical field strength E_c (corona inception) for different diameters of the inner conductor ($2r$) and relative air density δ was developed by Peek of the form:

$$\frac{E_c}{\delta} = 31.53 + \frac{9.63}{\sqrt{\delta r}} \quad (1.78)$$

where E_c is in kV/cm , r in cm .

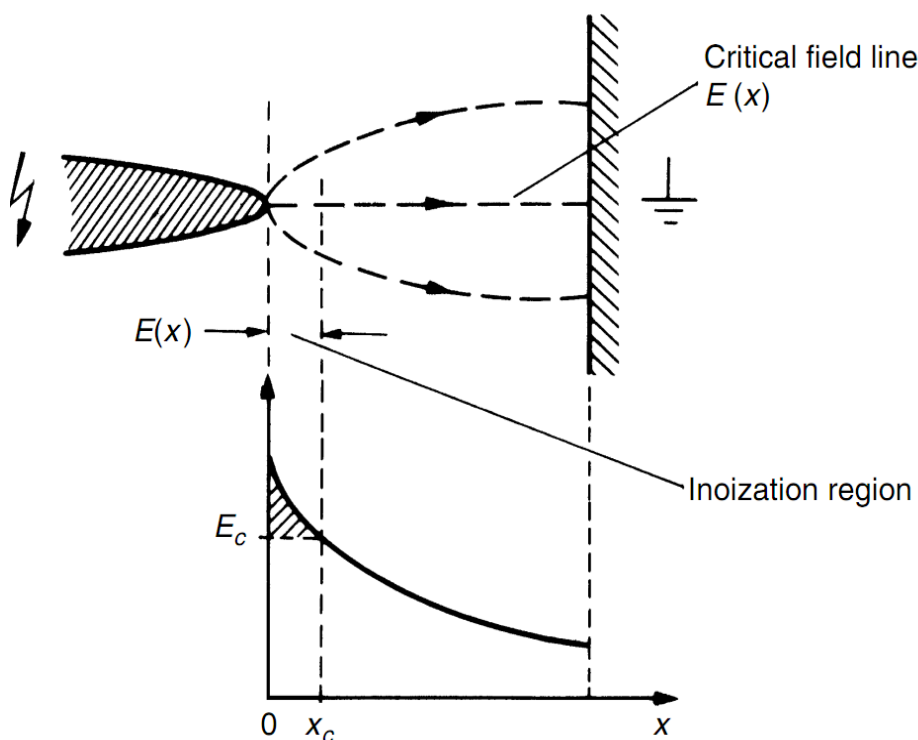


Figure 1.19 Electric field distribution in a non-uniform field gap

In uniform field and quasi-uniform field gaps the onset of measurable ionization usually leads to complete breakdown of the gap. In non-uniform fields various manifestations of luminous and audible discharges are observed long before the complete breakdown occurs. These discharges may be transient or steady state and are known as “*corona*”. An excellent review of the subject may be found in a book by Loeb [18]. The phenomenon is of particular importance in high voltage engineering where non-uniform fields are unavoidable. It is responsible for considerable power losses from high voltage transmission lines and often leads to deterioration of insulation by the combined action of the discharge ions bombarding the surface and the action of chemical compounds that are formed by the discharge. It may give rise to interference in communication systems. On the other hand, it has various industrial applications such as high-speed printing devices, electrostatic precipitators, paint sprayers, Geiger counters, etc.

The voltage gradient at the surface of the conductor in air required to produce a visual a.c. corona in air is given approximately by the Peek’s expression (1.78). There is a distinct difference in the visual appearance of a corona at wires under different polarity of the applied voltage. Under positive voltage, a corona appears in the form of a uniform bluish-white sheath

over the entire surface of the wire. On negative wires the corona appears as reddish glowing spots distributed along the wire. The number of spots increases with the current. Stroboscopic studies show that with alternating voltages a corona has about the same appearance as with direct voltages. Because of the distinctly different properties of coronas under the different voltage polarities it is convenient to discuss separately positive and negative coronas.

In this paragraph brief review of the main features of corona discharges and their effect on breakdown characteristics will be included.

The most convenient electrode configurations for the study of the physical mechanism of coronas are hemi-spherically capped rod-plane or point-plane gaps. In the former arrangement, by varying the radius of the electrode tip, different degrees of field non-uniformity can be readily achieved. The point – plane arrangement is particularly suitable for obtaining a high localized stress and for localization of dense space charge.

In discussing the corona characteristics and their relation to the breakdown characteristics it is convenient to distinguish between the phenomena that occur under pulsed voltage of short duration (impulse corona), where no space charge is permitted to drift and accumulate, and under long lasting (d.c.) voltages (static field corona).

Under impulse voltages at a level just above ionization threshold, because of the transient development of ionization, the growth of discharge is difficult to monitor precisely. However, with the use of “Lichtenberg figures” techniques, and more recently with high-speed photographic techniques, it has been possible to achieve some understanding of the various discharge stages preceding breakdown under impulse voltages.

The observations have shown that when a positive voltage pulse is applied to a point electrode, the first detectable ionization is of a filamentary branch nature, as shown diagrammatically in Fig. 1.20. This discharge is called a streamer and is analogous to the case of uniform field gaps at higher pd values. As the impulse voltage level is increased, the streamers grow both in length and their number of branches as indicated in Figs 1.20 (b) and (c). One of the interesting characteristics is their large number of branches which never cross each other. The velocity of the streamers decreases rapidly as they penetrate the low field region. Figure 1.21 shows velocities of impulse streamers recorded in air in a 2.5-cm gap under two different values of voltage. The actual mechanism of the transition from streamer to final breakdown is complex, and several models have been developed to explain this transition, but because of space limitation the reasons will not be discussed here.

When the voltage is applied for an infinitely long time (e.g. under

d.c. or 60 Hz) the ionization products will have sufficient time to wander

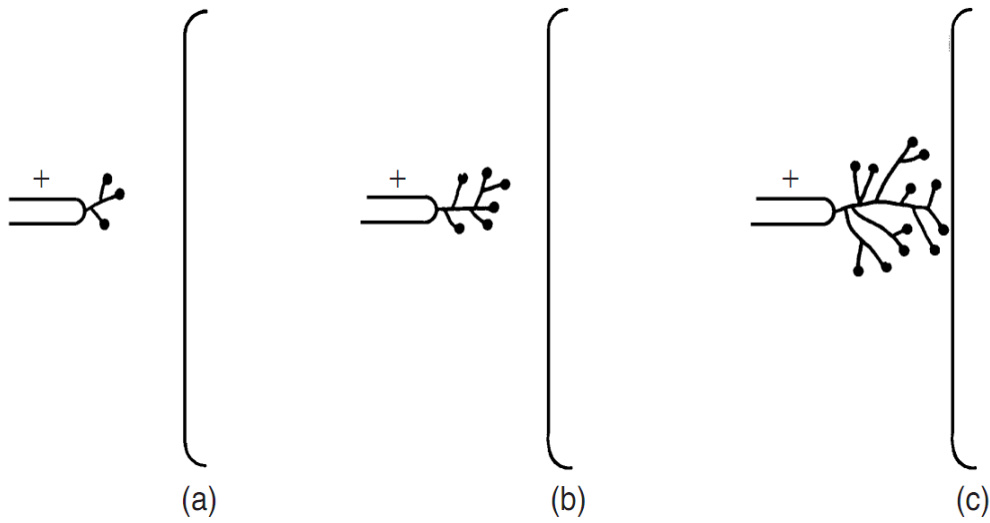


Figure 1.20 Scheme of the formation of streamers in rod-plane gap

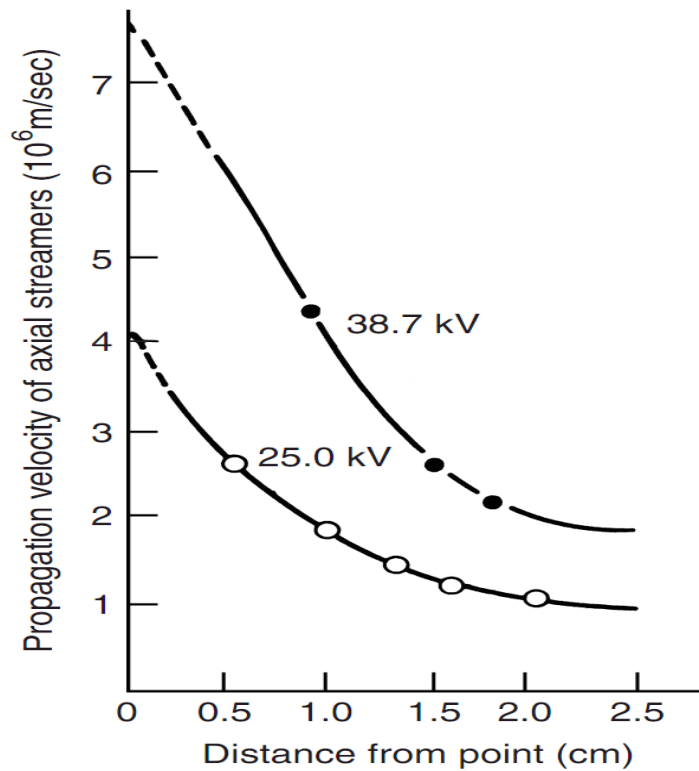


Figure 1.21 Streamer velocity in a gap of 2.5 cm under two different voltages in air

in the gap and accumulate in space, causing a distortion in the origi-

nal field. To study this phenomenon, let us choose the rod–plane gap with the rod tip of radius of 1 cm as shown in Fig. 1.22 and study the various discharge modes together with the breakdown characteristics for this arrangement in atmospheric air. Then if the gap length is small (less than about 2 cm) and the voltage is gradually raised no appreciable ionization is detected up to breakdown. As the gap is increased, the field distribution becomes more inhomogeneous, and on increasing the voltage at first a transient slightly branched filamentary discharge appears. These discharges have been shown to be identical with those observed under impulse voltages and are also called streamers. Under steady state the streamer develops with varying frequencies, giving rise to currents that are proportional to their physical length. These streamers are sometimes called onset streamers or burst pulses.

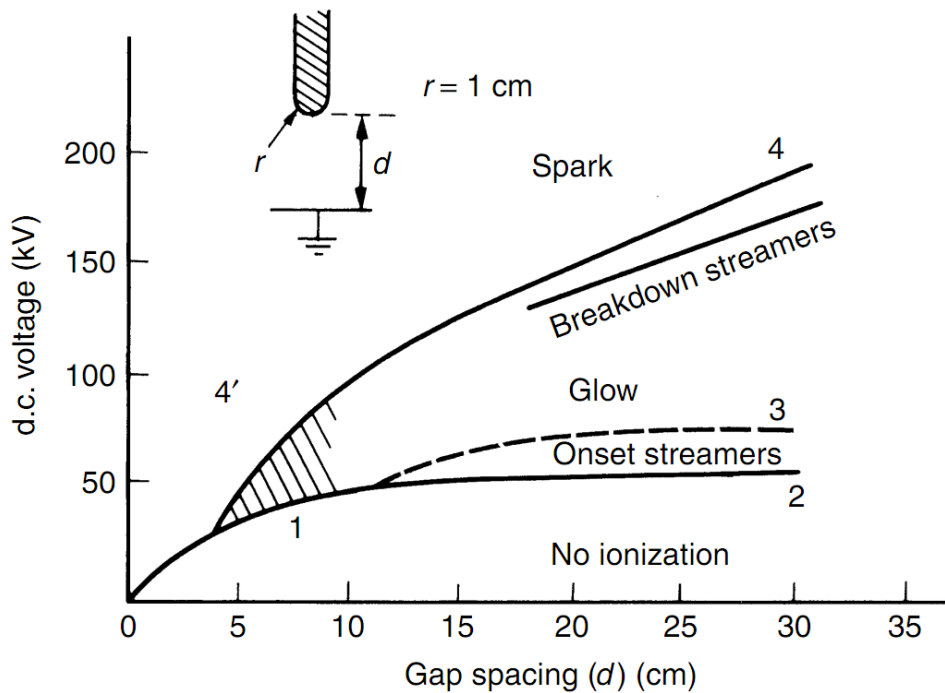


Figure 1.22 Threshold curves for various mode of anode corona

The onsets of the various discharge modes observed, as the gap length is increased, are illustrated schematically in Fig. 1.22 together with the corresponding discharge characteristics. At the smaller spacing when the voltage is still reasonably uniform the streamer is capable of penetrating the weaker field, reaching the cathode and initiating breakdown in the same manner as in uniform field gaps. This condition is shown by curve 1 of Fig. 1.22 with the larger spacing above 10 cm, streamers appear that do not cross the gap (shown by curve 2). Curve 3 represents transition from

streamers to steady glow corona without sparking. At the larger spacing there is a considerable spread in the voltage at which breakdown streamers develop preceding the complete breakdown of the gap. The dashed area represents the region of uncertain transitions; portion 1 indicates the onset of streamers followed immediately by transition to spark. If, however, the gap is increased to a point where glow is established and then reduced keeping the voltage constant, the glow discharge will have stabilized the gap against breakdown at a voltage that otherwise would have broken down. If the voltage is then raised, a spark is induced by glow corona (curve 4), but if it is lowered, a streamer breakdown is induced. By decreasing the gap further to lower values and increasing the voltage at the various points the glow–corona sparking voltage characteristic can be projected backwards as shown by curve 4. Thus if a steady corona glow is established, the sparking voltage is raised and the lower breakdown by streamer is suppressed. Figure 1.23 illustrates the onset voltage of different negative coronas plotted as a function of electrode separation for a typical example of a cathode of 0.75 mm radius. The lowest curve gives the onset voltage for pulses not greatly affected by the gap length. Raising the voltage does not change the mode of the pulses over a wide voltage range. Eventually at a much higher voltage a steady glow discharge is observed, but the transition from pulses to glow discharge is not sharply defined and is therefore shown as a broad transition region in Fig. 1.23. On increasing the voltage further, the glow discharge persists until breakdown occurs. It should be noted that breakdown under negative polarity occurs at considerably higher voltage than under positive voltage, except at low pressures; therefore, under alternating power frequency voltage the breakdown of non-uniform field gap invariably takes place during the positive half-cycle of the voltage wave. It was shown in Fig. 1.22 that in non-uniform field gaps in air the appearance of the first streamer may lead to breakdown or it may lead to the establishment of a steady state corona discharge which stabilizes the gap against breakdown. Accordingly we may have a corona stabilized or direct breakdown. Whether direct or corona stabilized breakdown occurs depends on factors such as the degree of field non-uniformity, gas pressure, voltage polarity and the nature of the gas. For example, in air the corona stabilized breakdown will extend to higher pressures than in SF_6 due to the relatively immobile SF_6^- ions (Figs 1.25 and 1.26). Figure 1.25 compares the positive and negative point–plane gap breakdown characteristics measured in air as a function of gas pressure. At very small spacing the breakdown characteristics for the two polarities nearly coincide and no corona stabilized region is observed.

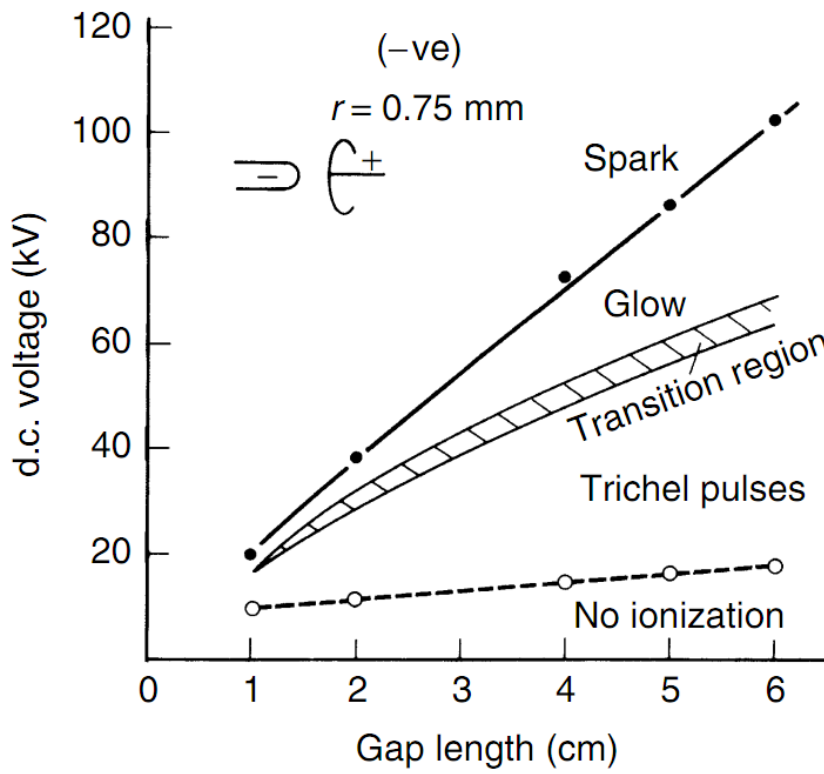


Figure 1.23 Negative rod-plane breakdown and corona characteristics in atmospheric air

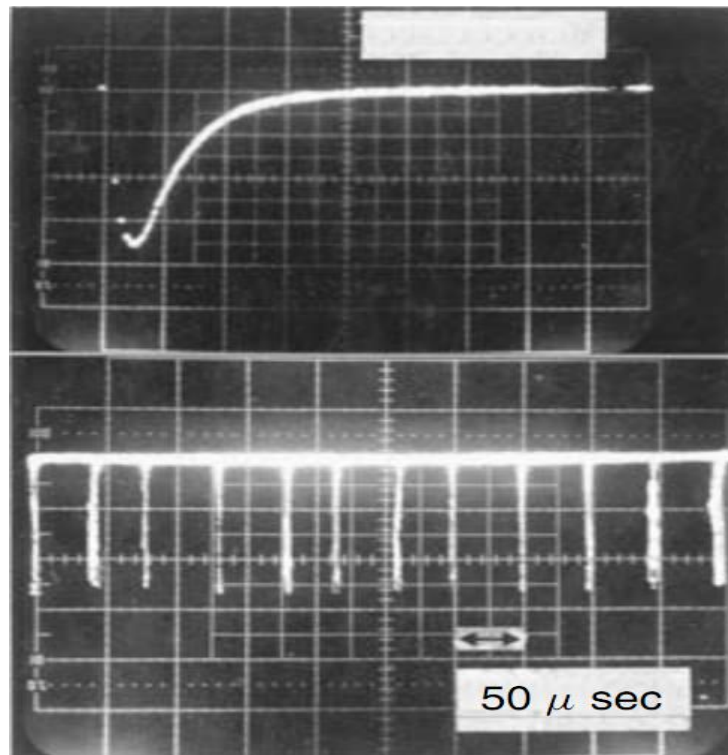


Figure 1.24 Pulse pattern of corona for the situation shown on Fig. 1.23

As the spacing is increased, the positive characteristics display the distinct high corona breakdown up to a pressure of approximately 7 bar, followed by a sudden drop in breakdown strengths. Under the negative polarity the corona stabilized region extends to much higher pressures.

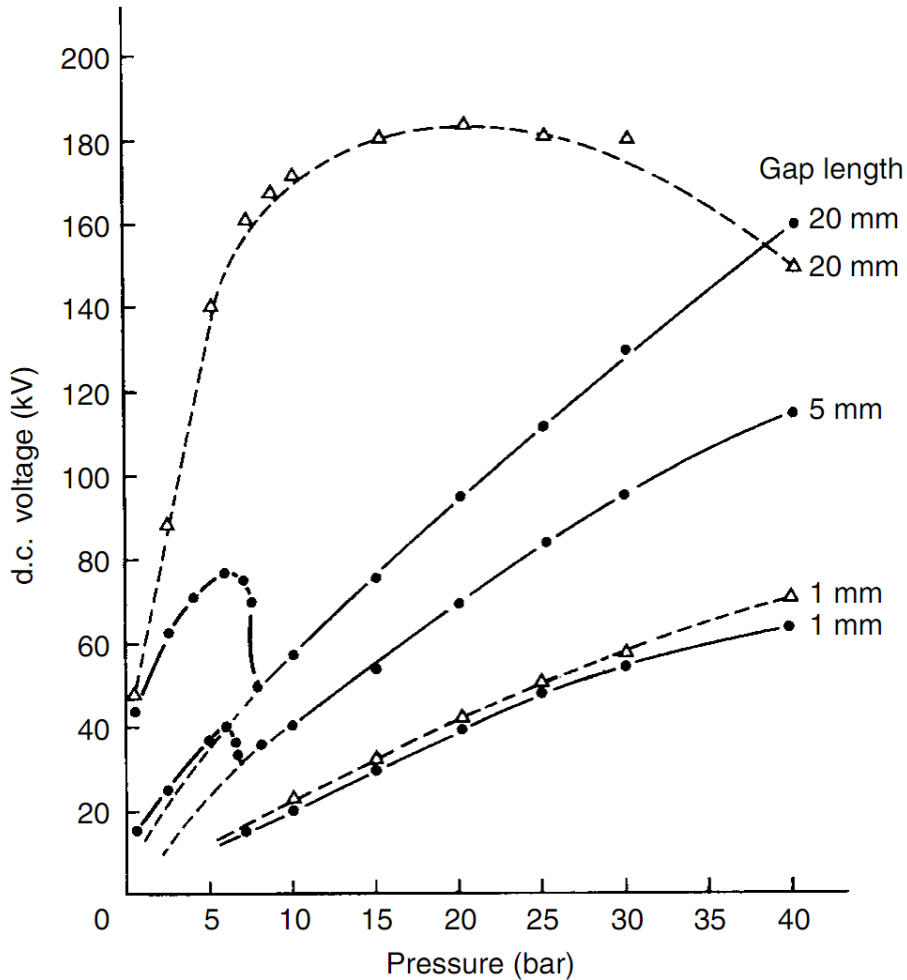


Figure 1.25 Corona inception and breakdown in point–plane gap in air:
 — positive point, --- negative point

A practical non–uniform field geometry that is frequently used in the construction of high voltage apparatus is the coaxial cylindrical arrangement. By properly choosing the radial dimensions for the cylinders it is possible to optimize such a system for the maximum corona–free breakdown. That’s why it is necessary to take into account both as a corona condition ignition and polarity if d.c. voltage is applied.

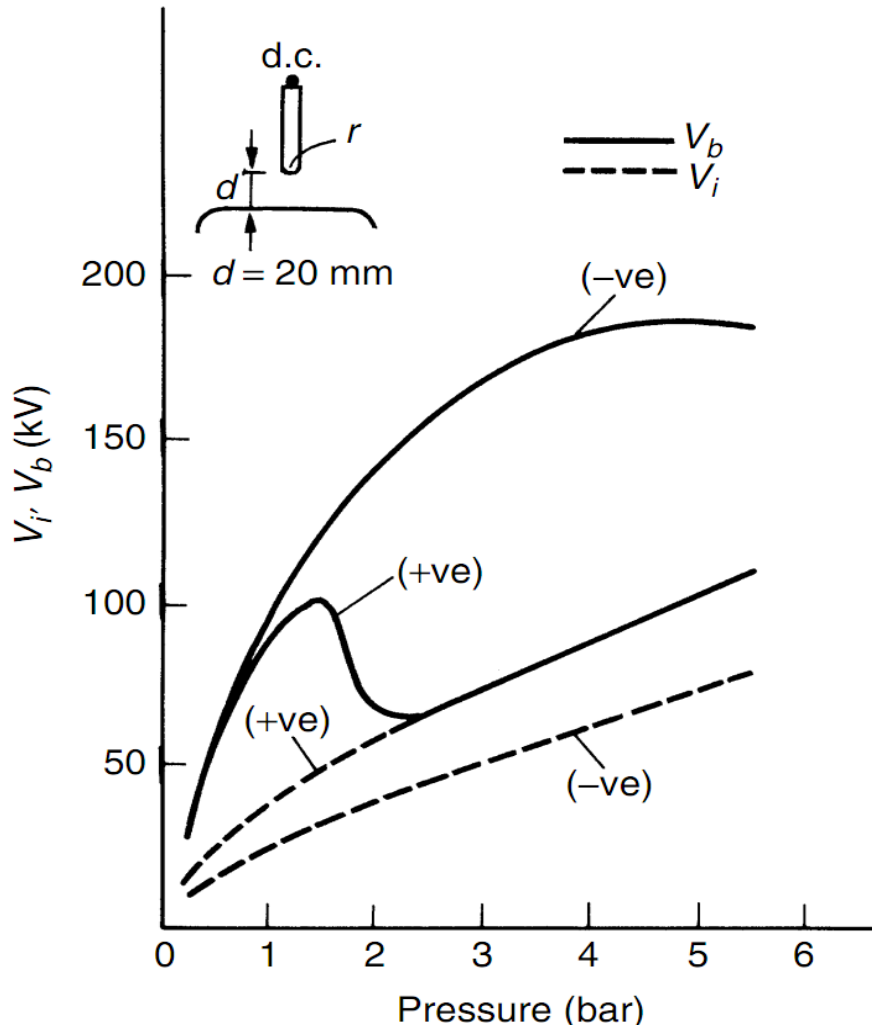


Figure 1.26 Corona inception and breakdown in rod-plane gap in SF₆

If we consider the case of a positive point-plane gap shown in Fig. 1.27(a) then an ionization by electron collision takes place in the high field region close to the point. Electrons because of their higher mobility will be readily drawn into the anode, leaving the positive space charge behind. The space charge will cause a reduction in the field strength close to the anode and at the same time will increase the field further away from it. The field distortion caused by the positive space charge is illustrated in Fig. 1.27(b). The dotted curve represents the original undistorted field distribution across the gap while the solid curve shows the distorted field. The high field region is in time moving further into the gap extending the region for ionization. The field strength at the tip of the space charge may be high enough for the initiation of a cathode directed streamer which subsequently may lead to complete breakdown. With the negative point (Fig. 1.27) the electrons are repelled into the low field region

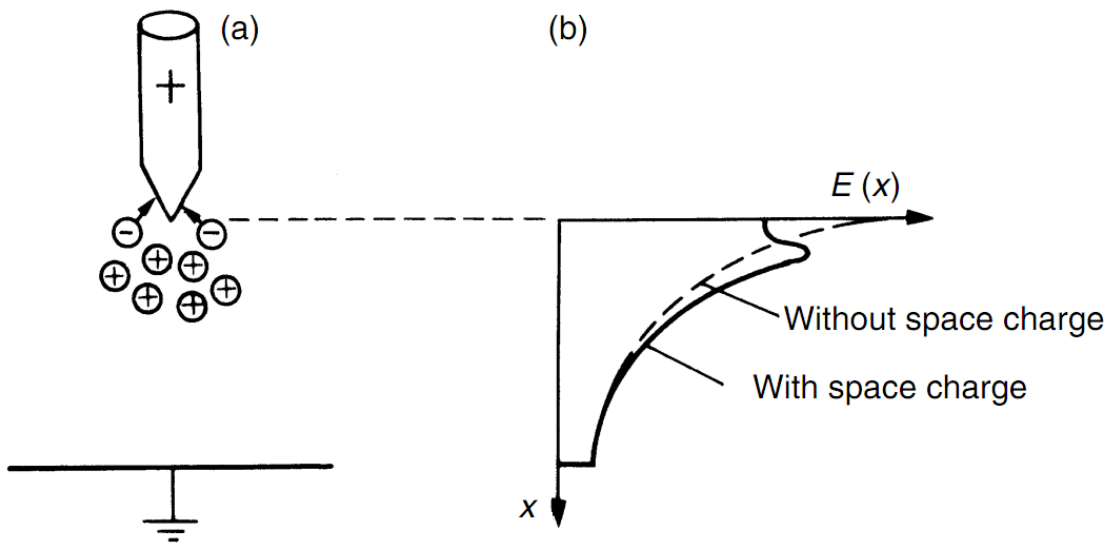


Figure 1.27 (a) Space charge build-up in positive point-plane gap,
 (b) field distortion by space charge

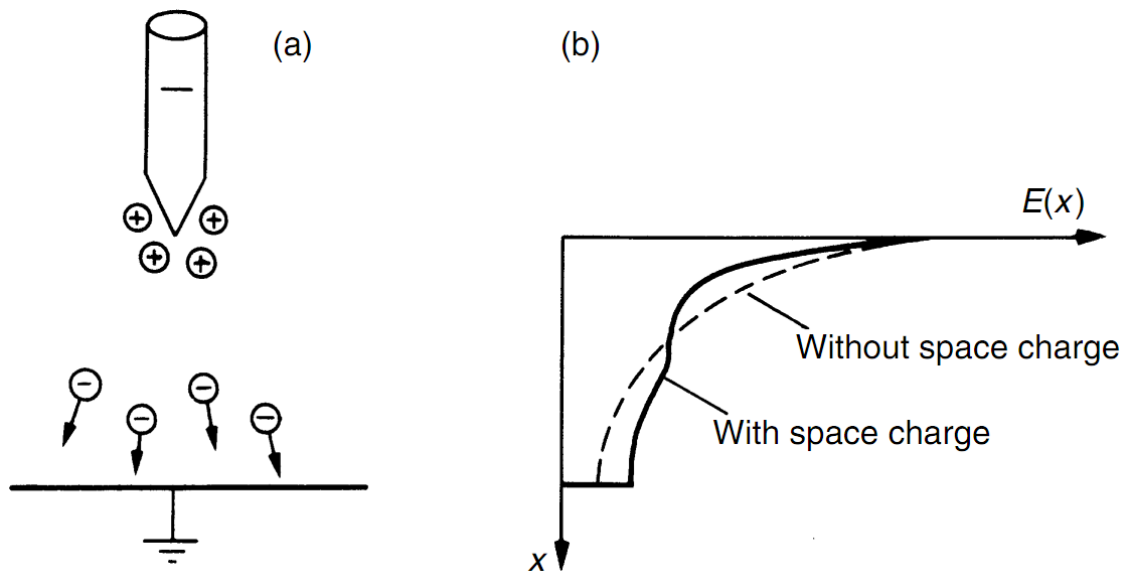


Figure 1.28 (a) Space charge build-up in negative point-plane gap,
 (b) field distortion by space charge

and in the case of attaching gases become attached to the gas molecules and tend to hold back the positive space charge which remains in the space between the negative charge and the point. In the vicinity of the point the

field is grossly enhanced, but the ionization region is drastically reduced.

For the initiation of breakdown an electron must be available to start the avalanche. With slowly rising voltages (d.c. and a.c.) there are usually sufficient initiatory electrons created by cosmic rays and naturally occurring radioactive sources. Under surge voltages and pulses of short duration, however, the gap may not break down as the peak voltage reaches the lowest breakdown value V_S unless the presence of initiatory electrons is ensured by using artificial irradiation. V_S is a voltage which leads to breakdown of the gap after a long time of application. With weak irradiation the peak value may have to be greatly increased so that the voltage remains above the d.c. value V_S for long intervals of time. Figure 1.29 illustrates the breakdown on a step-function voltage pulse; V_p represents the peak value of a step voltage applied at time $t=0$ to a gap that breaks down under V_S after a long time.

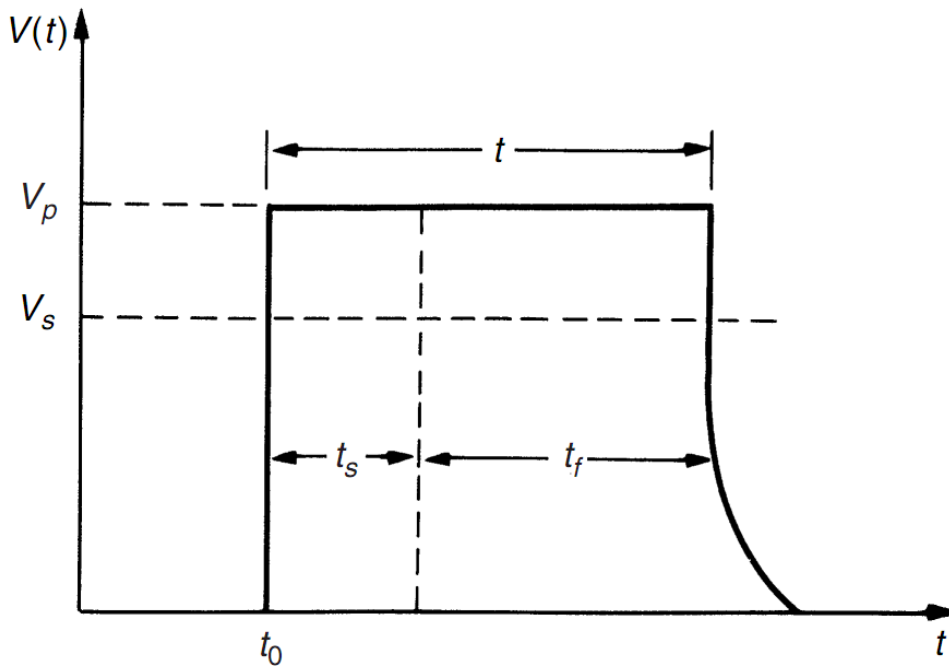


Figure 1.29 Time lag component under a step voltage

The time which elapses between the application of voltage to a gap sufficient to cause breakdown and the breakdown is called the *time lag* (t). It consists of two components: one is the time which elapses during the voltage application until a primary electron appears to initiate the discharge and is known as the statistical time lag t_s ; and the other is the time required for the breakdown to develop once initiated and is known as the formative time lag t_f . The statistical time lag depends upon the amount of preioniza-

tion in the gap. This in turn depends upon the size of the gap and the radiation producing the primary electrons. The appearance of such electrons is usually statistically distributed. The formative time lag t_f depends essentially upon the mechanism of spark growth in question. In cases when the secondary electrons arise entirely from electron emission at the cathode by positive ions, the transit time from anode to cathode will be the dominant factor determining the formative time. The formative time lag increases with the gap length and the field non-uniformity, but it decreases with the applied over-voltage.

When an impulse voltage of sufficiently high value is applied to a gap, breakdown will result on each voltage application. The time required for the spark development (time lag) will depend upon the rate of rise of voltage and the field geometry. Therefore, for each gap geometry it is possible to construct a volt-time characteristic by applying a number of impulses of increasing amplitude and noting oscillographically the time lag. In uniform and quasi-uniform field gaps the characteristic is usually sharply defined and it rises steeply with increasing the rate of rise of the applied voltage. In non-uniform field gaps, however, due to larger scatter in the results, the data fall into a dispersion band as shown in Fig. 1.30.

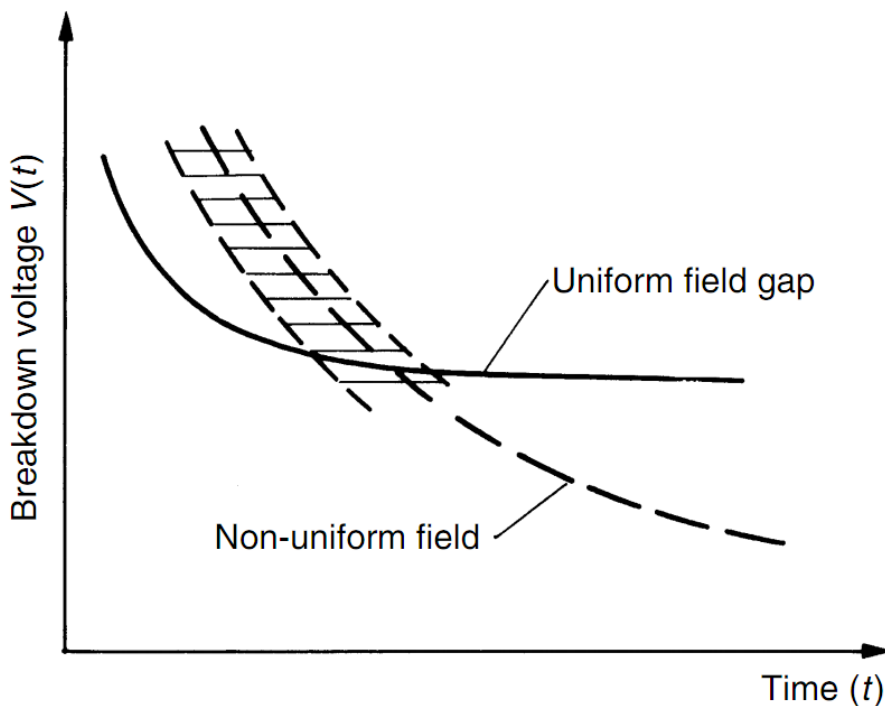


Figure 1.30 Schematic diagram of volt-time characteristics for uniform and non-uniform field gaps

The time to breakdown is less sensitive to the rate of voltage rise.

Hence, quasi-uniform field gaps (sphere – sphere) have often been used as protective devices against over-voltages in electric power systems. The volt–time characteristic is an important practical property of any insulating device or structure. It provides the basis for establishing the impulse strength of the insulation as well as for the design of the protection level against over-voltages.

So, all electrophysical processes begin with applying of electrical field, which should be intensive enough. In uniform electric fields breakdown voltage is determined by Paschen's law and depends on kind of gas, gas pressure and gap length. In non-uniform fields all electrophysical processes begin at the active electrode area. Active electrode has small radius of curve and rod or sharp form. Corona discharge is first step at the non-uniform fields. Depending on polarity in anode–cathode gap in case of d.c. regime, breakdown voltages can be quite different. If applied voltage is increased, corona passes to spark discharge. In case when external field is growth more, spark transforms to arc discharge. Arc discharge is high current (1 – 100 kA), low voltage (1 – 10 eV). Arcs have unique physical mechanism of existence which is based on cathode spots and explosive emission. These two factors provide unlimited emissive ability. Detailed consideration of arcs is given in [19–23]. If dielectric surface is placed in anode–cathode gap, streamer and next spark is formed in the surface. Breakdown voltages are lower in this case, especially if surface contains dirtiness and moisture. This fact is very important at the design and engineering of high voltage equipment. Practical application of flashover influence on insulation work is discussed in Chapter 4, 4.1 and [3, 22, 23]. This is important moment and non-uniformity degree of electric field have to be taken into account on the every step of design or engineering of electric energy system.

World of electrical discharges is very big and interesting. We have considered main discharge processes only. Flashover, glow in vacuum, atmosphere air and vacuum arcs and their practical application in electrical power engineering and industry are beyond of the textbook. These subjects are experimentally studied in laboratory workshops and of special master's course program.

Knowledge of laws of discharge processes are very important for every qualified specialist in electrical and power engineering.

REFERENCES

1. B. Loeb. The Kinetic Theory of Gases. Wiley, New York, 1963, Chapter 2.
2. W. Zaengl, E.Kuffel. High voltage engineering. Fundamentals. – Ox-

ford: Pergamon Press, 1984. – 488 p.

3. W. Zaengl, E. Kuffel, J. Kuffel. High voltage engineering. Fundamentals. – Butterworth – Heinemann, 2000. – 539 p.

4. E.W. McDaniel. Collision Phenomena in Ionised Gases. Wiley, New York, 1964. – 220 p.

5. R. Geballe and M.A. Harrison. *Phys. Rev.* 85 (1952), p. 372.

6. J.S. Townsend. Electricity in Gases. Oxford Press, 1914.

7. Raether. Electron Avalanches and Breakdown in Gases. Butterworths, London, 1964.

8. H. Raether. *Z. Phys.* 112 (1939), p. 464.

9. H. Raether. *Z. Phys.* 117 (1941), pp. 375, 524.

10. L.B. Loeb. Basic Processes of Gaseous Electronics. University of California Press, 1955.

11. L.B. Loeb. Formation of negative ions. Encyclopedia of Physics, Vol. 16, p. 445. Springer, Berlin, 1966.

12. J.M. Meek and J.D. Craggs. Electrical Breakdown of Gases. Clarendon Press, Oxford, 1953.

13. J.M. Meek. *Phys. Rev.* 57 (1940), p. 722.

14. L.B. Loeb and J.M. Meek. The Mechanism of Electric Spark. Stanford University Press, 1940.

15. W.S. Zaengl and N.U. Nyffenegger. Proc. 3rd Int. Conf. on Gas Discharges, 1974, p. 303.

16. W.S. Zaengl. Proc. 10th Symposium on Electrical Insulating Materials, Tokyo, 1977, p. 13.

17. W.S. Zaengl. Electronegative Gases, Present State of Knowledge and Application, Future Prospects. Nordic Symposium on Electric Insulation, June 13–15, 1988, Trondheim, pp. 11–139.

18. L.B. Loeb. Electrical Coronas. University of California Press, 1965. – 324 p.

19. G.A. Mesyats., D.I. Proskurovskiy. Pulsed electrical discharge in vacuum. – Berlin, Springer Verlag, 1989. – 293 p.

20. G.A. Mesyats. Explosive electron emission. – URO–Press, 1998.

21. G.A. Mesyats. Cathode phenomena in a vacuum discharge: the breakdown, the spark and the arc. – M.: Nauka, 2000. – 400 p.

22. Proceedings of XIV International Symposium on Discharges and Electrical Insulation in Vacuum. – Braunschweig, Germany, August, 30 – September, 3, 2010, V.1.

23. Proceedings of XV International Symposium on Discharges and Electrical Insulation in Vacuum. – Tomsk, Russia, September, 2 – 7, 2012, V.1.

CHAPTER 2. ELECTROPHYSICAL PROCESSES IN CONDENSED DIELECTRIC MATERIALS

Condensed dielectric materials are very widespread insulation in modern electrical engineering technology. They are divided on solid and liquid dielectric materials.

2.1 Electrophysical processes in solid dielectrics

Solid insulation forms an integral part of high voltage structures. The solid materials provide the mechanical support for conducting parts and at the same time insulate the conductors from one another. Frequently practical insulation structures consist of combinations of solids with liquid and/or gaseous media. Therefore, the knowledge of failure mechanisms of solid dielectrics under electric stress is of great importance.

In gases the transport of electricity is limited to positive and negative charge carriers, and the destruction of insulating properties involves a rapid growth of current through the formation of electron avalanches. The mechanism of electrical failure in gases is now understood reasonably clearly. This is not the case for solid insulation. Although numerous investigators have studied the breakdown of solids for nearly a century now, and a number of detailed theories have been put forward which aimed to explain quantitatively the breakdown processes in solids, the state of knowledge in this area is still very crude and inconclusive.

Electrical conduction studies in solids are obscured by the fact that the transport phenomena besides electronic and ionic carriers include also currents due to the slower polarization processes such as slow moving dipoles (orientation polarization) and interfacial polarization.

As the stress in solids is increased and approaches the breakdown stress, the current is found to increase exponentially, but does not vary so markedly with time for steady voltage. This increased current at high stresses is generally believed to result from the injection of carriers from an electrode or from electron multiplication in the bulk of the material or both. In addition, if impurities or structural defects are present they may cause local allowed energy levels (traps) in the forbidden band, and electrons may pass through the insulator by jumping from one trap to another (hopping effect).

From the electrodes the electrons are believed to be ejected by either the "Schottky's emission effect" or the "field emission effect" (tunnelling) discussed already in Chapter 1. Once injected into the material the electron multiplication is thought to be analogous to that in a gas discharge. Under

certain strictly controlled experimental conditions the breakdown of solids may therefore be accomplished by a process similar to gas breakdown. Under normal industrial conditions, however, the same solid materials are found to exhibit a wide range of dielectric strength, depending upon the conditions of the environment and the method of testing. The measured breakdown voltage is influenced by a large number of external factors such as temperature, humidity, duration of test, whether a.c., d.c., or impulse voltage is applied, pressure applied to the electrodes, discharges in the ambient medium, discharges in cavities and many other factors. The fundamental mechanisms of breakdown in solids are understood much less clearly than those in gases; nevertheless, several distinct mechanisms have been identified and treated theoretically. In this section the presently accepted breakdown mechanisms will be discussed briefly in a qualitative manner. Broadly speaking the mechanism of failure and the breakdown strength (BD strength) changes with the time of voltage application and for discussion purposes it is convenient to divide the time scale of voltage application into regions in which different mechanisms operate, as shown in Fig 2.1.

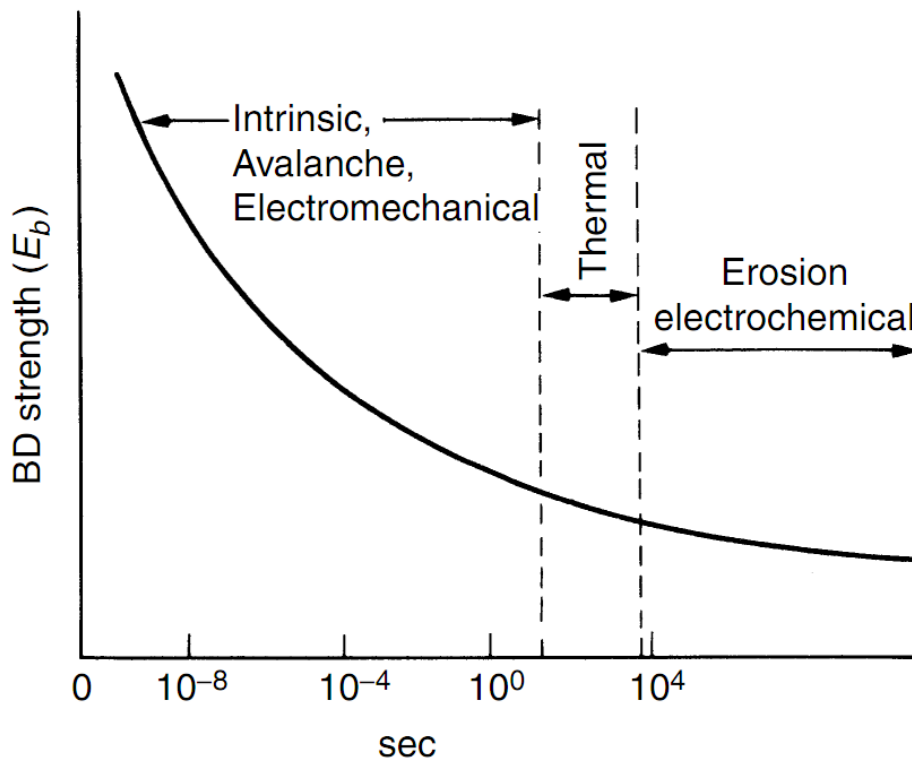


Figure 2.1 Mechanisms of failure and variation of breakdown strength in solids

2.1.1 Intrinsic breakdown

If the material under test is pure and homogeneous, the temperature and environmental conditions are carefully controlled, and the sample is so stressed that there are no external discharges. With undervoltages applied for a short time the electric strength increases up to an upper limit which is called the intrinsic electric strength. The intrinsic strength is a property of the material and temperature only. The intrinsic breakdown is accomplished in times of the order of 10^{-8} sec and has therefore been postulated to be electronic in nature. The stresses required for an intrinsic breakdown are well in excess of 10^6 V/cm. The intrinsic strength is generally assumed to be reached when electrons in the insulator gain sufficient energy from the applied field to cross the forbidden energy gap from the valence to the conduction band. The criterion condition is formulated by solving an equation for the energy balance between the gain of energy by conduction electrons from the applied field and its loss to the lattice. Several models have been proposed in an attempt to predict the critical value of the field which causes intrinsic breakdown, but no completely satisfactory solution has yet been obtained. The models used by various workers differ from each other in the proposed mechanisms of energy transfer from conduction electrons to the lattice, and also by the assumptions made concerning the distribution of conduction electrons. In pure homogeneous dielectric materials the conduction and the valence bands are separated by a large energy gap, and at room temperature the electrons cannot acquire sufficient thermal energy to make transitions from valence to conduction band. The conductivity in perfect dielectrics should therefore be zero. In practice, however, all crystals contain some imperfections in their structures due to missing atoms, and more frequently due to the presence of foreign atoms (impurities). The impurity atoms may act as traps for free electrons in energy levels that lie just below the conduction band, as illustrated schematically in Fig. 2.2.

At low temperatures the trap levels will be mostly filled with electrons caught there as the crystal was cooled down during its manufacture. At room temperature some of the trapped electrons will be excited thermally into the conduction band, because of the small energy gap between the trapping levels and the conduction level. An amorphous crystal will therefore have some free conduction electrons. When a field is applied to a crystal the conduction electrons gain energy from it, and due to collisions between them the energy is shared by all electrons. For a stable condition this energy must be somehow dissipated.

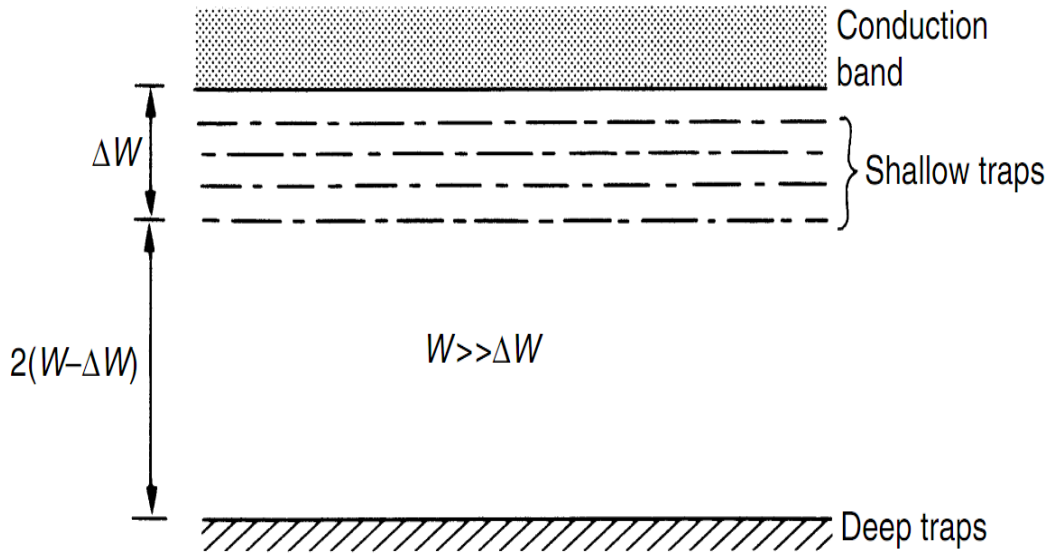


Figure 2.2 Energy level diagram for an amorphous dielectric

If there are relatively few electrons such as in pure crystals, most of the energy will be transferred to the lattice by electron – lattice interaction. In steady state conditions the electron temperature (T_e) will be nearly equal to the lattice temperature (T).

In amorphous dielectrics the electron interactions predominate, the field raises the energy of the electrons more rapidly than they can transfer it to the lattice, and the electron temperature T_e will exceed the lattice temperature T . The effect of the increased electron temperature will be a rise in the number of trapped electrons reaching the conduction band. This increases the material’s conduction and as the electron temperature continues to increase a complete breakdown is eventually reached known as “high– temperature breakdown”.

To date there has been no direct experimental proof to show whether an observed breakdown is intrinsic or not, except for plastic materials such as polyethylene and so conceptually it remains an ideal mechanism identified as the highest value obtainable after all secondary effects have been eliminated.

2.1.2 Streamer breakdown

Under certain controlled conditions in strictly uniform fields with the electrodes embedded in the specimen, breakdown may be accomplished after the passage of a single avalanche. An electron entering the conduction band of the dielectric at the cathode will drift towards the anode under the influ-

ence of the field gaining energy between collisions and losing it on collisions. On occasions the free path may be long enough for the energy gain to exceed the lattice ionization energy and an additional electron is produced on collision. The process is repeated and may lead to the formation of an electron avalanche similar to gases. The concept is similar to the streamer theory developed by Raether, and Meek and Loeb for gases discussed in Chapter 1, 1.3.

2.1.3 Electromechanical breakdown

Substances which can deform appreciably without fracture may collapse when the electrostatic compression forces on the test specimen exceed its mechanical compressive strength. The compression forces arise from the electrostatic attraction between surface charges which appear when the voltage is applied. The pressure exerted when the field reaches about 10^6 V/cm may be several kN/m^2 . If d_0 is the initial thickness of a specimen of material of *Young's modulus* Y , which decreases to a thickness of d (m) under an applied voltage V , then the electrically developed compressive stress is in equilibrium with the mechanical compressive strength if:

$$V^2 = d^2 \frac{2Y}{\epsilon_0 \epsilon_r} \ln \left(\frac{d_0}{d} \right) \quad (2.1)$$

where ϵ_0 and ϵ_r are the permittivity of free space and the relative permittivity of the dielectric.

2.1.4 Edge breakdown

In practical insulation systems, the solid material is stressed in conjunction with one or more other materials. If one of the materials is, for example, a gas or a liquid, then the measured breakdown voltage will be influenced more by the weak medium than by the solid.

A cross-section of a simplified example is shown in Fig. 2.3 which represents testing of a dielectric slab between sphere-plane electrodes. Ignoring the field distribution, i.e. assuming a homogeneous field, if we consider an elementary cylindrical volume of end area dA spanning the electrodes at distance x . For the case shown in Fig. 2.3, the stress in the gaseous part increases further as x is decreased, and reaches very high values as d_1 becomes very small (point B). Consequently the ambient breaks down at a relatively low applied voltage. The charge at the tip of the discharge will further disturb the applied local field and transform the arrangement

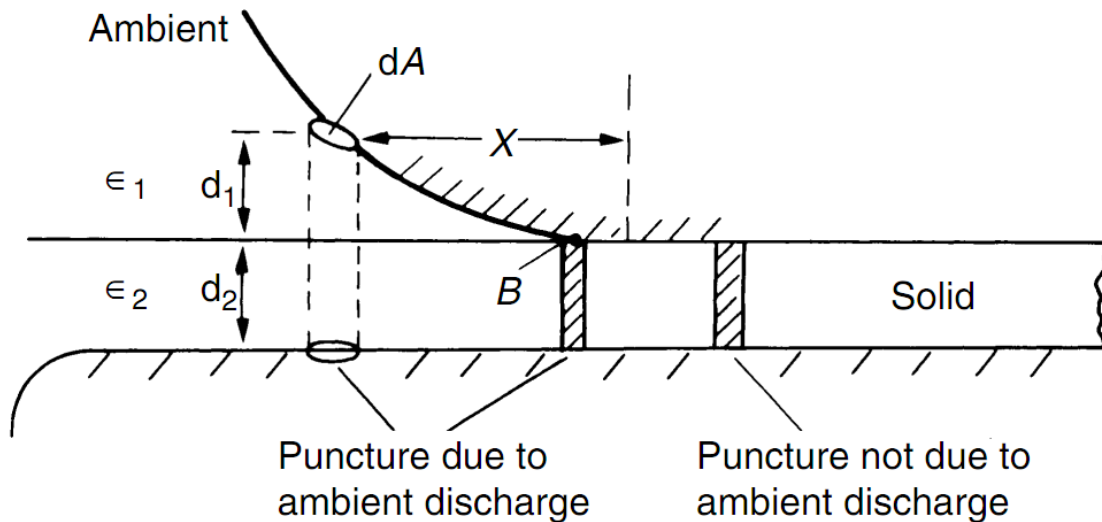


Figure 2.3 Breakdown of solid specimen due to discharge edge effect

to a highly non – uniform system. The charge concentration at the tip of a discharge channel has been estimated to be sufficient to give a local field of the order of 10 MV/cm , which is higher than the intrinsic breakdown field. A local breakdown at the tips of the discharge is likely, therefore, and complete breakdown is the result of many such breakdown channels formed in the solid and extending step by step through the whole thickness.

The breakdown event in solids in general is not accomplished through the formation of a single discharge channel, but assumes a **tree – like structure**. The tree – like pattern discharge is not limited specifically to the edge effect but may be observed in other dielectric failure mechanisms in which non – uniform field stresses predominate.

2.1.5 Thermal breakdown

When an insulation is stressed, because of conduction currents and dielectric losses due to polarization, heat is continuously generated within the dielectric. In general, the conductivity (σ) increases with temperature, conditions of instability are reached when the rate of heating exceeds the rate of cooling and the specimen may undergo **thermal breakdown**. The situation is illustrated graphically in Fig. 2.4 in which the cooling of a specimen is represented by the straight line and the heating at various field strengths by curves of increasing slope. Field (1) is in equilibrium at temperature T_1 , field (2) is in a state of unstable equilibrium at T_2 and field (3) does not reach a state of equilibrium at all. To obtain the basic equation for thermal breakdown let us consider a cube of face area A within dielectric.

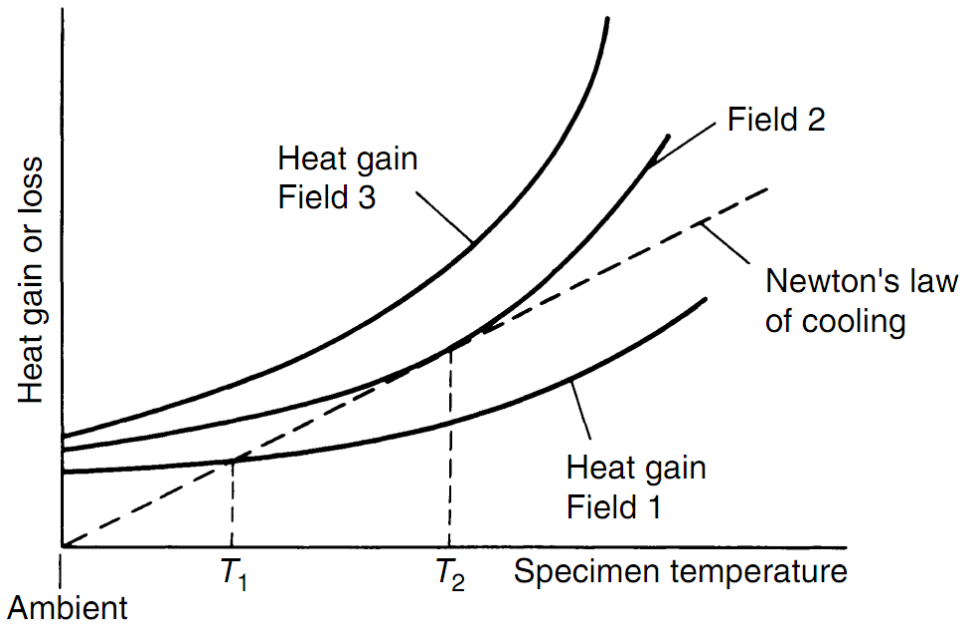


Figure 2.4 Thermal stability or instability under different applied fields

Assume that the heat flow in the x -direction is as shown in Fig. 2.5, then the

heat flow across face (1) = $KA \frac{dT}{dx}$ (K – thermal conductivity);

heat flow across face (2) = $KA \frac{dT}{dx} + KA \frac{d}{dx} \left(\frac{dT}{dx} \right) \Delta x$.

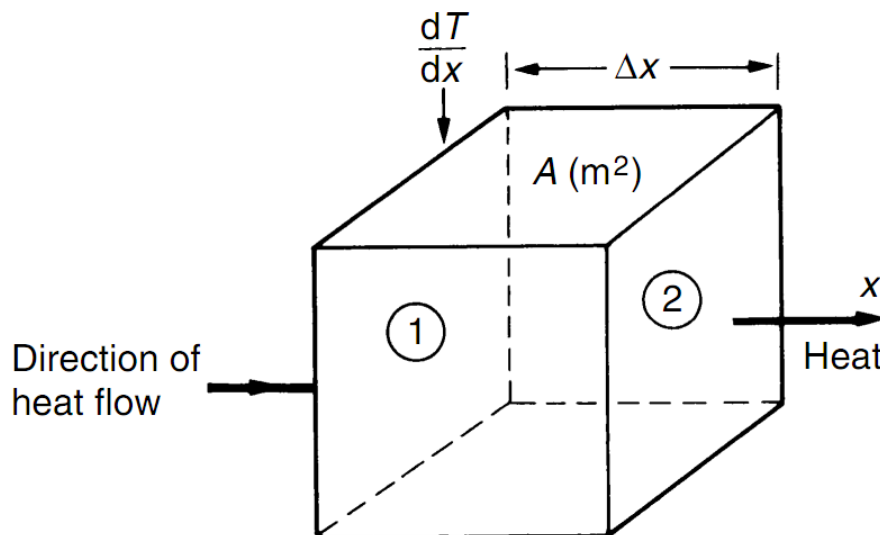


Figure 2.5 Heat input and output, cubical specimen

The second term represents the heat input into the block. Hence:

$$\frac{\text{heat flow}}{\text{volume}} \times K \frac{d}{dx} \left(\frac{dT}{dx} \right) = \text{div}(K \times \text{grad}T).$$

The conservation of energy requires that heat input into the element must be equal to the heat conducted away, plus the heat used to raise the temperature T of the solid or: heat generated = heat absorbed + heat lost to surroundings, i.e.:

$$C \frac{dT}{dt} + \text{div}(K \times \text{grad}T) = \sigma \times E^2 \quad (2.2)$$

where C is thermal capacity of dielectric, σ is the electrical conductivity. Calculation of the critical thermal situation involves the solution of equation (2.2). In solving it, one assumes that a critical condition arises and the insulation properties are lost, when at some point in the dielectric the temperature exceeds a critical temperature.

The voltage is independent of the thickness of the specimen, but for thin specimens the thermal breakdown voltage becomes thickness dependent and is proportional to the square root of the thickness tending asymptotically to a constant value for thick specimens. Under alternating fields the losses are much greater than under direct fields. Consequently the thermal breakdown strength is generally lower for alternating fields, and it decreases with increasing the frequency of the supply voltage. Table 2.1 shows thermal breakdown values for some typical dielectrics under alternating and direct voltages at 20°C. These results correspond to a thick slab of material. The thermal breakdown is a well – established mechanism, therefore the magnitude of the product $\tan \delta$ which represents the loss is a very essential parameter for the application of insulation material.

Thermal breakdown is often occurred in practical high voltage constructions. Any over – exceeding of heat output in some high voltage insulation part area such as bushing, different insulating sections of transformer and others can lead to thermal process intensification and next breakdown.

Among many points of view on solid dielectric breakdown, it is one advanced theory which is distinguished from others. This theory was created by Russian academician Yuriy N. Vershinin . Main state of the theory is breakdown channel is formed as result of transition “solid structure – plasma”. Detailed consideration of this phenomenon is given in [2-3].

Table 2.1 Thermal breakdown voltages for some typical dielectrics (20°C)

<i>Material</i>		<i>Thermal voltage in MV/cm</i>	
		<i>d.c.</i>	<i>a.c.</i>
Crystals:	Mica muscovite	24	7–18
Rock salts		38	1.4
Quartz:	Perpendicular to axis	12 000	–
	Parallel to axis	66	–
	Impure	–	2.2
Ceramics:	H.V. steatite	–	9.8
	L.F. steatite	–	1.5
	High-grade porcelain	–	2.8
Organic materials:	Capacitor paper	–	3.4–4
	Ebonite	–	1.45–2.75
	Polythene	–	3.5
	Polystyrene	–	5
	Polystyrene at 1 MHz	–	0.05
	Acrylic resins		0.3–1.0

2.1.6 Partial discharges

Practical insulation systems often contain cavities or voids within the dielectric material or on boundaries between the solid and the electrodes. These cavities are usually filled with a medium (gas or liquid) of lower breakdown strength than the solid. Moreover, the permittivity of the filling medium is frequently lower than that of the solid insulation, which causes the field intensity in the cavity to be higher than in the dielectric. Accordingly, under normal working stress of the insulation system the voltage across the cavity may exceed the breakdown value and may initiate breakdown in the void. Such electrophysical phenomenon is called *partial discharge*. Figure 2.6 shows a cross section of a dielectric of thickness d containing a cavity in the form of a disc of thickness t , together with an analogue circuit. In the analogue circuit the capacitance C_c corresponds to the

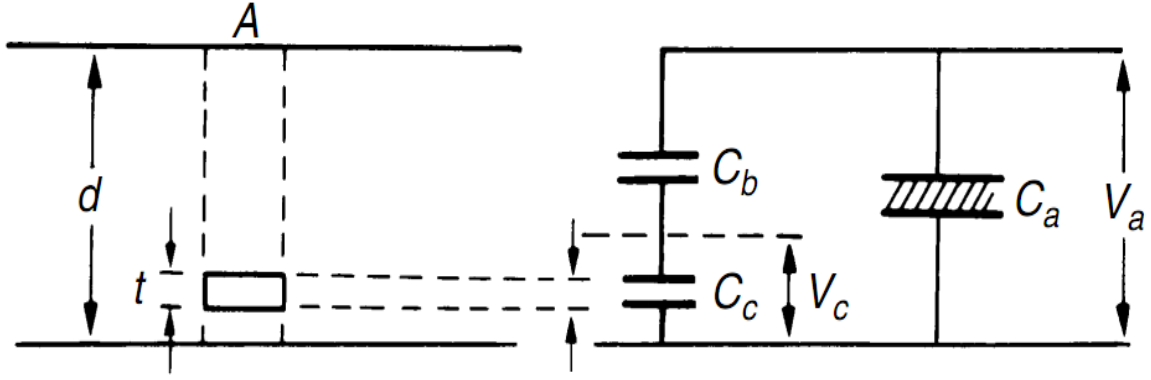


Figure 2.6 Electrical discharge in cavity and its equivalent circuit

cavity, C_b corresponds to the capacitance of the dielectric which is in series with C_c , and C_a is the capacitance of the rest of the dielectric. For $t \ll d$, which is usually the case, and assuming that the cavity is filled with gas, the field strength across C_c is given by the expression:

$$E_c = \varepsilon_r E_A \quad (2.3)$$

where ε_r is the relative permittivity of the dielectric. For the simple case of a disc-shaped dielectric in solid shown in Fig. 2.6, the discharge inception voltage applied across the dielectric can be expressed in terms of the cavity breakdown stress. Assuming that the gas – filled cavity breakdown stress is E_{cb} , then treating the cavity as series capacitance with the healthy part of the dielectric we may write:

$$C_b = \frac{\varepsilon_0 \varepsilon_r A}{d-t} \quad \text{and} \quad C_c = \frac{\varepsilon_0 A}{t} \quad (2.4)$$

And the voltage across the cavity is:

$$V_c = \frac{C_b}{C_c + C_b} \times V_a = \frac{V_a}{1 + \frac{1}{\varepsilon_r} \left(\frac{d}{t} - 1 \right)} \quad (2.5)$$

In practice a cavity in a material is often nearly spherical, and for such a case the internal field strength is:

$$E_c = \frac{3\varepsilon_r E}{\varepsilon_{rc} + 2\varepsilon_r} = \frac{3}{2}E \quad (2.6)$$

for $\varepsilon_r \gg \varepsilon_{rc}$, where E is in the average stress in the dielectric, under an applied voltage V_a when V_c reaches breakdown value V^+ of the gap t , the cavity may break down. The sequence of breakdowns under sinusoidal alternating voltage is illustrated in Fig. 2.7. The dotted curve shows qualitatively the voltage that would appear across the cavity if it did not break down. As V_c reaches the value V^+ , a discharge takes place, the voltage V_c collapses and the gap extinguishes. The voltage across the cavity then starts increasing again until it reaches V^+ , when a new discharge occurs. Thus several discharges may take place during the rising part of the applied voltage. Similarly, decreasing the applied voltage the cavity discharges as the voltage across it reaches V^- . In this way groups of discharges originate from a single cavity and give rise to positive and negative current pulses on raising and decreasing the voltage respectively.

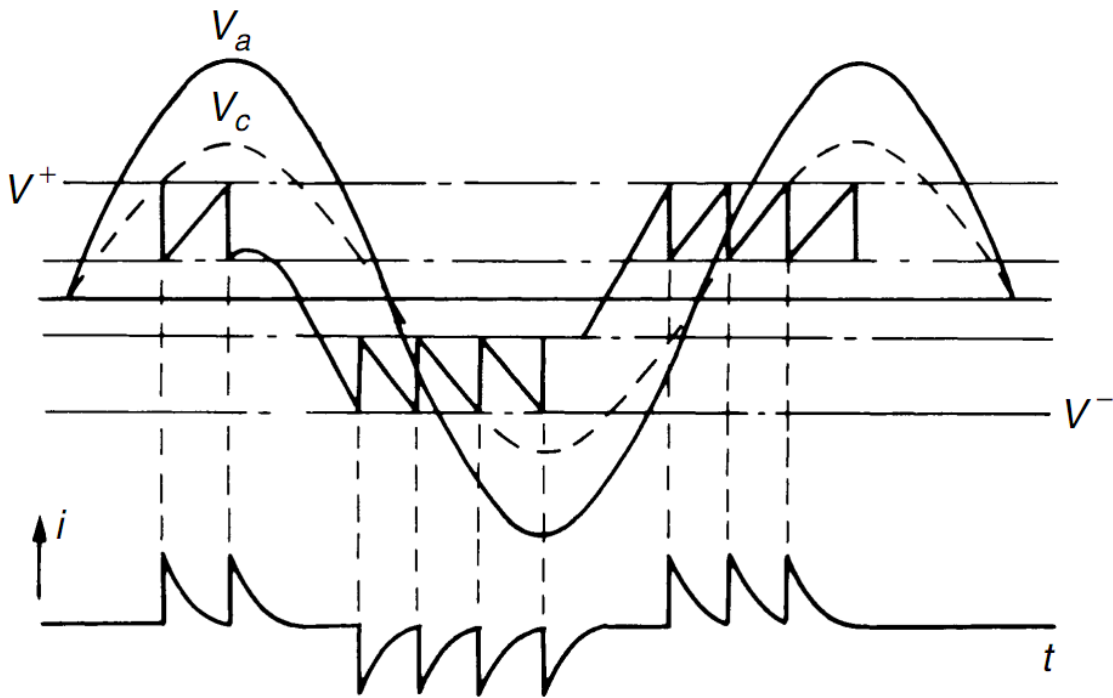


Figure 2.7 Sequence of cavity breakdown under alternating voltages

When the gas in the cavity breaks down, the surfaces of the insulation provide instantaneous cathode and anode. Some of the electrons impinging

upon the anode are sufficiently energetic to break the chemical bonds of the insulation surface. Similarly, bombardment of the cathode by positive ions may cause damage by increasing the surface temperature and produce local thermal instability. Also channels and pits are formed which elongate through the insulation by the “*edge mechanism*”.

Additional chemical degradation may result from active discharge products, e.g. O_3 or NO_2 , formed in air which may cause deterioration. Whatever is the deterioration mechanism operating, the net effect is a slow erosion of the material and a consequent reduction of the breakdown strength of the solid insulation.

When the discharges occur on the insulation surface, the erosion takes place initially over a comparatively large area. The erosion roughens the surface and slowly penetrates the insulation and at some stage will again give rise to channel propagation and “*tree-like*” growth through the insulation.

For practical application it is important that the dielectric strength of a system does not deteriorate significantly over a long period of time (years). In practice, however, because of imperfect manufacture and sometimes poor design, the dielectric strength decreases with the time of voltage application (or the life).

One of the reason solid insulation degradation is *tracking* formation. Tracking is the formation of a permanent conducting path, usually carbon, across a surface of insulation and in most cases the conduction path results from degradation of the insulation. For tracking to occur the insulation must contain some organic substance. In an outdoor environment insulation will in time become covered with contaminant which may be of industrial or coastal origin. In the presence of moisture the contamination layer gives rise to leakage current which heats the surface and causes interruption in the moisture film; small sparks are drawn between the separating moisture films. This process acts effectively as an extension to the electrodes. The heat resulting from the small sparks causes carbonization and volatilization of the insulation and leads to formation of permanent ‘carbon track’ on the surface. The phenomenon of tracking severely limits the use of organic insulation in the outdoor environment. That’s why polymer materials are being more and more popular in electric energy systems, especially at the insulation strings production. The rate of tracking depends upon the structure of the polymers and it can be drastically slowed down by adding appropriate fillers to the polymer which inhibit carbonization.

Moisture is not essential to tracking. The conducting path may arise from metallic dust; for example, in oil – immersed equipment with moving parts which gradually wear and deposit on the surface.

2.2 Electrophysical processes in liquid dielectrics

The general state of knowledge on the electrical breakdown in liquids is less advanced than is in case of gases or even solids. Many aspects of liquid breakdown have been investigated over the last decades, but the findings and conclusions of the many workers cannot be reconciled and so produce a general theory applicable to liquids, as the independent data are at variance and sometimes contradictory. The principal reason for this situation is the lack of comprehensive theory concerning the physical basis of the liquid state which would form the skeleton structure in which observations could be compared and related.

2.2.1 Electronic breakdown

Both the field emission and the field – enhanced thermionic emission mechanisms discussed earlier in Chapter 1, 1.2, have been considered responsible for the current at the cathode in liquids. Conduction studies in insulating liquids at high fields show that most experimental data for current fit well the Schottky – type equation in which the current is temperature dependent. Breakdown measurements carried out over a wide range of temperatures, however, show little temperature dependence. This suggests that the cathode process is field emission rather than thermionic emission. It is possible that the return of positive ions and particularly positively charged foreign particles to the cathode will cause local field enhancement and give rise to local electron emission. Once the electron is injected into the liquid it gains energy from the applied field. In the electronic theory of breakdown it is assumed that some electrons gain more energy from the field than they lose in collisions with molecules. These electrons are accelerated until they gain sufficient energy to ionize molecules on collisions and initiate avalanche.

The condition for the onset of electron avalanche is obtained by equating the gain in energy of an electron over its mean free path to that required for ionization of the molecule.

Electrical strength is strictly depending on admixture presence and purity degree of liquid dielectric. Typical strengths for several highly pure liquids are included in Table 2.2. The electronic theory satisfactorily predicts the relative magnitude of breakdown strength of liquids, but the observed formative time lags are much longer than predicted by electronic theory.

Table 2.2 Electric strength of highly purified liquids

<i>Liquid</i>	<i>Strength (MV/cm)</i>
Hexane	1.1–1.3
Benzene	1.1
Good oil	~1.0–4.0
Silicone	1.0–1.2
Oxygen	2.4
Nitrogen	1.6–1.88

2.2.2 Suspended solid particle breakdown mechanism

Solid impurities may be present in the liquid either as fibres or as dispersed solid particles. Let us consider a spherical particle of radius r and permittivity ε to be suspended in dielectric liquid of permittivity ε_{liq} . Then in a field the particle will become polarized and it will experience a force given by expression:

$$F_e = \varepsilon_{liq} \times r^3 \times \frac{\varepsilon - \varepsilon_{liq}}{\varepsilon + 2\varepsilon_{liq}} \times E \times gradE \quad (2.7)$$

This force is directed towards a place of maximum stress if $\varepsilon > \varepsilon_{liq}$, but for bubbles $\varepsilon < \varepsilon_{liq}$, it has the opposite direction. The force given by equation (2.7) increases as the permittivity of the suspended particle (ε) increases, and for a conducting particle for which $\varepsilon \rightarrow \infty$ the force becomes:

$$F_e = F_\infty = r^3 \times E \times gradE \quad (2.8)$$

Thus the force will urge the particle to move to the strongest region of the field. In a uniform field gap or sphere gap of small spacing the strongest field is in the uniform region. In this region ***grad E is equal to zero*** so that the particle will remain in equilibrium there. Accordingly, particles will be dragged into the uniform field region. If the permittivity of the particle is higher than that of the medium, then its presence in the uniform field region will cause flux concentration at its surface. Other particles will be attracted into the region of higher flux concentration and in time will become aligned

head to tail to form *a bridge across the gap*. The field in the liquid between the particles will be enhanced, and if it reaches critical value breakdown will follow.

The movement of particles by electrical force is opposed by viscous drag, and since the particles are moving into the region of high stress, diffusion must also be taken into account. For a particle of radius r slowly moving with a velocity v in a medium of viscosity, the drag force F_{drag} is given by Stokes relation:

$$F_{drag} = 6\pi r \eta v(x) \quad (2.9)$$

Equating the electrical force with the drag force ($F_e = F_{drag}$) we obtain:

$$v_E = \frac{r^2 \times E \times dE}{6 \times \pi \times \eta \times dx} \quad (2.10)$$

where v_E is the velocity of the particle towards the region of maximum stress. If the diffusion process is included, the drift velocity due to diffusion will be given by the equation:

$$v_D = -\frac{DdN}{Ndx} = -\left(\frac{kT}{6 \times \pi \times r \times \eta}\right) \times \frac{dN}{Ndx} \quad (2.11)$$

2.2.3 Cavity breakdown

Insulating liquids may contain gaseous inclusions in the form of bubbles. The processes by which bubbles are formed include:

- *gas pockets on the electrode surface,*
- *changes in temperature and pressure,*
- *dissociation of products by electron collisions giving rise to gaseous products,*
- *liquid vaporization by corona-type discharges from points and irregularities on the electrodes.*

The electric field in a spherical gas bubble which is immersed in a liquid of permittivity ϵ_{liq} is given by:

$$E_B = \frac{3E_0}{\epsilon_{liq} + 2} \quad (2.12)$$

where E_0 is the field in the liquid in the absence of the bubble. When the

field E_B becomes equal to the gaseous ionization field, discharge takes place which will lead to decomposition of the liquid and breakdown may follow.

Commercial insulating liquids cannot readily be subjected to highly elaborated purification treatment, and the breakdown strength will usually depend upon the nature of impurities present.

So, in solid dielectric three kinds of breakdown are possible: electrical, thermal and material ageing due to partial discharges. They are differed each other ionization reason nature and time duration. Time range is very extensive: from microseconds (electrical breakdown) up to years (partial discharge deterioration).

As for liquid dielectric two contradictory points of view are in modern breakdown theories. One of them is affirmed that ionization processes play main role at breakdown channel formation. Other one is stated that most important role in breakdown channel formation play bubbles presence in liquid dielectric media. In inner bubble area all ionization processes have the same nature as in gases (this material is detailed considered in Chapter 1) and discharge in liquid is generated as result of gas bubble media breakdown.

REFERENCES

1. W. Zaengl, E. Kuffel, J. Kuffel. High voltage engineering. Fundamentals. – Butterworth – Heinemann, 2000. – 539 p.
2. Yu. N. Vershinin. Domain mechanism of dielectric breakdown. – WELC, Moscow, 1977. – 19 p.
3. Yu. N. Vershinin. Overheating instability in crystalline insulations subjected to pre-breakdown electric field. – SPSS, 1975, V.17, 3, pp. 526 – 530.
4. D.M. Taylor and T.J. Lewis. J. Phys. D4, 1971, p. 1346.
5. J. O'Dwyer. The Theory of Electrical Conduction and Breakdown in Solid Dielectrics. Clarendon Press, Oxford, 1973.
6. J.A. Kok. Electrical Breakdown in Insulating Liquids. Philips Tech. Library, 1961.
7. Z. Krasucki. Breakdown of commercial liquid and liquid solid dielectrics, in High Voltage Technology (Alston), p. 129. Oxford University Press, 1968.
8. A.A. Zaky and R. Hawley. Conduction and Breakdown in Mineral Oils. Pergamon Press, Oxford, 1973.
9. D. Kind, H. Karner. High voltage insulation technology. – Braunschweig, Wiesbaden, Germany, 1985. – 192 p.

CHAPTER 3. GENERATION AND MEASUREMENT OF HIGH VOLTAGES

This chapter consists of two parts. First one deals with scheme and process of different kind high voltage generation. Second one is devoted to measurement procedure of those.

3.1. Generation of high voltages

Three main kinds of high voltages are used in modern industry – alternating, direct and pulsed ones.

3.1.1 Alternating voltages

As electric power transmission with high alternating current (a.c.) voltages predominates in our transmission and distribution systems, the most common form of testing high voltage (h.v.) apparatus is related to high a.c. voltages. It is obvious then that most research work in electrical insulation systems has to be carried out with this type of voltage.

In every laboratory high voltage alternating current (HVAC) supplies are therefore in common use. As far as the voltage levels are concerned, these may range from about 10 kV to more than 5 MV today, as the development of transmission voltages up to about 1200 kV has proceeded for many years [1]. For routine testing, the voltage levels for power–frequency testing are always related to the highest phase–to–phase voltage V_m of power transmission systems. This “rated power–frequency short duration withstand voltage” V_t is different for different apparatus used within the transmission systems and also dependent upon the type of insulation coordination applied (see Chapter 4). For $V_m < 300$ kV, the ratio V_t/V_m is up to about 1.9 and may decrease with higher values of V_m . If, nevertheless, higher nominal voltages for the a.c. testing supplies are foreseen, the necessity for the determination of safety factors are most responsible for this fact [2].

In general, all a.c. voltage tests are made at the nominal power frequency of the test objects. Typical exceptions are related to the testing of iron–cored windings, i.e. potential or instrument transformers, or to fundamental studies on insulating materials or systems. For iron–cored windings, the frequency has to be raised to avoid saturation of the core. Depending upon the type of testing equipment used, the methods for the generation of variable–frequency voltages might be expensive.

The power frequency single–phase transformer is the most common

form of HVAC testing apparatus. Designed for operation at the same frequency as the normal working frequency of the test objects (i.e., 60 or 50 Hz), they may also be used for higher frequencies with rated voltage, or for lower frequencies, if the voltages are reduced in accordance to the frequency, to avoid saturation of the core.

From the considerations of thermal rating, the *kVA output* and the fundamental design of the iron core and windings there is not a very big difference between a testing and a single-phase power transformer. The differences are related mainly to a smaller flux density within the core to avoid unnecessary high magnetizing currents which would produce higher harmonics in the voltage regulator supplying the transformer, and to a very compact and well-insulated h.v. winding for the rated voltage. Therefore, a single-phase testing unit may be compared with the construction of a potential transformer used for the measurement of voltage and power in power transmission systems.

For a better understanding of advanced circuits, the fundamental design of such “single unit testing transformers” will be illustrated. Figure 3.1 shows the well-known circuit diagram. The primary winding “2” is usually rated for low voltages of 1 kV, but might often be split up in two or more windings which can be switched in series or parallel (not shown here) to increase the regulation capabilities. The iron core “1” is fixed at earth potential as well as one terminal of each of the two windings. Simplified cross-sections of two possible constructions for the unit widespread itself is given in Figs 3.2 a, b.

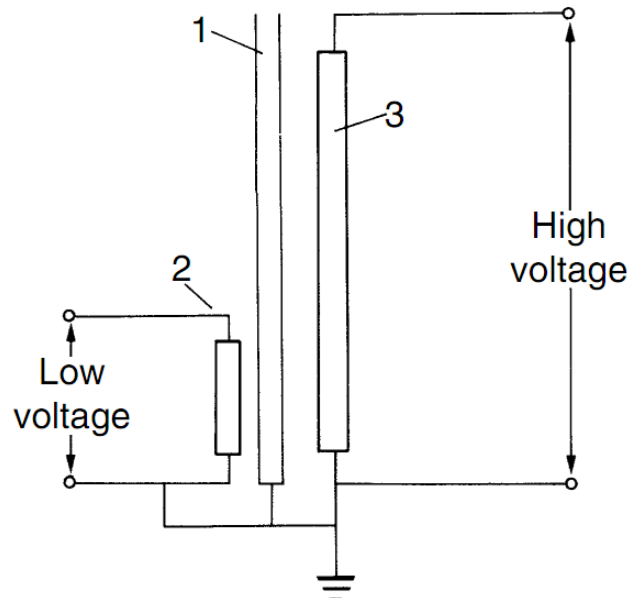


Figure 3.1 Scheme of single unit testing transformer:
 1 - iron core, 2 - primary low voltage, 3 - secondary high voltage wind-

ing

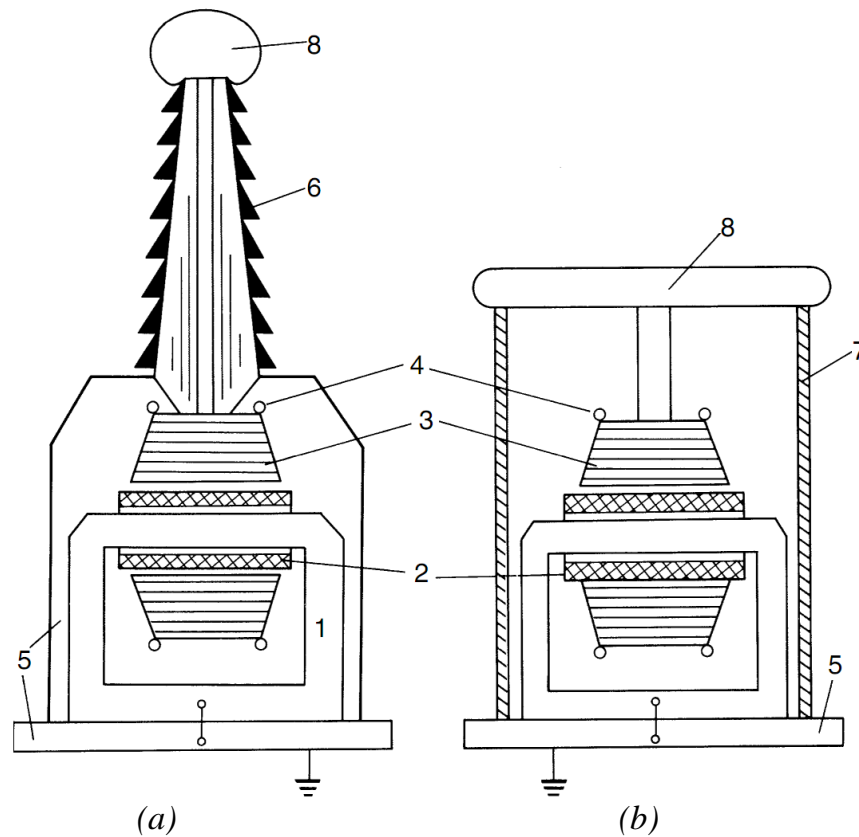


Figure 3.2 Different construction units of testing transformers:
1 - iron core, 2 - primary low voltage, 3 - secondary high voltage winding, 4 - field grading shield, 5 - grounded metal tank and base, 6 - high voltage bushing, 7 - insulating shell or tank, 8 - high voltage electrode

In both cases the vessels would be filled with high-quality transformer oil, as most of the windings are oil-paper insulated. The sectional view of the windings shows the primary winding close to the iron core and surrounded by the h.v. winding “3”. This coaxial arrangement reduces the magnetic stray flux and increases, therefore, the coupling of both windings. The shape of the cross-sectional view of winding no. 3 is a hint to the usual layout of this coil: the beginning (grounded end) of the h.v. winding is located at the side close to the core, and the end close to a sliced metal shield, which prevents too high field intensities at h.v. potential. Between both ends the single turns are arranged in layers, which are carefully insulated from each other by solid materials. Adjacent layers, therefore, form coaxial capacitors of high values, and if those capacitances are equal – produced by the reduced width of the single layers with increasing diameters – the potential distribution for transient volt-

ages can be kept constant. By this procedure, the trapezoidal shape of the cross-section is originated.

It may well be understood that the design of the h.v. winding become difficult if voltages of more than some 100 kV must be produced within one coil. Better constructions are available by specialized techniques, mainly by “*cascadin transformers*”.

For voltages higher than about 300 kV, the cascading of transformers is a big advantage, as the weight of a whole testing set can be subdivided into single units and therefore transport and erection becomes easier. The cascading principle is illustrated with the basic scheme shown in Fig. 3.3. The low voltage supply is connected to the primary winding “1” of transformer I, designed for an high voltage output of V as are the other two transformers. The exciting winding “3” supplies the primary of the second transformer unit II; both windings are dimensioned for the same low voltage, and the potential is fixed to the high potential V . The h.v. or secondary windings “2” of both units are series connected, so that a voltage of $2V$ is produced hereby. The addition of the stage III needs no further explanation. The tanks or vessels containing the active parts (core and windings) are indicated by dashed lines only. For a metal tank construction and the non-subdivided h.v. winding assumed in this basic scheme, the core and tank of each unit would be tapped to the low voltage terminal of each secondary winding as indicated. Then the tank of transformer I can be earthed; the tanks of transformers II and III are at high potentials, namely V and $2V$ above earth, and must be suitably insulated. Through bushings the leads from the exciting coils “3” as well as the tapplings of the h.v. windings are brought up to the next transformer. If the h.v. windings of each transformer are of mid-point potential type, the tanks are at potentials of $0.5V$, $1.5V$ and $2.5V$ respectively.

The disadvantage of transformer cascading is the heavy loading of primary windings for the lower stages. In Fig. 3.3 this is indicated by the letter P , the product of current and voltage for each of the coils. For this three-stage cascade the output kVA rating would be $3P$, and therefore each of the windings “2” would carry a current of $I = P/V$. Also, only the primary winding of transformer III is loaded with P , but this power is drawn from the exciting winding of transformer II. Therefore, the primary of this second stage is loaded with $2P$. Finally, the full power $3P$ must be provided by the primary of transformer I. Thus an adequate dimensioning of the primary and exciting coils is necessary. As for testing of insulation, the load is primarily a capacitive one, a compensation of this capacitive load by low voltage reactors, which are in parallel to the primary windings, is possible. As these reactors must be switched in accordance to the variable load, however, one usually tries to avoid this additional expense.

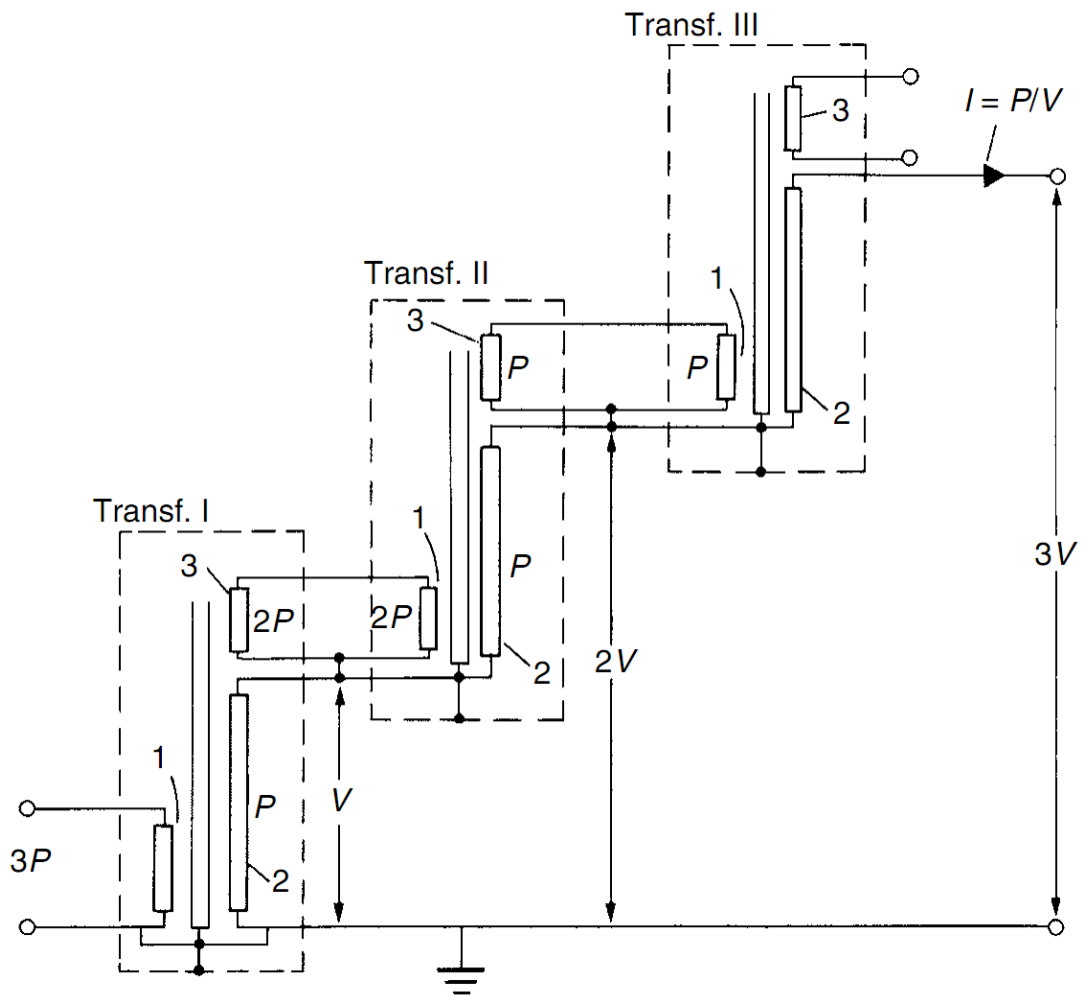


Figure 3.3 Circuit of cascaded transformers:
 1 – primary windings, 2 – secondary windings, 3 – tertiary exciting windings

3.1.2 Direct voltages

In high voltage technology direct voltages are mainly used for pure scientific research work and for testing equipment related to high voltage direct current (HVDC) transmission systems. High d.c. voltages are even more extensively used in applied physics (accelerators, electron microscopy, etc.), electromedical equipment (X-rays), industrial applications (precipitation and filtering of exhaust gases in thermal power stations and the cement industry; electrostatic painting and powder coating, etc.), or communications electronics (TV, broadcasting stations). Therefore, the requirements on voltage shape,

voltage level, and current rating, short- or long-term stability for every HVDC generating system may differ strongly from each other. With the knowledge of the fundamental generating principles it will be possible, however, to select proper circuits for a special application.

The rectification of alternating currents is the most efficient means of obtaining HVDC supplies. For a clear understanding of all a.c. to d.c. conversion circuits the *single-phase half-wave rectifier* with voltage smoothing is of basic interest (Fig. 3.4(a)). If we neglect the leakage reactance of the transformer and the small internal impedance of the diodes during conduction –

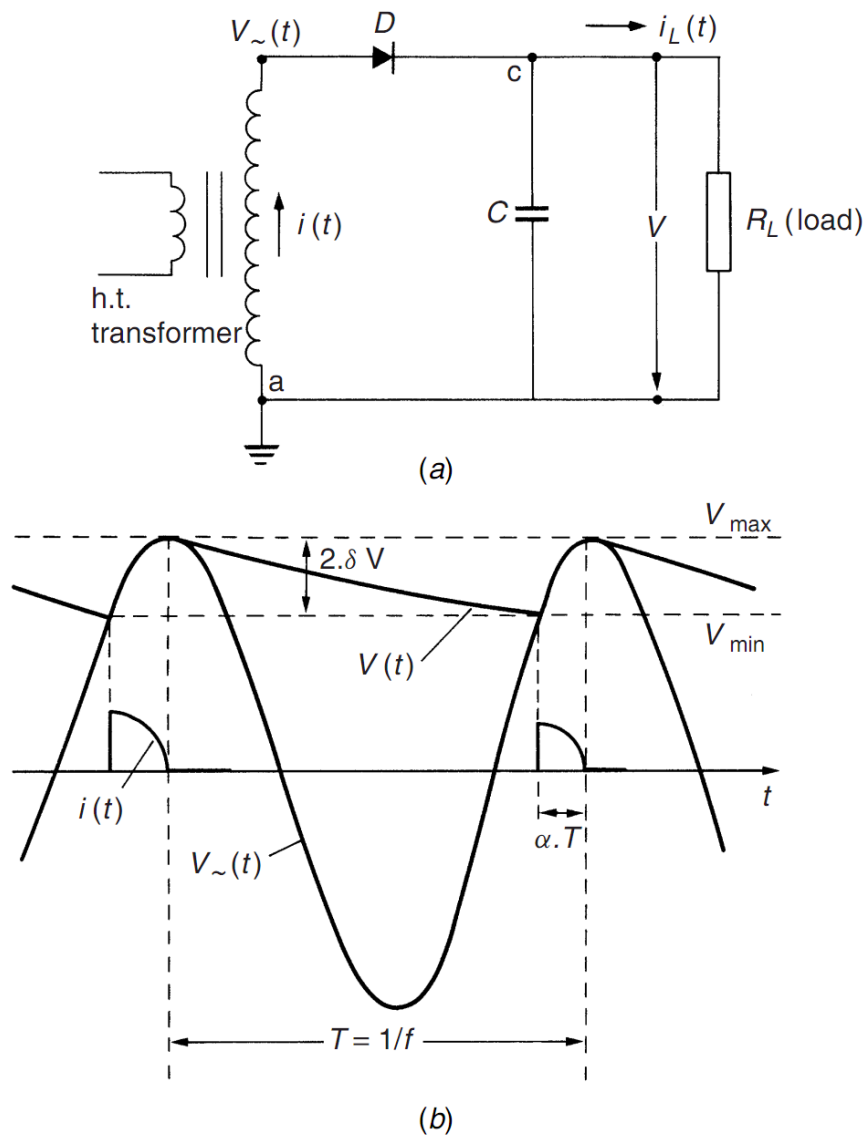


Figure 3.4 Single-phase half-wave rectifier:
a – circuit scheme, *b* - voltages and currents with load R_L

– impedance of the diodes during conduction – and this will be done throughout unless otherwise stated – the reservoir or smoothing capacitor C is charged to the maximum voltage $+V_{max}$ of the a.c. voltage $V(t)$ of the transformer, when D conducts. This is the case as long as $V < V(t)$ for the polarity of D assumed. If $I = 0$, i.e. the output load being zero $R_L = \infty$, the d.c. voltage across C remains constant ($+V_{max}$), whereas $V(t)$ oscillates between $\pm V_{max}$. The diode D must be dimensioned, therefore, to withstand a peak reverse voltage of $2V_{max}$. The output voltage V does not remain any more constant if the circuit is loaded. During one period, $T = 1/f$ of the a.c. voltage a charge Q is transferred to the load R_L , which is represented as:

$$Q = \int_T i_L(t) dt = \frac{1}{R_L} \int_T V(t) dt = I \times T = \frac{I}{f} \quad (3.1)$$

where I is therefore the mean value of the d.c. output $i_L(t)$, and $V(t)$ the d.c. voltage which includes a ripple as shown in Fig. 3.4(b).

The size of such circuits is unnecessarily large for pure d.c. supplies. The other disadvantage of the single-phase half-wave rectifier concerns the possible saturation of the h.v. transformer, if the amplitude of the direct current is comparable with the nominal alternating current of the transformer is comparable with the nominal alternating current of the transformer. The bi-phase half-wave (or single-phase full-wave) rectifier as shown in Fig. 3.5 overcomes this disadvantage, but it does not change the fundamental efficiency, considering that two h.v. windings of the transformer are now available. When high voltages more than 300 kV d.c. is necessary, cascaded scheme is used. Detailed description of Cockcroft – Walton generator, electrostatic generator of Van de Graaf, is beyond of this textbook and is subject of special seminars.

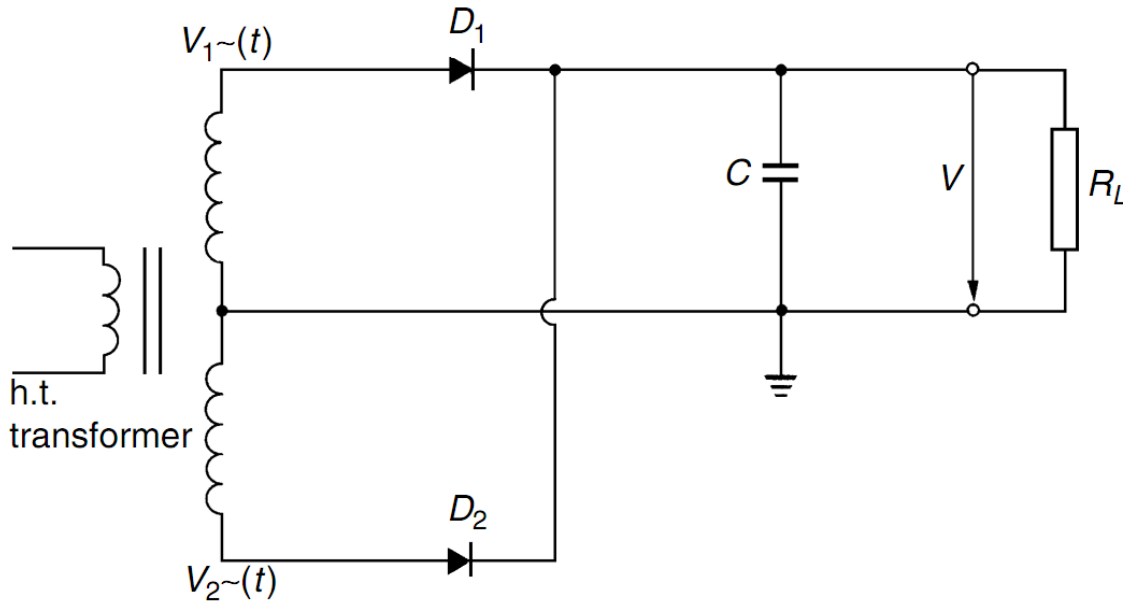


Figure 3.5 Biphas half-wave rectifier circuit with smoothing capacitor C

3.1.3 Impulse voltages

Impulse voltages have applications in such areas as plasma, discharge, particle beam sources, nuclear and thermonuclear researches, overvoltage pulses modeling, high voltage testing of high voltage equipment and others.

Voltage pulsed amplitude is in range $100 - 5\,000$ kV, pulse duration has range $10^{-3} - 10^{-9}$ sec. To provide such pulse parameters, single-stage and multi-stage circuits are used.

Basic circuits for single-stage impulse generators are shown in Fig. 3.6. The capacitor C_1 is slowly charged from a d.c. source until the spark gap G breaks down. This spark gap acts as a voltage-limiting and voltage-sensitive switch, whose ignition time (time to voltage breakdown) is very short in comparison to front time. As such single-stage generators may be used for charging voltages from some kV up to about $1\,MV$, the sphere gaps will offer proper operating conditions. An economic limit of the charging voltage V_0 is, however, a value of about 200 to $250\,kV$, as too large diameters of the spheres would otherwise be required to avoid excessive inhomogeneous field distributions between the spheres. The resistors R_1 , R_2 and the capacitance C_2 form the waveshaping network. R_1 will primarily damp the circuit and control the front time. R_2 will discharge the capacitors and therefore essentially control the wavetail. The capacitance C_2 represents the full load, i.e. the object under test as well as all other capacitive elements which are in parallel to the test object.

One of the most significant parameter of impulse generators is the

maximum stored energy:

$$W = \frac{1}{2} C_1 (V_{0\max})^2 \quad (3.2)$$

where the C_1 is discharge capacitance. As C_1 is always much larger than C_2 , this figure determines mainly the cost of a generator. For the circuit Fig. 3.6 the output voltage is thus given by the expression:

$$V(t) = \frac{V_0}{t} \times \frac{Z_2}{Z_1 + Z_2}$$

where Z is complex resistance of respective circuit parts.

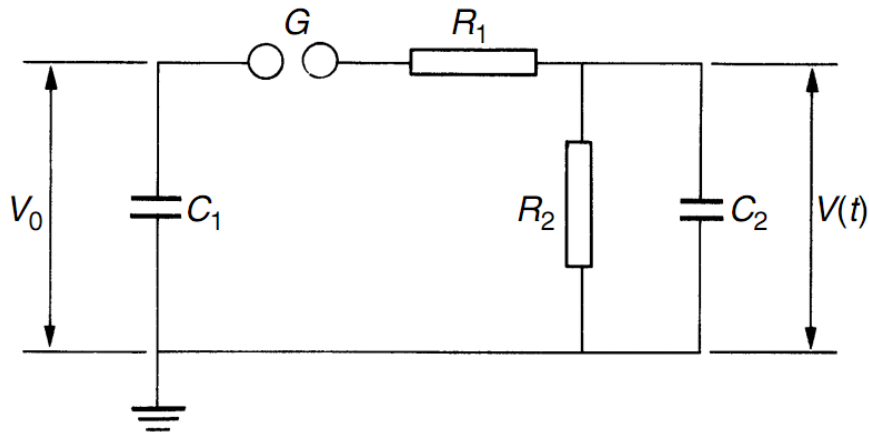


Figure 3.6 Single-stage impulse generator circuits:
 C_1 - discharge capacitance, C_2 - load capacitance,
 R_1 - front or damping resistance, R_2 - discharge resistance

The difficulties encountered with spark gaps for the switching of very high voltages, the increase of the physical size of the circuit elements, the efforts necessary in obtaining high d.c. voltages to charge C_1 and, last but not least, the difficulties of suppressing corona discharges from the structure and leads during the charging period make the one-stage circuit inconvenient for higher voltages.

In order to overcome these difficulties, in 1923 German researcher and engineer Marx suggested an arrangement where a number of condensers are charged in parallel through high ohmic resistances and then discharged in series through spark gaps [3].

There are many different, although always similar, multistage circuits in use. To demonstrate the principle of operation, a typical circuit is presented in Fig. 3.7 which shows the connections of a six-stage generator.

The d.c. voltage charges the equal stage capacitors C_1 in parallel through the high value charging resistor R' as well as through the discharge (and also charging) resistances R'_2 , which are much smaller than the resistors R' and are comparable with R_2 in Fig. 3.6. At the end of the relatively long charging period (typically several seconds up to 1 minute), the points A, B, \dots, F will be at the potential of the d.c. source, e.g. $-V$ with respect to earth, and the points G, H, \dots, N will remain at the earth potential, as the voltage drop during charging across the resistor R'_2 is negligible. The discharge or firing of the generator is initiated by the breakdown of the lowest gap G_1 which is followed by a nearly simultaneous breakdown of all the remaining gaps. According to the traditional theory, which does not take into account the stray capacitances indicated by the dotted lines, this rapid breakdown would be caused by high overvoltages across the second and further gaps: when the first gap fires, the potential at point A changes rapidly from $-V$ to zero, and thus the point H increases its potential to $+V$. As the point B still would remain at the charging potential, $-V$, thus a voltage of $2V$ would appear across G_2 . This high overvoltage would therefore cause this gap to break down and the potential at point I would rise to $+2V$, creating a potential difference of $3V$ across gap G_3 , if again the potential at point C would remain at the charging potential. This traditional interpretation, however, is wrong, since the potentials B and C can – neglecting stray capacitances – also follow the adjacent potentials of the points A and B , as the resistors R' are between. We may only see up to now that this circuit will give an output voltage with a polarity opposite to that of the charging voltage. In practice, it has been noted that the

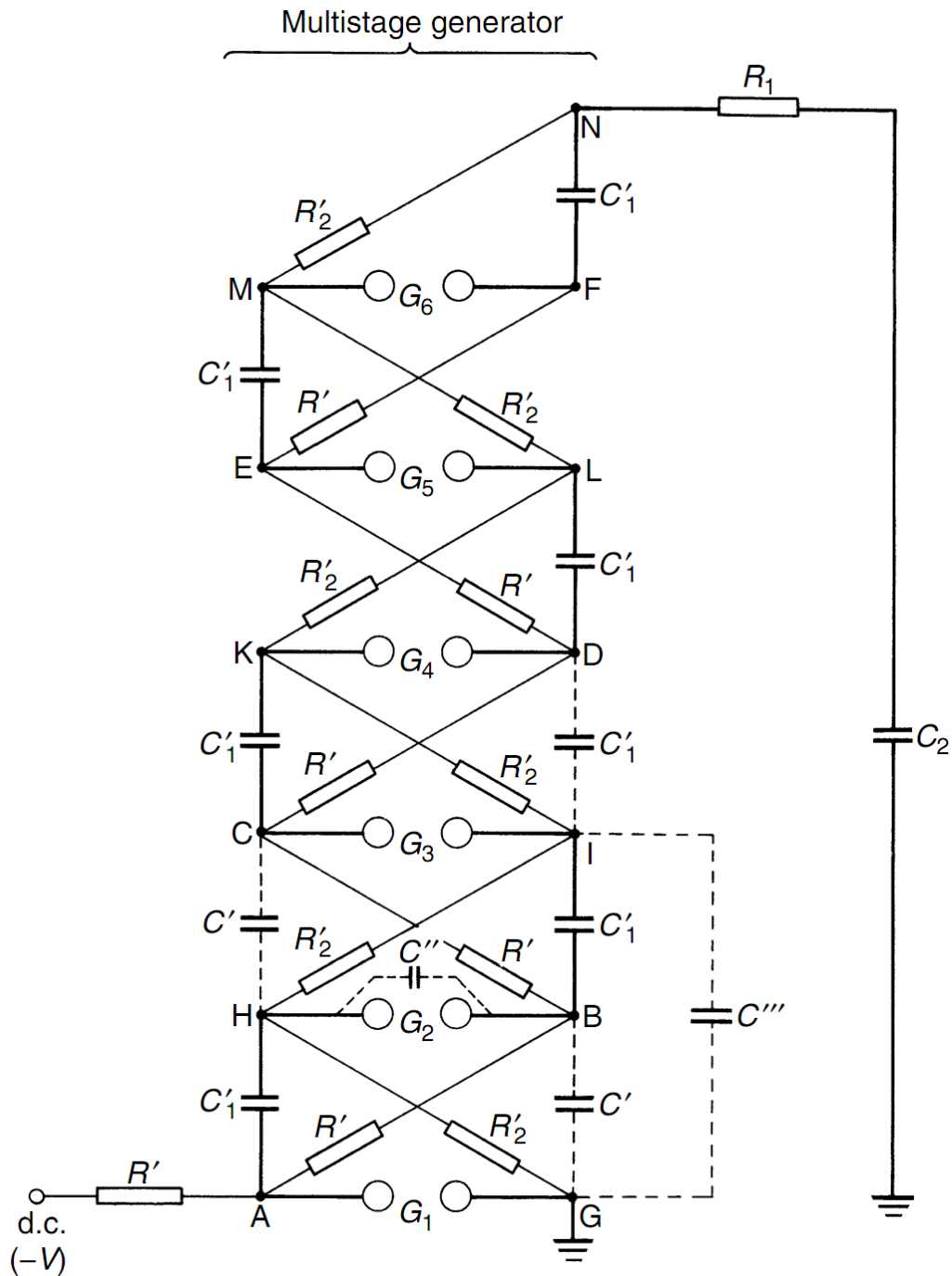


Figure 3.7 Circuit scheme of six-stage impulse Marx generator

gap G_2 must be set to a gap distance only slightly greater than that at which G_1 breaks down; otherwise it does not operate. More detailed studying of Marx generator work is made during laboratory workshop. Other impulse generator types are described in [1-3]. Information concerning high voltage generation could be found also in [4-7].

3.2. Measurement of high voltages

Measurement of high voltages – d.c., a.c. or impulse voltages – involves unusual problems that may not be familiar to specialists in the common electrical measurement techniques. These problems increase with the magnitude of the voltage, but are still easy to solve for voltages of some 10 kV only, and become difficult if hundreds of kilovolts or even megavolts have to be measured. The difficulties are mainly related to the large structures necessary to control the electrical fields, to avoid flashover, corona and sometimes to control the heat dissipation within the circuits.

This subchapter is devoted to the measurement of voltages applied for the testing of h.v. equipment or in research. Voltage-measuring methods used within the electric power transmission systems, e.g. instrument transformers, conventional or non-conventional ones, are not discussed. Such methods are summarized in specialized courses and given in references.

The classification of the measuring methods by sections according to the type of voltages to be measured would be difficult and confusing. A basic principle of quantifying a voltage may cover all kinds of voltage shapes and thus it controls the classification. The essential part of a measuring system relates also to the elements or apparatus representing the individual circuit elements. These could be treated separately, but a preferred treatment is within the chapter, in which special problems first arise [8]. Due to space limitation no constructional details are given, but the comments referring to such problems should carefully be noted. The classification used here could introduce difficulties in selecting proper methods for the measurement of given voltages [9]. Below state of the art methods of high voltage measurement are described.

It is general review of high voltage measurement technique will be overviewed below.

Simple *spark gaps* insulated by atmospheric air can be used to measure the amplitude of a voltage above about 10 kV. The complex mechanism of this physical effect, often employed in protecting equipment from overvoltages (protection gaps), is treated in Chapter 1. Although spark gaps for measurement purposes might be applied following given rules and recommendations only, a misuse can be avoided through an adequate study of the physical phenomena. As the fast transition from an either completely insulating or still highly insulating state of a gap to the high conducting arc state is used to determine a voltage level, the disruptive discharge does not offer a direct reading of the voltage across the gap. A complete short-circuit is the result of a spark, and therefore the voltage source must be capable to allow such a short-circuit, although the currents may and sometimes must be limited by

resistors in series with the gap. *This method is used to measure of peak voltage.* There are two types of sphere gap construction – horizontal and vertical. Peak voltage is determined by means of tables with data. Data are sphere diameter, gap distance and peak voltage corresponding geometry measurement. Gap could be both uniform and non-uniform electric field. Detailed description of the process measurement is given in [10, 11].

Electrostatic voltmeter is used to measure both – *d.c. and a.c. voltages.* Main part of the device is pair measuring electrodes. Electrical field forces on metal electrode with some mechanical force. This force is proportional to voltage square. Electrode is connected with device scale. Scale shows the value which is corresponding electrical field force, which, in turn, corresponds to measuring voltage. The electrostatic measuring device can be used for *absolute* voltage measurements, since the calibration can be made in terms of the fundamental quantities of length and forces. The very important advantage is the extremely low loading effect, as only electrical fields have to be built up. The atmospheric air, high-pressure gas or even high vacuum between the electrodes provide very high resistivity, and thus the active power losses are mainly due to the resistance of insulating materials used elsewhere. The measurement of voltages lower than about 50 V is, however, not possible, as the forces become too small. Detailed description of the construction is given in [1, 8].

Basic principles Ohm's law provides a method to reduce high voltages to measurable quantities, i.e. adequate currents or low voltages. The simplest method employs a micro-ammeter in series with a resistor of sufficiently high value to keep the loading of an h.v. source as small as possible. If the voltage drop across the ammeter is neglected, which is usually allowable due to the small terminal impedance of such instruments. For d.c. voltage measurements, average current-indicating instruments such as moving coil or equivalent electronic meters are used giving the arithmetic mean value of voltage. This method is called ***ammeter in series with high ohmic resistors and high ohmic resistor voltage dividers.*** Scheme of this measurement technique is shown on Fig. 3.8 a, b.

The main difficulties encountered in this method are related to the stability of the resistance R . All types of resistors are more or less temperature dependent and often may show some voltage dependency. Such variations are directly proportional to the voltage to be measured and increase the uncertainty of the measurement result.

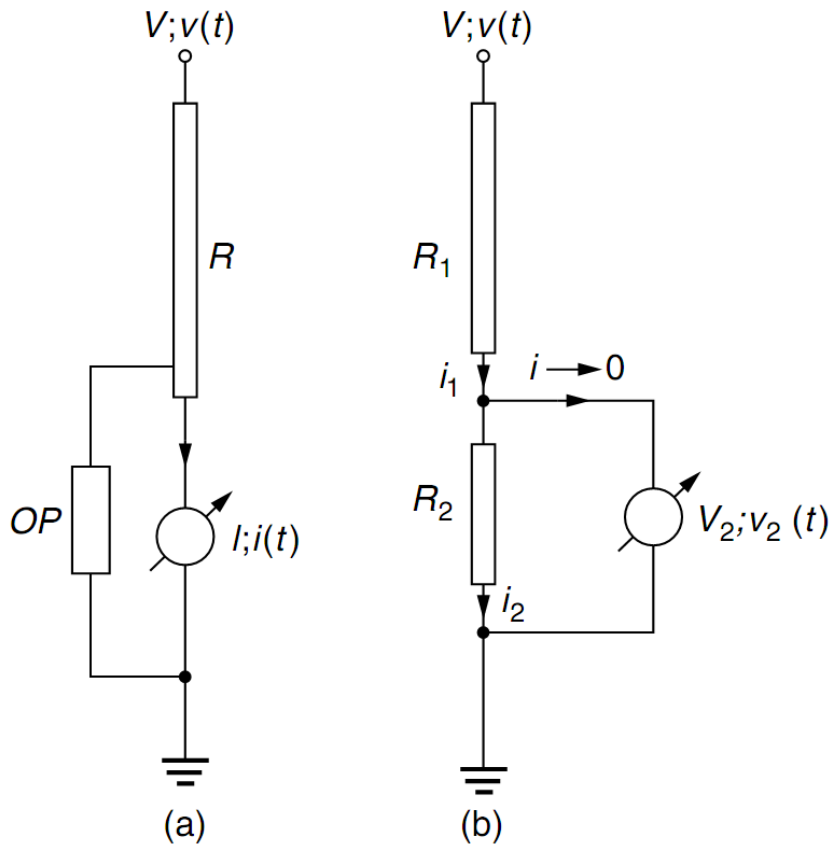


Figure 3.8 Measurement of high d.c. and a.c. voltages by means of:
 a - ammeter in series with resistor R , b - voltage divider R_1, R_2 ,
 OP - over voltage protection

As both resistors pass the same current $i_1=i_2$, the influence of voltage and temperature coefficients of the resistors can be eliminated to a large extent, if both resistors employ equal resistor technology, are subjected to equal voltage stresses, and if provisions are made to prevent accumulation of heat within any section of the resistor column. Thus the uncertainty of the measurement can be greatly reduced. Accurate measurement of V_2 was difficult in earlier times as only electrostatic voltmeters of limited accuracy had been available. In practice this high ohmic resistor R, R_1 is composed of a large number of individual elements connected in series, as no commercial types of single unit resistors for very high voltages are available.

Wire-wound metal resistors made from $Cu - Mn, Cu - Ni$ and $Ni - Cr$ alloys or similar compositions have very low temperature coefficients down to about $10^{-5} /K$ and provide adequate accuracy of measurement procedure.

The simple but accurate method for the measurement of peak values of a.c. voltages was proposed by Chubb and Fortescue and is named "**the Chubb - Fortescue method**". The basic diagram (Fig. 3.9(a)) comprises a

standard capacitor, two diodes and a current integrating ammeter (i.e. moving coil or equivalent instrument) only. The displacement current i_c is subdivided into positive and negative components by the back-to-back connected diodes. The voltage drop across these diodes (less than 1 V for Si diodes) may completely be neglected when high voltages are to be measured.

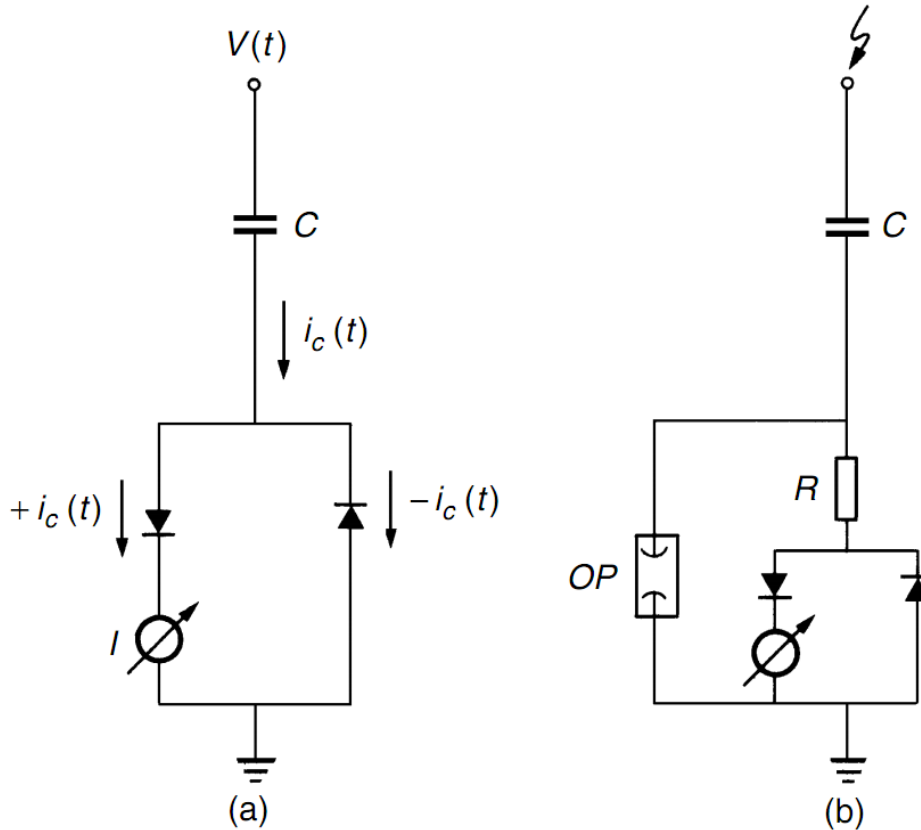


Figure 3.9 A.C. peak voltage measurement by Chubb – Fortescue method: a - fundamental circuit, b - actual circuit

But due to the back-to-back connection of the diodes, the reverse voltages are low. However, the diodes as well as the instrument become highly stressed by short impulse currents during voltage breakdowns. A suitable protection of the rectifying circuit is thus recommended as shown in Fig. 3.9(b). The resistor R introduces a required voltage drop during breakdown to ignite the overvoltage protector OP (e.g. a gas discharge tube).

The influence of the frequency on the reading can be eliminated by electronically controlled gates and by sensing the rectified current by analogue-to-digital converters.

The important influence of the effective capacitance of any h.v. capacitors as used, e.g., in the Chubb – Fortescue circuit in most of the peak reading circuits for a.c. voltages, makes it necessary to present a short treatment

about the *technology of high voltage capacitor* units widely used in testing and research laboratories.

In comparison to h.v. capacitors used within h.v. transmission and distribution systems for load or series compensation, the requirements for “measuring capacitors” are different. First, the effective capacitor values are quite low and range between some *10 and 100 pF* only. These low values are sufficient to provide the energy or power needed for the measurement and to provide low load for the voltage source. The second requirement is related to the stability of the *C* values relative to atmospheric conditions (temperature, humidity), external fields and voltage range, including all effects associated with this magnitude, i.e. partial discharges or non-linearity.

An h.v. capacitor may consist of a single capacitance unit, defined basically as a two-electrode arrangement, or of a chain of capacitor units rated for relative “low voltages” (kV range) electrically connected in series. The technology as well as the electrical behaviour is quite different for the two cases and therefore a separate discussion is appropriate [1, 8].

Ultra high vacuum would provide the ideal dielectric between metal plates forming an arrangement with known and fixed field distribution. Ultra high vacuum has excellent electrical strength although it is limited by well-known, electrode effects. The difficulties and associated costs, however, to place such electrodes in large vessels or tanks providing ultra high vacuum conditions without maintenance are the reasons why vacuum is not used for very high voltages.

According to Paschen’s law (Chapter 1, 1.3) high electric strength can also be achieved with gases at high pressure. Atmospheric pressure may be treated as the lower limit of a high pressure and, dependent upon the type of gas used, the upper limit is set again by predominantly electrode surface effects which place an economic limit given by the decreasing relative dielectric strength of the gas and the increasing cost of pressure vessels. Gases are dielectrics with predominantly electronic polarization only (see section 7.1), providing a very low relative permittivity which is not influenced up to very high frequencies and only by the particle density. Hence a gaseous dielectric is adequate for the construction of h.v. capacitors. Scheme and description of work of some h.v. capacitor measurement technology is given in [1, 8].

The main requirements for technology of H.V. capacitors are:

- the capacitance *C* shall be independent of magnitude of voltage level and shall not change with time of application (no ageing effects);
- the temperature coefficient shall be small or very small;
- dependent on the kind and temperature range of application, and shall at least be known;

- the effective inductivity of C shall be as small as possible, if used for high–frequency applications, i.e. voltage dividers for impulse voltages.

Voltage dividers for d.c., a.c. or impulse voltages consist of resistors or capacitors or convenient combinations of these elements. Inductors are in general not used for voltage dividers for testing purposes, although ‘inductance voltage dividers’ do exist and are used for the measurement of power frequency voltages, independent from inductive voltage transformers as used in power transmission.

Voltage dividers are very popular and often used device for high voltage measurement. Any voltage divider consists of two main parts: high voltage arm and low voltage arm. *Main condition of measurement procedure is following: signal form on low voltage arm must exactly repeat signal form in measurement circuit.*

Voltage dividers are three main types, depending on which kind of circuit element is used for dividing purpose: resistive, capacitive and resistive-capacitive (mixed type). Signal level on low voltage arm is appropriate to match it with accurate measurement device which allows to analyze the signal parameters. As rule this is electronic oscilloscope. Common measuring schemes of different divider types and their matching with cable are shown on Fig. 3.10.

More detailed consideration of voltage dividers and other measuring techniques is much more useful to study during practice course in high voltage laboratories. Whole workshop course is connected with all kind of high voltage measurement. During this course doing all specific features, constructions, measurement principles and its result interpretations are fulfilled.

REFERENCES

1. W. Zaengl, E.Kuffel, J. Kuffel. High voltage engineering. Fundamentals. – Butterworth – Heinemann, 2000. – 539 p.
2. A. Rodewald and K. Feser. The generation of lightning and switching impulse voltages in the UHV region with an improved Marx circuit. Trans. IEEE PAS 93, 1974, pp. 414 – 420.
3. Marx E. Deutsches Reichspatent (German Patent) No. 455933.
4. D. Kind and H. Wehinger. Transients in testing transformers due to the generation of switching voltages. Trans. IEEE PAS 97, 1978, pp. 563 – 568.
5. J.D. Cockcroft and E.S. Walton. Experiments with high velocity ions. Proc. Roy. Soc. London, Series A, 136, 1932, pp. 619 – 630.

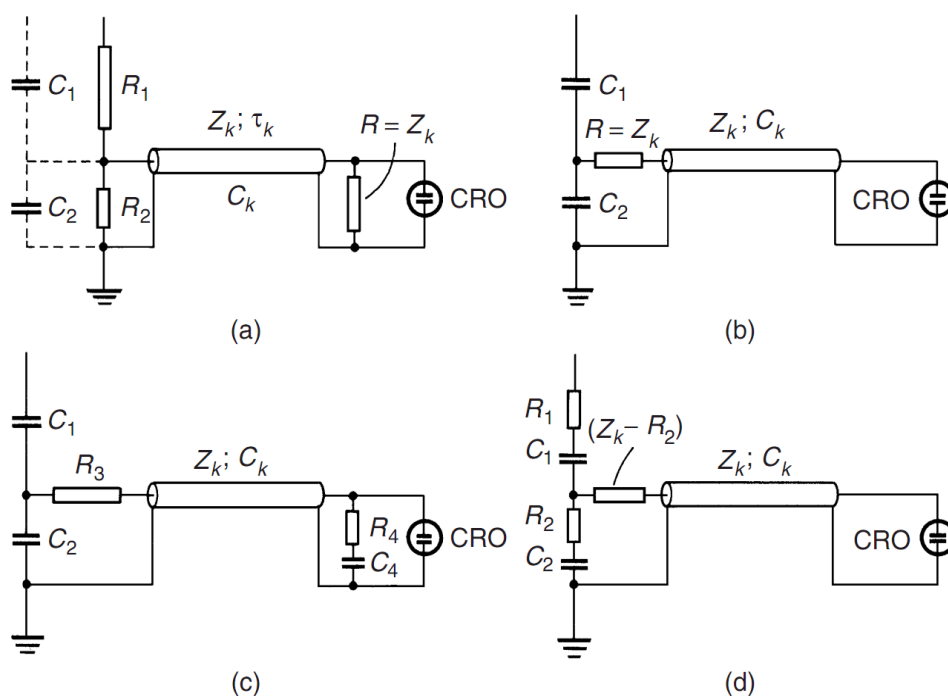


Figure 3.10 Circuits for signal cable matching:

a - resistor or parallel-mixed capacitor-divider, b - capacitor divider, simple matching, c - capacitor divider, compensated matching, d - damped capacitor divider

6. H. Frank, W. Hauschild, I. Kantelberg and H. Schwab. HV DC Testing Generator for Short Time Reversal on Load. 4th Int. Symposium on High Voltage Engineering, Athens, 1983, paper 5105.
7. W. Schufft and Y. Gotanda. A new DC Voltage Test System with Fast Polarity Reversal. 10th Int. Symposium on High Voltage Engineering, Montreal 1997, Vol. 4, pp. 37 – 40.
8. A.J. Schwab. High Voltage Measurement Techniques. MIT Press, Cambridge, London, England, 1972.
9. Comparative Calibration of Reference Measuring Systems for Lightning Impulse Voltages. Proc. Int. Symposium on High Voltage Engineering, Graz, Austria, 1995, p. 4469.
10. IEC Publication 52, 2nd Edition (1960). Recommendations for Voltage Measurements by Means of Sphere-gaps (one sphere earthed).
11. F.S. Edwards and J.F. Smee. The Calibration of the Sphere Spark-Gap for Voltage Measurement up to One Million Volts at 50 Hz. JIEE 82, 1938, pp. 655 – 657.
12. High voltage measurements, present state and future developments. Rev. Gen. Electricity, Special Issue, June 1978.

CHAPTER 4. OVERVOLTAGES: NATURE AND PROTECTION

4.1 General characteristic of overvoltages

Electrical and power systems are always subjected to overvoltages that have their origin in atmospheric discharges in which case they are called *external* or *lightning overvoltages*, or they are generated internally by connecting or disconnecting the system, or due to the systems fault initiation or extinction. The latter type is called *internal overvoltages*. This class may be further subdivided into *temporary overvoltages*, if they are oscillatory of power frequency or harmonics, and *switching overvoltages*, if they are heavily damped and of short duration. Temporary overvoltages occur almost without exception under no load or very light load conditions. Because of their common origin the temporary and switching overvoltages occur together and their combined effect has to be taken into account in the design of high voltage systems insulation.

The magnitude of the external or lightning overvoltages remains essentially independent of the system's design, whereas that of internal or switching overvoltages increases with increasing the operating voltage of the system. Hence, with increasing the system's operating voltage a point is reached when the switching overvoltages become the dominant factor in designing the system's insulation. Up to approximately 300 kV, the system's insulation has to be designed to withstand primarily lightning surges. Above that voltage, both lightning and switching surges have to be considered. For ultra high voltage systems, 750 kV and above switching overvoltages in combination with insulator contamination become the predominating factor in the insulation design. For the study of overvoltages occurring in power systems, a thorough knowledge of surge propagation laws is needed which can be found in a number of textbooks and will not be discussed here.

4.2 Nature of overvoltages

One of most dangerous source of overvoltage is lightning. Physical manifestations of lightning have been noted in ancient times, but the understanding of lightning is relatively recent. Franklin carried out experiments on lightning in 1744–1750, but most of the knowledge has been obtained over the last 50 to 70 years. The real incentive to study lightning came when electric transmission lines had to be protected against lightning.

Fundamentally, lightning is a manifestation of a very large electric discharge and spark. Several theories have been advanced to explain accumulation of electricity in clouds. The present section reviews briefly the lightning

discharge processes.

In an active thunder cloud the larger particles usually possess negative charge and the smaller carriers are positive. Thus the base of a thunder cloud generally carries a negative charge and the upper part is positive, with the whole being electrically neutral. The physical mechanism of charge separation is still a topic of research and will not be treated here. As will be discussed later, there may be several charge centres within a single cloud. Typically the negative charge centre may be located anywhere *between 500 m and 10 000 m above ground*. Lightning discharge to earth is usually initiated at the fringe of a negative charge centre. To the eye a lightning discharge appears as a single luminous discharge, although at times branches of variable intensity may be observed which terminate in midair, while the luminous main channel continues in a zig-zag path to earth. High-speed photographic technique studies reveal that most lightning strokes are followed by repeat or multiple strokes which travel along the path established by the first stroke. The latter ones are not usually branched and their path is brightly illuminated. The various development stages of a lightning stroke from cloud to earth as observed by high-speed photography is shown diagrammatically in Fig. 4.1. together with the current to ground. The stroke is initiated in the region of the negative charge centre where the local field intensity approaches ionization field intensity. During the first stage the leader discharge, known as the “*stepped leader*”, moves rapidly downwards in steps of 50 m to 100 m, and pauses after each step for a few tens of microseconds. From the tip of the discharge a ‘pilot streamer’ having low luminosity and current of a few amperes propagates into the virgin air with a velocity of about 1×10^5 m/sec. The pilot streamer is followed by the stepped leader with an average velocity of about 5×10^5 m/sec and a current of *some 100 A*. For a stepped leader from a cloud *some 3 km above ground* shown in Fig. 4.1 it takes about *60 m/sec* to reach the ground. As the leader approaches ground, the electric field between the leader and earth increases and causes point discharges from earth objects such as tall buildings, trees, etc. At some point the charge concentration at the earthed object is high enough to initiate an upwards positive streamer. At the instance when the two leaders meet, the “main” or “return” stroke starts from ground to cloud, travelling much faster ($\approx 50 \times 10^6$ m/sec) along the previously established ionized channel. The current in the return stroke is in the order of *a few kA to 250 kA* and the temperatures within the channel are *15 000° C to 20 000° C* and are responsible for the destructive effects of lightning giving high luminosity and causing explosive air expansion. The return stroke causes the destructive effects generally associated with lightning.

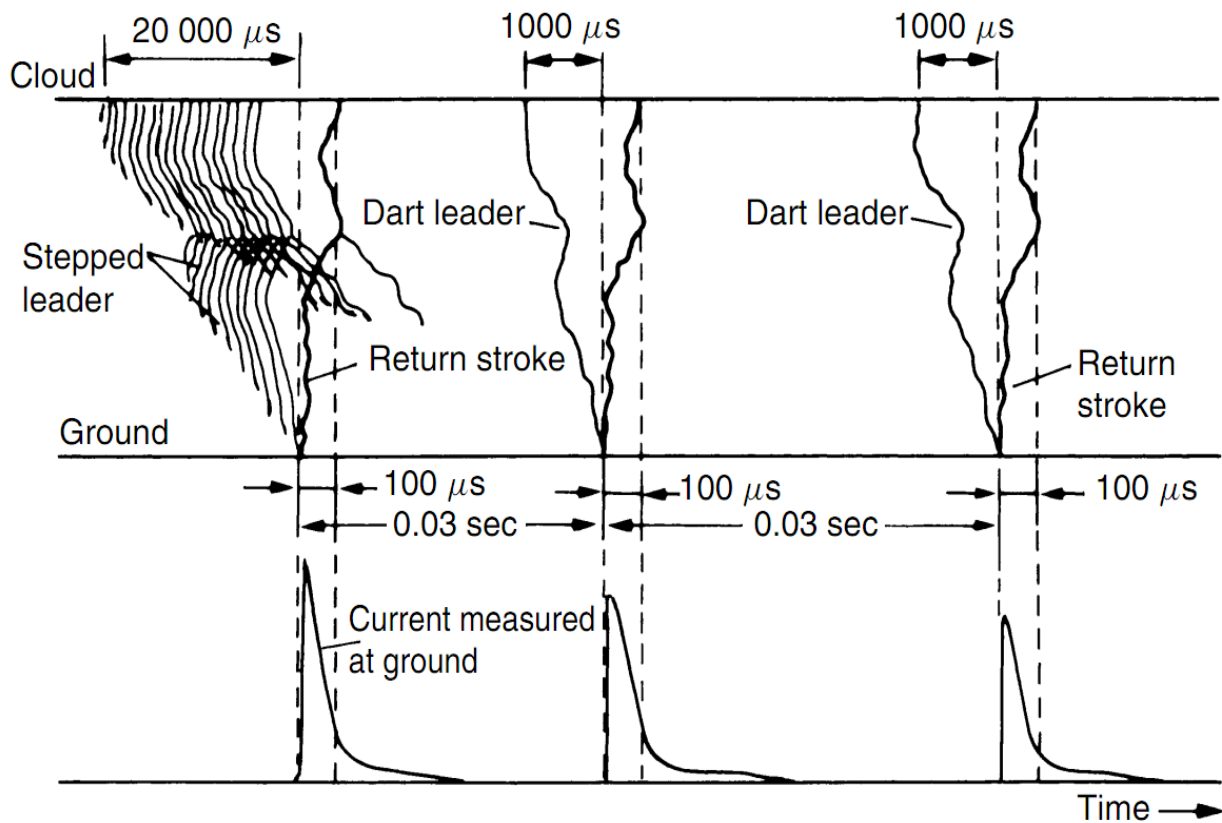
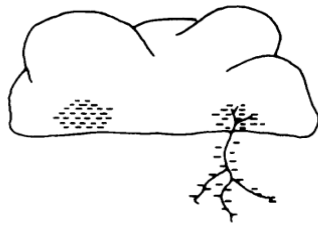


Figure 4.1 Representation of lightning mechanism and ground current

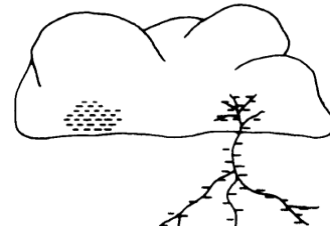
The return stroke is followed by several strokes at 10 to $300\ \text{m/sec}$ intervals. The leader of the second and subsequent strokes is known as the “*dart leader*” because of its dart-like appearance. The dart leader follows the path of the first stepped leader with a velocity *about 10 times faster* than the stepped leader. The path is usually not branched and is brightly illuminated.

A diagrammatic representation of the various stages of the lightning stroke development from cloud to ground in Figs 4.2(a) to (f) gives a clearer appreciation of the process involved. In a cloud several charge centres of high concentration may exist. In the present case only two negative charge centres are shown. In (a) the stepped leader has been initiated and the pilot streamer and stepped leader propagate to ground, lowering the negative charges in the cloud. At this instance the striking point still has not been decided; in (b) the pilot streamer is about to make contact with the upwards positive streamer from earth; in (c) the stroke is completed, a heavy return stroke returns to cloud and the negative charge of cloud begins to discharge; in (d) the first centre is completely discharged and streamers begin developing in the second charge centre; in (e) the second charge centre is discharging to ground via the first charge centre and dart leader, distributing negative

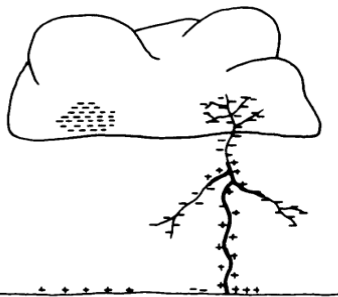
charge along the channel. Positive streamers are rising up from ground to meet the dart leader; (f) contact is made with streamers from earth,



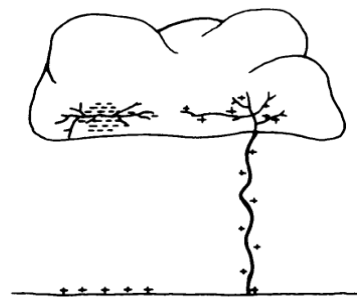
(a) Charge centres in cloud; pilot streamer and stepped leader propagate earthward; outward branching of streamers to earth. Lowering of charge into space beneath cloud.



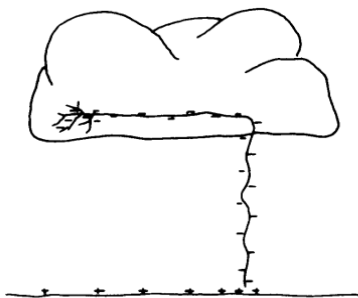
(b) Process of (a) almost completed; pilot streamer about to strike earth.



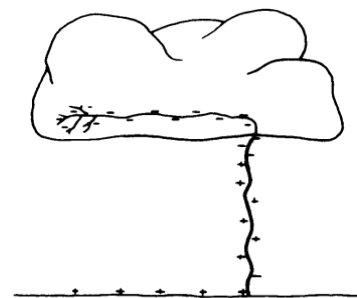
(c) Heavy return streamer; discharge to earth of negatively charged space beneath cloud.



(d) First charge centre completely discharged; development of streamers between charge centres within cloud.



(e) Discharge between two charge centres; dart leader propagates to ground along original channel; dart leader about to strike earth; negative charge lowered and distributed along stroke channel.



(f) Heavy return streamer discharge to earth of negatively charged space beneath cloud.

Figure 4.2 Schema of various stages of lightning stroke

heavy return stroke proceeds upwards and begins to discharge negatively charged space beneath the cloud and the second charge centre in the cloud.

Lightning strokes from cloud to ground account only for about 10 percent of

lightning discharges, the *majority of discharges during thunderstorms take place between clouds*. Discharges within clouds often provide general illumination known as “*sheath lightning*”.

It is very important to make an estimation of lightning parameters. To estimate the amount of energy in a typical lightning discharge let us assume a value of potential difference of 10^7 V for a breakdown between a cloud and ground and a total charge of 20 coulombs. Then the energy released is 20×10^7 Ws or about 55 kWh in one or more strokes that make the discharge. The energy of the discharge dissipated in the air channel is expended in several processes. Small amounts of this energy are used in ionization of molecules, excitations, radiation, etc. Most of the energy is consumed in the sudden expansion of the air channel. Some fraction of the total causes heating of the struck earthed objects. In general, lightning processes return to the global system the energy that was used originally to create the charged cloud.

The degree of hazard depends on circumstances. To minimize the chances of being struck by lightning during thunderstorm, one should be sufficiently far away from tall objects likely to be struck, remain inside buildings or be well insulated.

A direct hit on a human or animal is rare; they are more at risk from indirect striking, usually:

- (a) *when the subject is close to a parallel hit or other tall object,*
- (b) *due to an intense electric field from a stroke which can induce sufficient current to cause death,*
- (c) *when lightning terminating on earth sets up high potential gradients over the ground surface in an outwards direction from the point or object struck.*

Figure 4.3 illustrates qualitatively the current distribution in the ground and the voltage distribution along the ground extending outwards from the edge of a building struck by lightning. The potential difference between the person's feet will be largest if his feet are separated along a radial line from the source of voltage and will be negligible if he moves at a right angle to such a radial line. In the latter case the person would be safe due to element of chance. The danger to electric systems and apparatus comes from the potentials that lightning may produce across insulation. Insulation of power systems may be classified into two broad categories: ***external and internal insulation***.

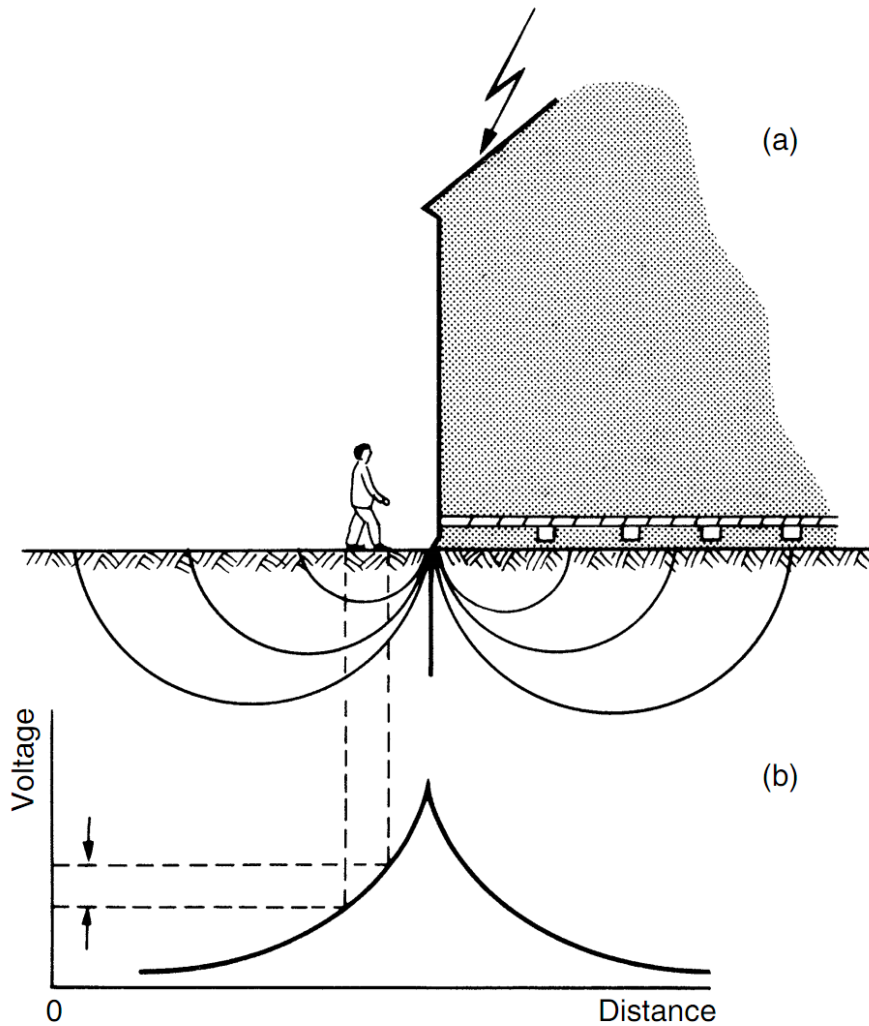


Figure 4.3 Current distribution and voltage distribution in ground due to lightning stroke to a building

External insulation is comprised of air and/or porcelain, special glass, etc., such as conductor-to-tower clearances of transmission lines or bus supports. If the potential caused by lightning exceeds the strength of insulation, a flashover or puncture occurs. Flashover of external insulation generally does not cause damage to equipment. Flashover is spark discharge on the dielectric surface. This phenomenon is described in Chapter 1, 1.4. The insulation is “self-restoring”. At the worst a relatively short outage follows to allow replacement of a cheap string of damaged insulation. *Internal insulation* most frequently consists of *paper*, *oil* or other *synthetic insulation* which insulates high voltage conductors from ground in expensive equipment such as transformers, generators, reactors, capacitors, circuit-breakers, etc. Failure of internal insulation causes much longer outages. If power arc follows damage to

equipment it may be disastrous and lead to very costly replacements.

The system's insulation has to be designed to withstand lightning voltages and be tested in laboratories prior to commissioning. Exhaustive measurements of lightning currents and voltages and long experience have formed the basis for establishing and accepting what is known as the standard surge or impulse voltage to simulate external or lightning overvoltages. *The international standard lightning impulse voltage* waveshape is an aperiodic voltage impulse that does not cross the zero line which reaches its peak in $1.2 \mu\text{sec}$ and then decreases slowly (in $50 \mu\text{sec}$) to half the peak value. The characteristics of a standard impulse are its polarity, its peak value, its front time and its half value time.

Extensive laboratory tests have shown that for external insulation the lightning surge flashover voltages are substantially proportional to gap length and that positive impulses give significantly lower flashover values than negative ones. In addition, for a particular test arrangement, as the applied impulse crest is increased the instant of flashover moves from the tail of the wave to the crest and ultimately to the front of the wave giving an impulse voltage – time (“V – T”) characteristic as was discussed in Chapter 1.

Internal, first of all, switching overvoltages are a result of repeated regular switching on – switching off procedure. It takes place in any electric energy system due to its working singularity. In power transmission systems with systems voltages of 220 kV and above, the electrical strength of the insulation to switching overvoltages becomes important for the insulation design. A considerable amount of data on breakdown under switching surges is available [8-10]. Many tests have shown that the flashover voltage for various geometrical arrangements under unidirectional switching surge voltages decreases with increasing the front duration of the surge, reaching the lowest value somewhere in the range between 100 and $500 \mu\text{sec}$. The time to half-value has less effect upon the breakdown strength because flashover almost always takes place before or at the crest of the wave.

4.3 Insulation coordination

Insulation coordination is the correlation of insulation of electrical equipment with the characteristics of protective devices such that the insulation is protected from excessive overvoltages. In a substation, for example, the insulation of transformers, circuit breakers, bus supports, etc., should have insulation strength in excess of the voltage provided by protective devices.

Electric systems insulation designers have two options available to them:

- *choose insulation levels for components that would withstand all kinds of overvoltages,*
- *consider, design and engineering protective devices that could be installed at the sensitive points in the system that would limit overvoltages there.*

The first alternative is unacceptable especially for ultra high voltage operating levels because of the excessive insulation required. Hence, there has been great incentive to develop and use protective devices. The actual relationship between the insulation levels and protective levels is a question of economics. Conventional methods of insulation coordination provide a margin of protection between electrical stress and electrical strength based on predicted maximum overvoltage and minimum strength, the maximum strength being allowed by the protective devices.

“**Insulation level**” is defined by the values of test voltages which the insulation of equipment under test must be able to withstand.

In the earlier days of electric power, insulation levels commonly used were established on the basis of experience gained by utilities. As laboratory techniques improved, so that different laboratories were in closer agreement on test results, an international joint committee, the Committee on Insulation Coordination, was formed and was charged with the task of establishing insulation strength of all classes of equipment and to establish levels for various voltage classification. In 1941 a detailed document was published giving basic insulation levels for all equipment in operation at that time. The presented tests included standard impulse voltages and one-minute power frequency tests.

In the early days insulation levels for lightning surges were determined by evaluating the 50 per cent flashover values (*BIL*) for all insulations and providing a sufficiently high withstand level that all insulations would withstand. For those values a volt – time characteristic was constructed. Similarly the protection levels provided by protective devices were determined. The two volt – time characteristics are shown in Fig. 4.4. The upper curve represents the common BIL for all insulations present, while the lower represents the protective voltage level provided by the protective devices. The difference between the two curves provides the safety margin for the insulation system. Present-day practices of insulation coordination rely on a statistical approach which relates directly the electrical stress and the electrical strength.

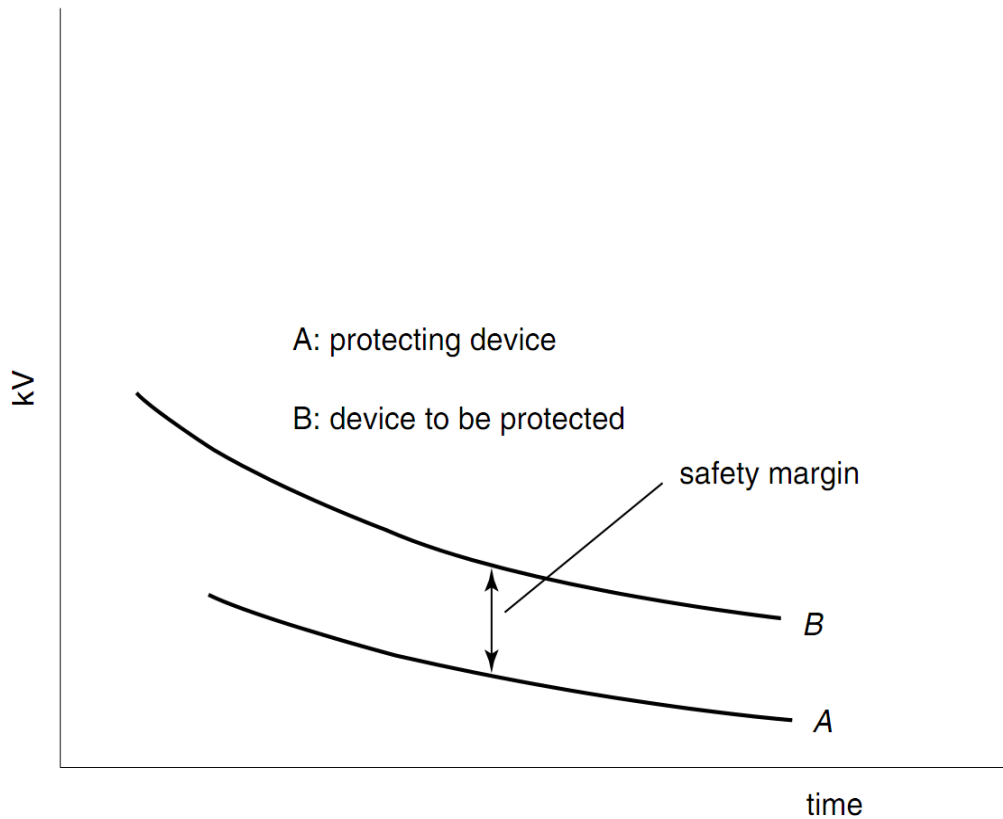


Figure 4.4 Coordination and protection levels

This approach requires a knowledge of the distribution of both the anticipated stresses and the electrical strengths. The statistical nature of overvoltages, in particular switching overvoltages, makes it necessary to compute a large number of overvoltages in order to determine with some degree of confidence the statistical overvoltages on a system.

In engineering practice it would become uneconomical to use the complete distribution functions for the occurrence of overvoltage and for the withstand of insulation and a compromise solution is accepted as shown in Figs 4.5 (a, b) for guidance. Curve on Fig. 4.5 (a) represents probability of occurrence of overvoltages of such amplitude V_S that only 2 per cent (shaded area) has a chance to cause breakdown. V_S is known as the “statistical overvoltage”. In Fig. 4.5 (b) the voltage V_W is so low that in 90 per cent of applied impulses, breakdown does not occur and such voltage is known as the “statistical withstand voltage” V_W .

The “**protection level**” provided by *arresters* is established in a similar manner to the “**insulation level**”; the basic difference is that the insulation of *protective devices* (arresters) **must not withstand the applied voltage**.

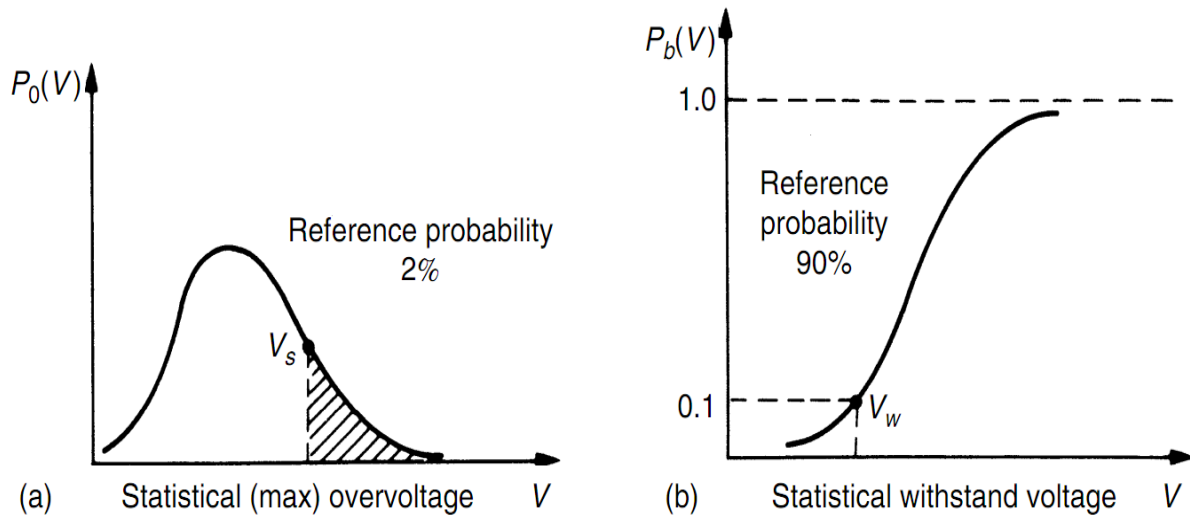


Figure 4.5 Diagram of probability for overvoltages (a) and insulation withstand strength (b)

In practice, the protective gap will in general break down before the insulation and will cause a reduction (to a safe limit) in overvoltage reaching the protected insulation.

4.4 Protection devices

Special protective devices from overvoltages are called arresters. The development of metal oxide arresters (MOA) represented a breakthrough in overvoltage protection devices. It became possible to design arresters without using gaps which were indispensable in the conventional lightning arresters, which utilized non-linear resistors made of silicon carbide (SiC) and spark gaps. Figs 4.6 and 4.7 show a block diagram of the valve arrangements in the two types of arrester. In device of Fig. 4.6 the elements and the spark gaps are connected in series. In other arrester's type (Fig.4.7) the elements are stacked on top of each other without the need for spark gaps.

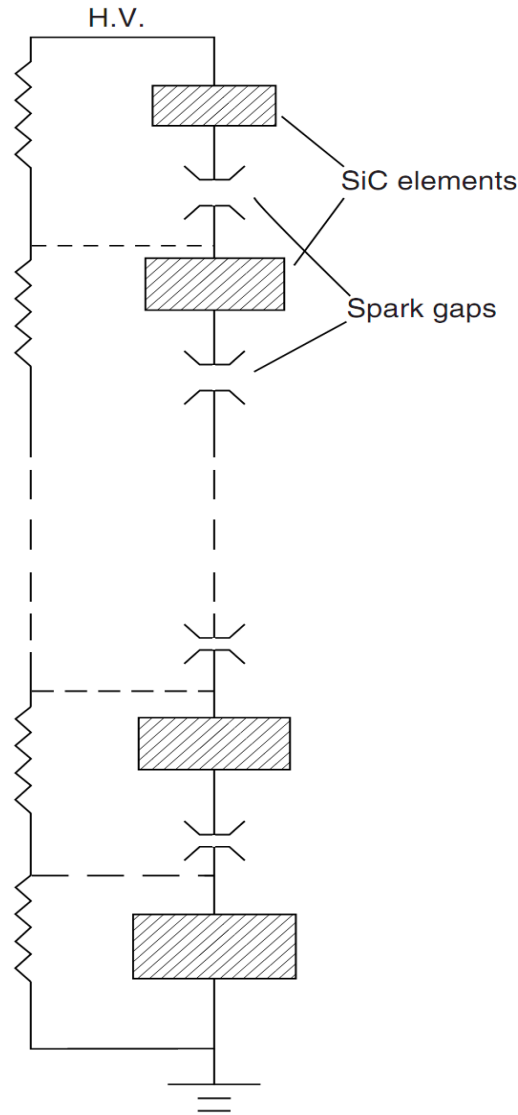


Figure 4.6 Block diagram of valve SiC-type arrester

An ideal lightning arrester should:
conduct electric current at a certain voltage above the rated voltage;
hold the voltage with little change for the duration of overvoltage;
substantially cease conduction at very nearly the same voltage at which
conduction started.

In SiC arrester type the three functions are performed by the combination of the series spark gaps and the SiC elements. In the case of MOA arrester the metal oxide valve elements perform all three functions because of their superior non-linear resistivity. The volt – current characteristics for the two types of arresters can be represented by the following equations:

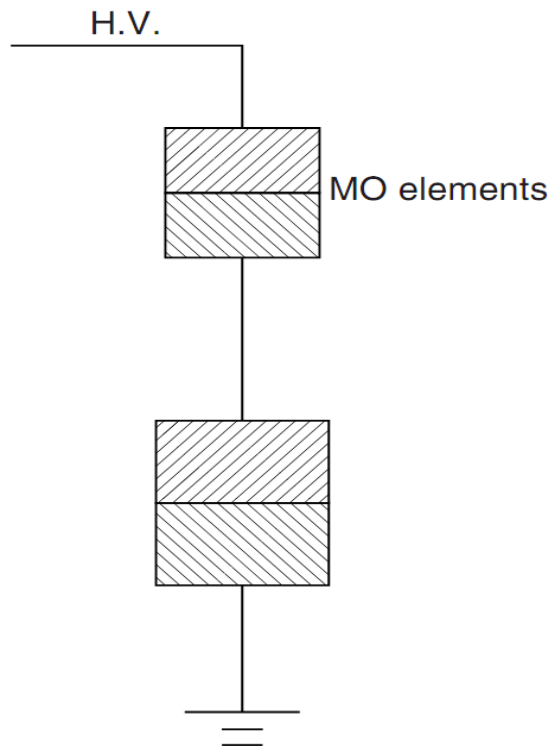


Figure 4.7 Block diagram of valve arrester MOA-type

$$\text{For SiC valves: } I = kV^a \text{ where } a=4-6 \quad (4.1)$$

$$\text{For ZnO valves: } I = kV^b \text{ where } k=\text{const, } b=25-30 \quad (4.2)$$

Typical volt – current characteristics for the valve elements used in the two types of arresters are plotted in Fig. 4.8. The metal oxide varistors, which consist of compacted and sintered granules of zinc oxide with a small amount of other carefully selected metal oxide additives (Bi_2O_3 , MnO , Cr_2O_3 , Sb_2O_3) to improve the ***V–I non-linearity***, were first introduced in the electronics industry in 1968 by Matsushita Electric Industrial Co. in Japan.

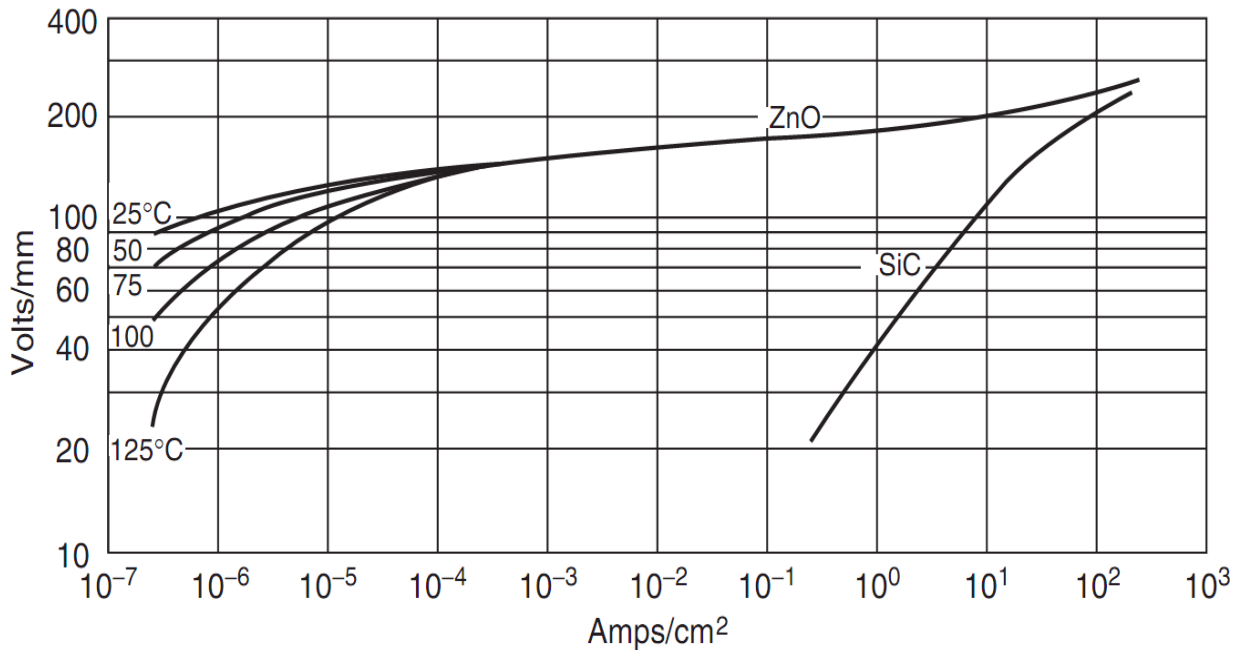


Figure 4.8 Volt-ampere characteristics of zinc oxide and silicon carbide valve elements

The ZnO grains have a low resistivity, while the additives (oxides) which form the boundaries between the grains provide high resistance. The two are strongly bonded when sintered at high temperature.

From Fig. 4.8 it can be seen that for a change in current from 10^{-3} to 10^2 A/cm², the voltage increase for ZnO is only 56 per cent. With such a high degree of non-linearity it is entirely feasible to use these elements without series gaps in an arrester with a current of only tens of μ A at operating voltage.

The elements are manufactured in the form of discs of several sizes. The disc voltage rating has been increasing with the improvement in the manufacturing technology and the microstructure composition, e.g. Fig. 4.9 compares the V – I characteristics of an older type ZnO element with that of a new type, both developed by Mitsubishi.

It is noted that the voltage rating per unit valve has been approximately doubled. For higher voltage and current ratings the discs are arranged in series and in parallel.

Figure 4.10 shows a schematic structure of a three-column arrangement of the arrester valves in an advanced MOA compact structure.

In Fig. 4.11 is shown part of an assembled advanced 500 kV MOA. The percentages indicate the reduction in size by replacing the older type MOA with the advanced MOA elements whose V – I characteristics are shown in Fig. 4.11.

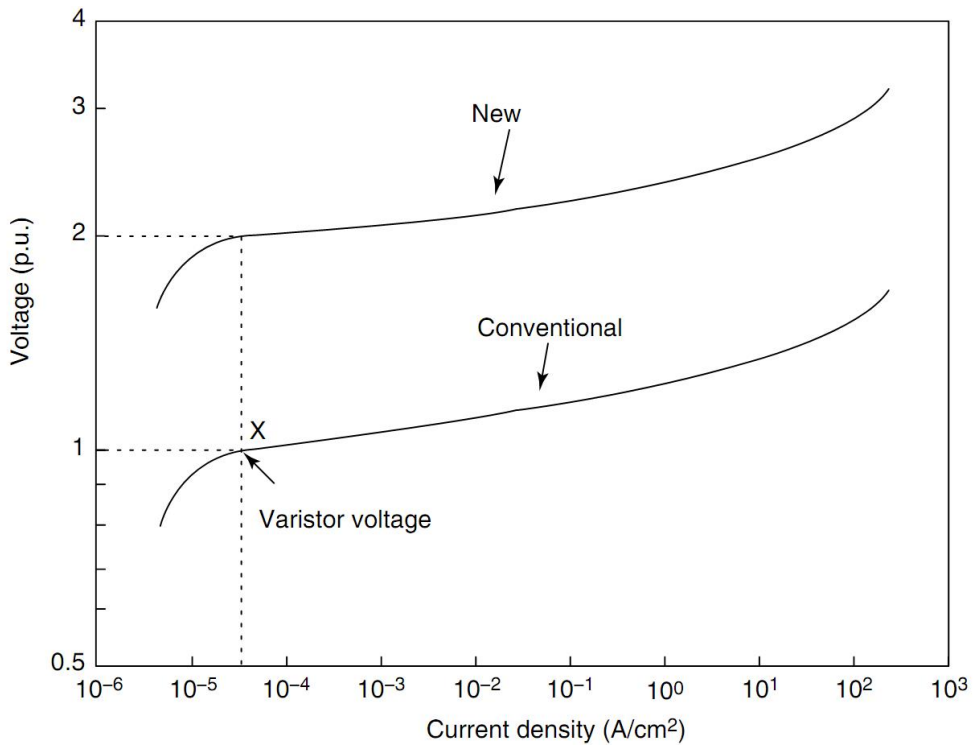


Figure 4.9 Comparison of volt – current characteristics of advanced MOA (new) with that of an older type MOA (conventional)

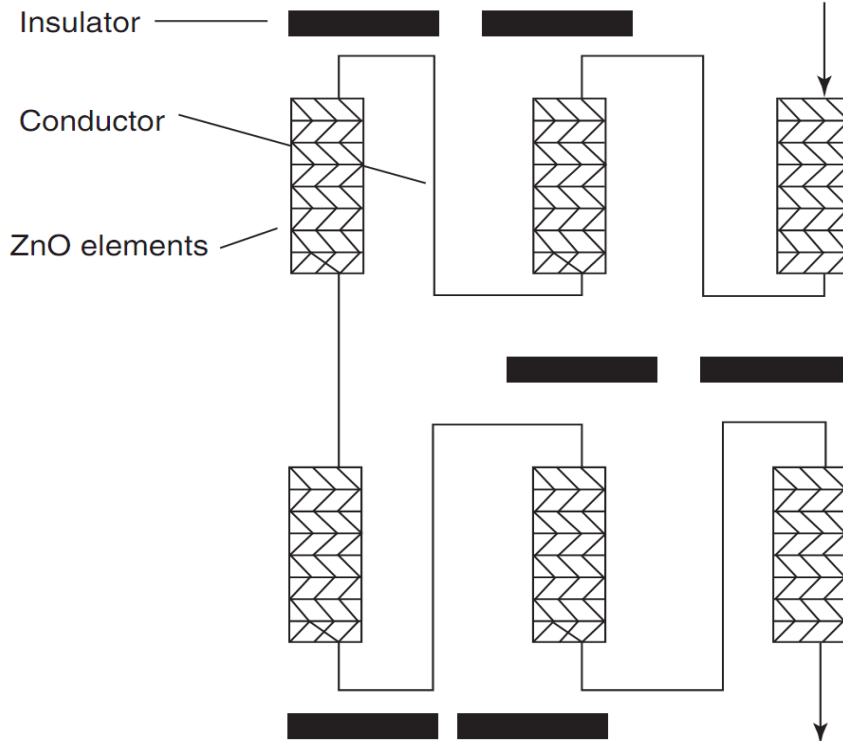


Figure 4.10 Structure of a three column arrangement of arrester elements

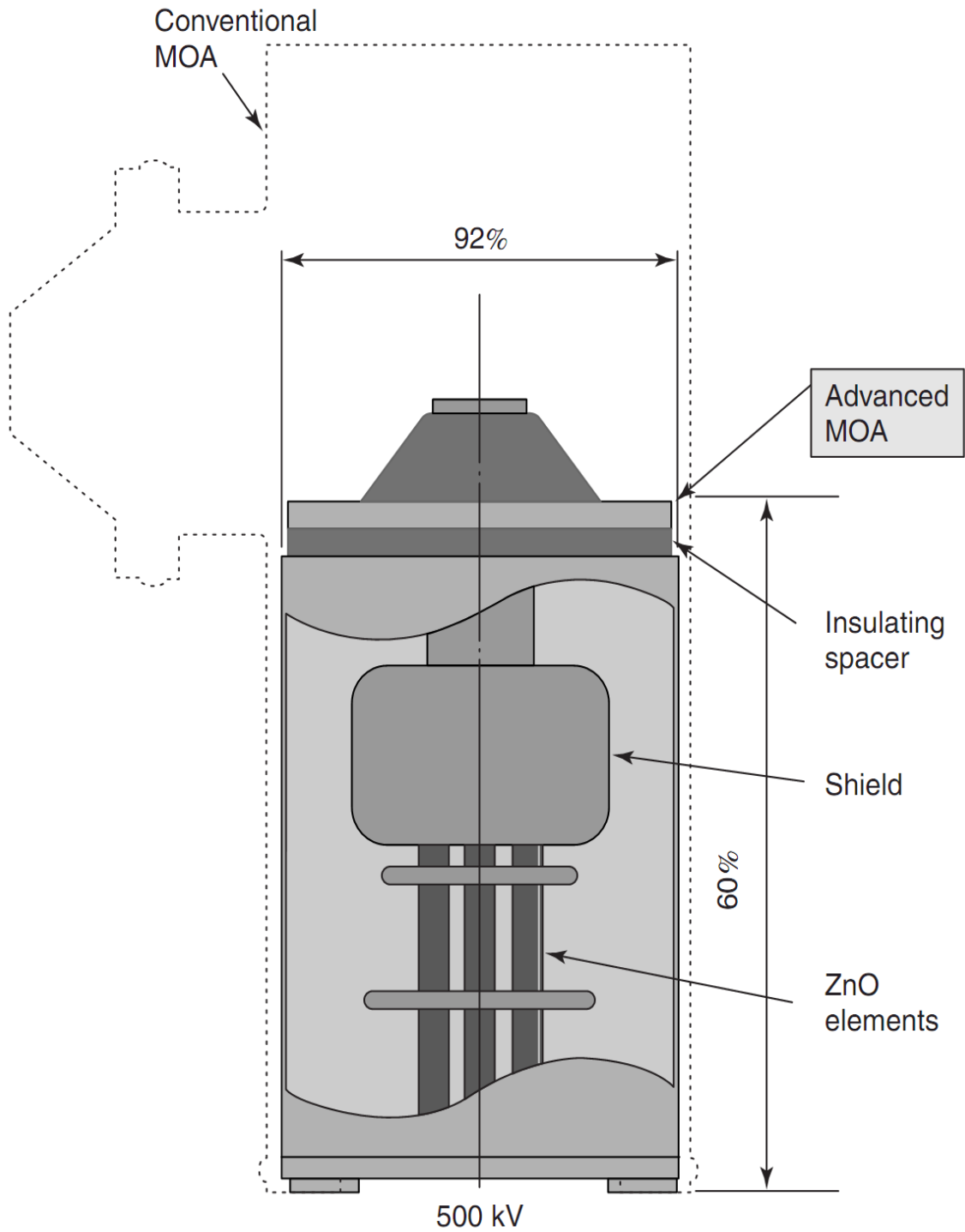


Figure 4.11 Part of an assembled 500 kV MOA arrester.

In this construction the individual surge arresters are interconnected by means of corona-free stress distributors. The modular design and the light-weight construction allow easy on-site engineering and in the event of any

units failing the individual unit may be readily replaced.

The advantages of the polymeric-housed arresters over their porcelain-housed equivalents are several and include:

- *No risk to personnel or adjacent equipment during fault current operation.*
- *Simple light modular assembly – no need for lifting equipment.*
- *Simple installation.*
- *High-strength construction eliminates accidental damage during transport.*
- *The use of polymer materials and/or silicon rubber reduces pollution flashover problems.*

Thus the introduction of ZnO arresters and their general acceptance by utilities since late 1980s, and in 1990s in protecting high voltage substations, has greatly reduced power systems protection problems.

In the earlier construction the valve elements were mounted within a ceramic housing. The metal oxide elements were surrounded by a gaseous medium and the end fittings were generally sealed with rubber O-rings. With time in service, especially in hostile environments, the seals tended to deteriorate allowing the ingress of moisture. In the 1980s polymeric-housed surge arresters were developed. Bowthorpe EMP (UK) manufactures a complete range of polymeric-housed arresters extending from distribution to heavy duty station arresters for voltages up to 400 kV. In their design the surface of the metal oxide elements column is bonded homogeneously with glass fibre reinforced resin. This construction is void free, gives the unit a high mechanical strength, and provides a uniform dielectric at the surface of the metal oxide column. The housing material is a *polymer (EPDM) – Ethylene propylene diene monomer* – which is a hydrocarbon rubber, resistant to tracking and is particularly suitable for application in regions where pollution causes a problem. A cross-section detailing the major features of a polymeric-housed arrester is given in Fig. 4.12.

The ZnO elements are separated by aluminium blocks which serve as heat sinks. To achieve higher voltages and higher current ratings a modular construction with the individual units mounted in series – parallel arrangement is shown in Fig. 4.13.

Arresters are important part of every electric energy system. Valve arresters are used in majority of World's electric energy systems. Design and engineering of ZnO-type arrester allowed make protection degree more high and technological. Essential more rapid non-linearity of ZnO, absence of spark gaps makes this arrester type very prospective for electric energy systems around the World.

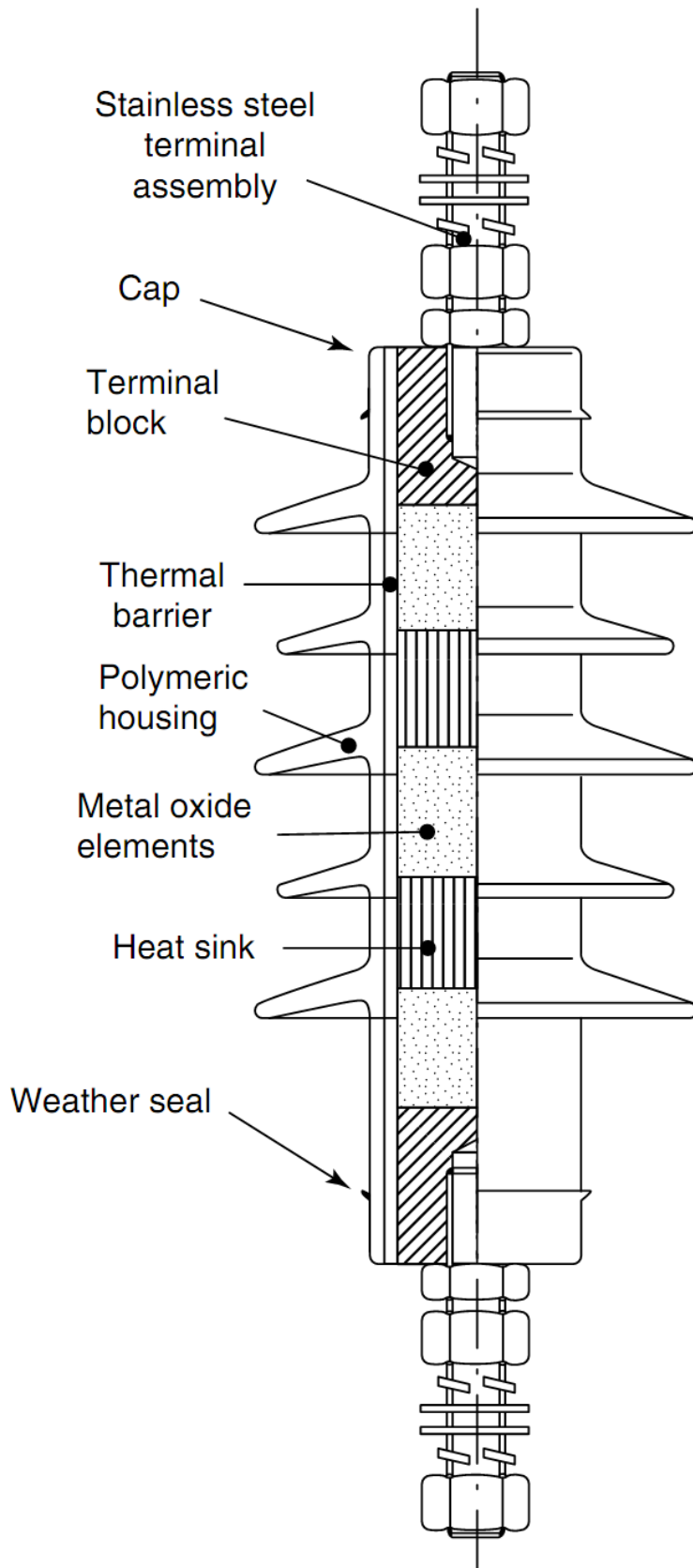


Figure 4.12 Cross section of a polymer-housed arrester

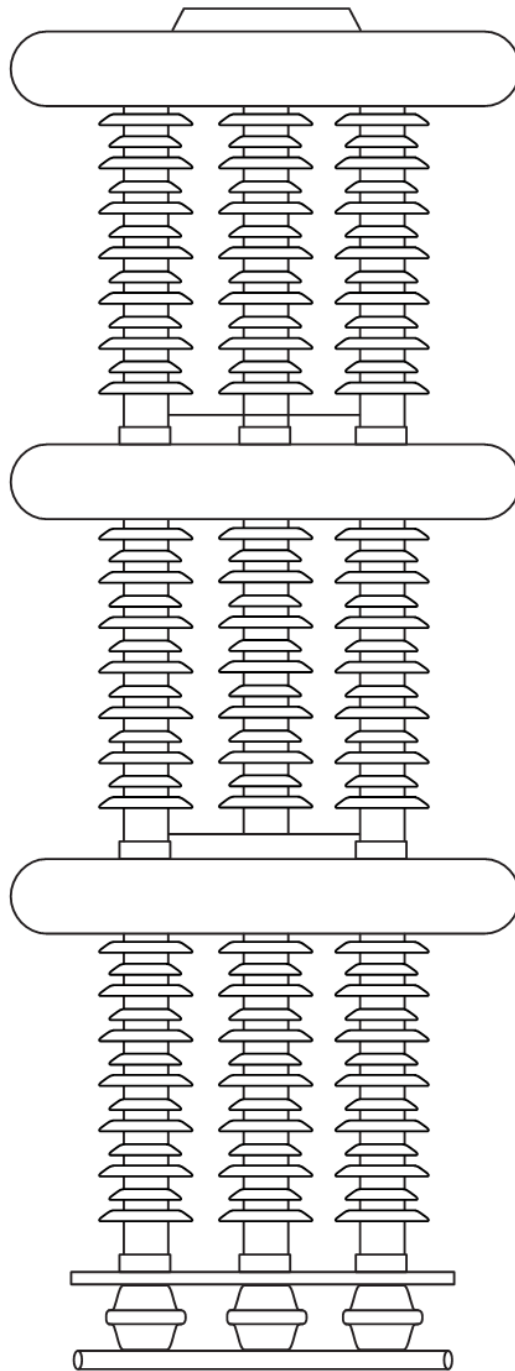


Figure 4.13 Construction of a series-parallel polymeric-housed arrester

REFERENCES

1. Hydro-Quebec Symposium on Extra-High Voltage Alternating Current, Oct. 1973.
2. W.W. Lewis. *The Protection of Transmission Systems against Lightning*. Dover Publications, Inc., New York, 1965.
3. Dielectric Stresses and Coordination of Insulation. Brown Boveri Publication No. CH-A050020E No. 4, 1972.
4. International Electrotechnical Commission. IEC Intern. Standard IEC 71-2 1996 'Insulation Coordination Part 2. Application Guide'.
5. R. Kuffel, J. Giesbrecht, T. Maguire and P. McLaren. 'RTDS' A Fully Digital Power System Simulator Operating in Real Time, Proceedings of the First International Conference on Digital Power System Simulators, pp. 19 – 24, April 1995.
6. E.C. Sakshang *et al.* A new concept in Station Design. IEEE Trans. PAS, Vol. 96, No. 2, 1977, pp. 647 – 656.
7. A. Sweetana *et al.* Design, development and testing of 1200 kV and 550 kV gapless surge arresters. IEEE Trans. PAS Vol. 101, No. 7, 1982, pp. 2319 – 2327.
8. W. Zaengl, E.Kuffel, J. Kuffel. High voltage engineering. Fundamentals. – Butterworth – Heinemann, 2000. – 539 p.
9. C. Wadhwa. High voltage engineering. – New age international limited, New Delhi, India, 2001. – 282 p.
10. V. Ushakov. High voltage engineering. – Tomsk, TPU, 2001. – 253 p.

CHAPTER 5. ADVANCED HIGH VOLTAGE TECHNOLOGIES

5.1 New approaches to high voltage equipment diagnostics

5.1.1 Dielectric spectroscopy technology

The main aim of this paragraph is to present and to recall the fundamentals of advanced method high voltage insulation diagnostic of high voltage equipment, first of all power transformers. It is based on dielectric spectroscopy. These are *dielectric response in time- and frequency-domain* by introducing into the basic equations. From these fundamentals, identifying and diagnostic methods can be derived which become more and more attractive for a condition based maintenance of electric power equipment which has to be applied in future.

Today, the catchword in utility companies is condition-based or detective testing and maintenance, or even life management, as opposed to time-based or preventive maintenance only. The reasons for this evolution are well known. In North America, for instance, their roots can be found in restructuring and re-regulation of the Electric Utility Industry, and here in Europe, it was the adoption of the “Single Market Directive” which became the norm in February 1999, whereas it was still the exception many years before [1]. The main issue of this regulation of the electricity market, which becomes now subdivided into independent power producers, transmission companies, system operators and distribution companies, is to encourage competition still maintaining basic public policy and service objectives. All partners within this new scheme are thus forced to cut costs in maintenance and operation without endangering steady supply of electricity to demanding customers. Costs can be reduced first of all by a transition from time-based maintenance (TBM) to condition based maintenance (CBM), if the actual conditions of the expensive high voltage (HV) components within the electric power transmission systems are reliably known. The application of “unscheduled maintenance”, the philosophy of which is based on a reactive mode of operation, will not at all reduce costs. Unscheduled maintenance means that only then repairs and maintenance will be made if the equipment, as e.g. a transformer or cable, breaks down. But this causes in general a downtime of the electricity supply so that breakdowns become much more costly than planned maintenance. A CBM based on diverse, reliable diagnostic tools should be applied today. Driving forces for the development and application of improved diagnostic methods are the steadily increasing age of expensive HV components. In many parts of the world, the majority of e.g. large power

transformers have been installed in the 60's of the last century. Also, cable technology did change at this time and the first generations of PE or XLPE cables are still prone to breakdowns. All these facts are very well known. It is not the aim of this contribution to discuss the full complexity of all the different diagnostic techniques as already successfully applied to different HV components. Most of the dangerous breakdowns, however, are caused by ageing effects of the HV insulation systems as used within these components, and there is still some lack of appropriate tools to diagnose insulation materials non-destructively and reliably in the field of application. New methods have been published in the last decade and even before, for which reliable diagnostics are claimed. Many of these methods are based on changes of dielectric properties of the insulation, whose basics are often not very well known. Therefore, this contribution will predominantly introduce into such basics but will also provide some hints to more recent instruments, which are able to quantify dielectric properties in the field.

Experience shows that most of electric power engineers are not too familiar with the fundamentals of “dielectric response functions” and their background. The following short introduction may contribute to close this gap. Every kind of insulation material consists at an atomic level of negative and positive charges balancing each other in microscopic as well as in more macroscopic scales (if no uni-polar charge was deposited within the material before by well known charging effects). Macroscopically, some localised space charge may be present, but even then an overall charge neutrality exists. As soon as the material is exposed to an electric field (as generated by a voltage across electrodes between which the dielectric is embedded), very different kinds of dipoles become excited even within atomic scales. A local charge imbalance is thus “induced” within the neutral species (atoms or molecules) as the “centres of gravity” for the equal amount of positive and negative charges, $\pm q$, become separated by a small distance d , thus creating a dipole with a dipole moment, $p = qd$, which is related to the “local” or “microscopic” or a slow process as e.g. active in cable material electric field E acting in close vicinity of the species. Thus, the dipole moment can also be written as $p = \alpha E$, where α is the “polarisability” of the species or material under consideration. Note that p , d and E are vectors not marked here. As the distance d will be different for different species as well as the number of dipoles per unit volume, also their polarisability is different. Due to chemical interactions between dissimilar atoms forming molecules, many molecules will have a constant and stable distance d between the charge centers thus forming “permanent dipole moments”, which are in general not uniformly distributed within the matter as long as no external field is applied. (Note, that any kind of “permanent polarisation”, as effec-

tive in *electrets* or *ferroelectrics*, is not considered here). The macroscopic effect of the polarisation–ability of individual species is finally manifested in a general relation between the **macroscopic polarisation P** and the number of polarised species N per unit volume of the matter. These relationships are known, but not treated here. But let us recall now the main mechanisms producing polarisation P : “**Electronic Polarisation**” is effective in every atom or molecule as the centre of gravity of the electrons surrounding the positive atomic cores will be displaced by the electric field E . This effect is extremely fast and thus effective up to optical frequencies. – “**Ionic (or molecular) Polarisation**” refers to matter containing molecules forming ions, which do not separate by low electric fields or working temperatures. - “**Dipolar (or orientation) Polarisation**” belongs to matter containing molecules with *permanent* dipole moments with orientations statistically distributed due to the action of thermal energy. Under the influence of E , the dipoles will be oriented only partially, so again, a linear dependency of P and E exists. Ionic and dipolar polarisation are still quite fast effects and may follow AC frequencies up to MHz or GHz. - “**Interfacial Polarisation**” is predominantly effective in insulating materials composed of different dielectric materials *as e.g. oil impregnated paper/cellulose*. The mismatch of the products permittivity by electric conductivity for the different dielectrics forces movable positive and negative charges to become deposited on the interfaces of different insulating materials, thus forming dipoles. This phenomena is often *very slow* and in general active in a very low frequency range up to power frequencies. – Finally, **hopping of charge carriers** between localised sites of charges may occur creating also polarisation. This is in general also a slow process as e.g. active in cable materials (PE etc.). For more detail see e.g. [2, 3].

So, the dielectric polarisation is the result of a relative shift of positive and negative charges in the matter. During all of these processes, the electric field is therefore *not able to force the charges to escape from the matter*, which would cause inherent electric condition.

Dielectric Response Methods are based on fundamental interactions between well known electric quantities: Usually, HV insulation materials (also called dielectrics) are isotropic and in general homogeneous, at least at macroscopic scales. Then, the vectors of (macroscopic) polarisation P and the electric field E are of equal direction and interrelated by:

$$P = \chi \varepsilon_0 E \quad (5.1)$$

where χ is the dielectric susceptibility of the matter, a dimensionless number which is zero for ideal vacuum. Thus, the susceptibility χ accounts

for all kinds of polarisation processes as effective within a dielectric, ε_0 is the permittivity of vacuum. This provides already a hint that all polarisation processes induce also electric charges at the electrodes, between which the dielectric is sandwiched. From equation (5.1) it can well be deduced that the polarisation P will change or vanish if the field E is changed or set to zero. A reduction of E will thus lead to a *depolarisation* process, which will follow with some delay or retardation to the reduction of E . Dielectric properties become thus *dynamic* events which can be detected in **time-** as well as in **frequency domain**.

In a *vacuum-insulated* electrode arrangement, the vector of *electric displacement* (or “*dielectric flux density*” or “*electrical induction*”) D is exactly proportional to the electric field E ,

$$D = \varepsilon_0 E \quad (5.2)$$

or, if the electric field is generated by a time-varying voltage,

$$D(t) = \varepsilon_0 E(t) \quad (5.3)$$

here, ε_0 is again the permittivity of vacuum. The origin of D and E is in general provided by a voltage source connected to the electrodes of any electrode arrangement under consideration. No time delay at all will exist between both magnitudes, if the time scales considered produce still “electrostatic field conditions”. Note, however, that D represents the (positive and negative) electric charges per unit area as induced at the electrode surface, these charges are the origin – sources and sinks – of all electric field lines. For time-varying fields, $E(t)$, the so called “displacement current” must be supplied by the voltage source to maintain the area charge density at the electrodes. This current is governed by dQ/dt , where Q is the total electric charge deposited on each of the electrodes. If now the vacuum is replaced by any kind of isotropic dielectric material, the electric displacement D of equation (5.2 and 5.3) increases by its inherent (macroscopic) polarisation P as defined in equation (5.1):

$$D(t) = \varepsilon_0 E(t) + P(t) = \varepsilon_0 (1 + \chi) E(t) \quad (5.4)$$

This equation is quite essential as it separates the two kinds of charge induction. As for *isotropic* materials both vectors, P and D , are still in parallel to E , we can further on avoid bold letters to mark vectors. However, the time dependency of $P(t)$ will not any more be the same as that of $E(t)$, as

the different polarisation processes have different time delays with respect to the appearance of E . This delay is obviously caused by the time-dependent behaviour of the susceptibility $\chi = \chi(t)$. This time delay may be understood best with the following reflections: Let us assume, that a step-like constant electric field of magnitude E_0 is applied within the dielectric at any time t_0 and that this field remains constant for $t \geq t_0$. The dielectric can then be completely characterised by its time dependent susceptibility $\chi(t)$ or its specific polarisation $P(t)$ as a **response in time domain**, i.e. the formation and evolution of the different kinds of polarisation processes, which develop as well within extremely short times (as e.g. electronic polarisation) or are much slower or even very slower (as e.g. interfacial polarisation). For $t \leq t_0$, the magnitude of the susceptibility or polarisation is still zero. Figure 5.1 illustrates this situation:

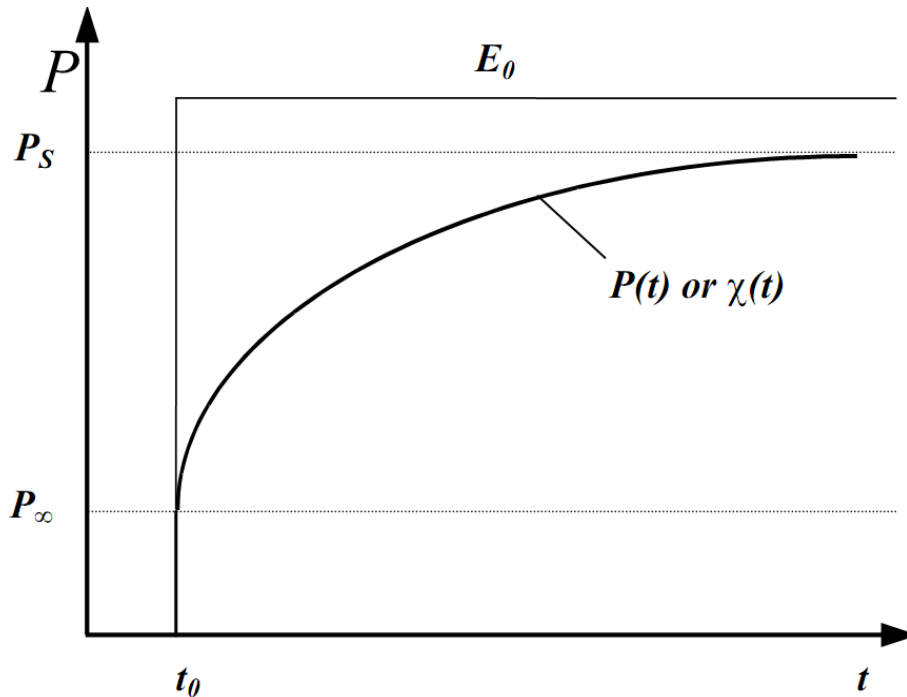


Figure 5.1 Polarization of a dielectric exposed to a step field magnitude E_0

This, according to equation. (5.1), can be expressed as

$$\frac{P(t)}{E_0} = \varepsilon_0 \chi(t) l(t) \quad (5.4)$$

where $\chi(t)$ as well as $P(t)$ represent “*step response functions*”. The factor $I(t)$ is used to indicate the unit step. It is necessary to note, however, that in fig. 1 the first part of these functions are simplified by an ideal step to account for the very fast polarisation processes, marked by an “*instantaneous polarisation*”, $P(t = t_0) = P_\infty$. This step can in general not be recorded neither in time— nor in an adequate frequency domain. As all kinds of polarisation become finite and will settle at longer times, the polarisation becomes finally “static”, $P(t \rightarrow \infty) = P_s$, i.e. for a selected time static. Due to fig. 1, the step response of this somewhat simplified polarisation can now be written as:

$$P(t) = P_\infty + (P_s - P_\infty)g(t - t_0) \quad (5.5)$$

where $g(t)$ is dimensionless, monotonically increasing function. The equation (5.4) may also be written as:

$$P(t) = \varepsilon_0 [\chi_\infty + (\chi_s - \chi_\infty)g(t - t_0)]E_0 \quad (5.6)$$

As known from general circuit theory, it is now possible to compute any other time dependent polarisation $P(t)$ for *any other* time dependent excitation $E(t)$ of a test object, as the special solutions for the step excitation are already known. This can be done by means of “*Duhamel’s Integral*” or convolution in the time domain. For the quantities as used in equation. (5.6), the result is:

$$P(t) = \varepsilon_0 \chi_0 E(t) + \varepsilon_0 \int_{-\infty}^t f(t - \tau) E(\tau) d\tau \quad (5.7)$$

where $f(t)$ is the so called dielectric response function.

$$f(t) = (\chi_s - \chi_\infty) \frac{\partial g(t)}{\partial t} = (\varepsilon_s - \varepsilon_\infty) \frac{\partial g(t)}{\partial t} \quad (5.8)$$

$f(t)$ is obviously a ***monotonically decreasing*** function and inherent to the dielectric investigated.

The polarisation $P(t)$ is not an observable magnitude by itself, but it produces the main part of the ***polarisation*** (or absorption, or charging) ***current*** in a test object if the electric field, $E(t)$, is ***suddenly*** applied. But up to now, we have not yet considered any inherent or “pure” dc conductivity σ_0 ,

which represents the movement of the free charges in the dielectric and which is **not** involved in polarisation. As already postulated by Maxwell in 1891 [4], this field $E(t)$ generates a total current density $j(t)$, which can be written as the sum of conduction, vacuum and polarisation displacement current:

$$j(t) = \sigma_0 E(t) + \frac{\partial D(t)}{\partial t} = \sigma_0(E) + \varepsilon_0 \frac{\partial E(t)}{\partial t} + \frac{\partial P(t)}{\partial t} \quad (5.9)$$

Taking into account $\varepsilon_\infty = 1 + \chi_\infty$ equation (5.9) can be written as:

$$j(t) = \sigma_0 E(t) + \varepsilon_0 [\varepsilon_\infty \delta(t) + f(t)] E(t) \quad (5.10)$$

Equation (8a) is thus a first basis for the measurement of the dielectric response function $f(t)$. For doing so, a step-like dc charging voltage of magnitude U_C which must be constant and free of ripple, is suddenly switched to the test object which has been totally discharged before. Then a **polarisation current** $i_{pol}(t)$ through the test object can be recorded according to the equation:

$$i_{pol}(t) = C_0 U_C \left[\frac{\sigma_0}{\varepsilon_0} + \varepsilon_\infty \delta(t) + f(t) \right] \quad (5.11)$$

where C_0 is the geometric or vacuum capacitance of the test object and $\delta(t)$ is the delta function originated from the applied step voltage at $t=t_0$.

This polarisation current contains three parts. The first one is related to the intrinsic conductivity of the object, the last one represents all polarisation processes as activated during the time of voltage application and the middle part with the delta function can not be recorded in practice due to the large dynamic range of the current amplitudes.

A polarisation current measurement can be stopped if the current becomes either stable due to the *dc* term or very low. Immediately following the polarisation, the **depolarisation** (or discharging) **current** i_{depol} can be measured by a subsequent short-circuiting of the sample, as shown on figure 5.2.

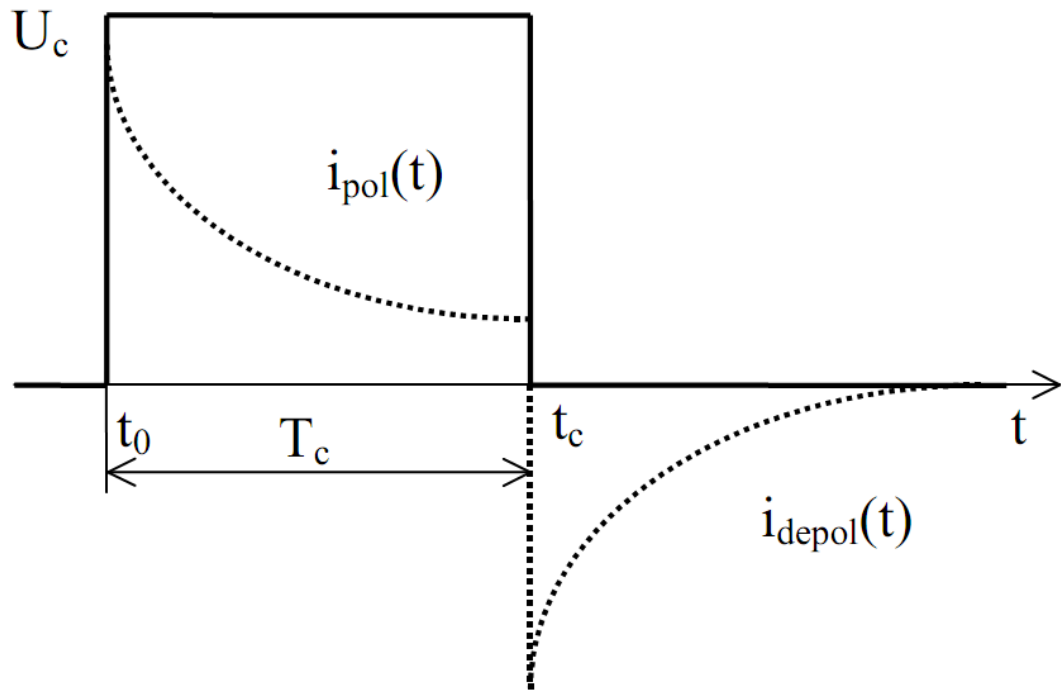


Figure 5.2 Principle of relaxation current measurement

According to the superposition principle and neglecting the second term in equation.(5.11) which is again a very short current pulse, we get for $t \geq (t_0 + T_c)$:

$$i_{depol}(t) = -C_0 U_c [f(t) - t(t + T_c)] \quad (5.12)$$

where T_c is the time during which the step voltage for polarisation was applied. ***This current is of opposite polarity.***

In practice, the polarisation and depolarisation or relaxation currents are measured with a “two electrode” technique as shown in figure 5.3.

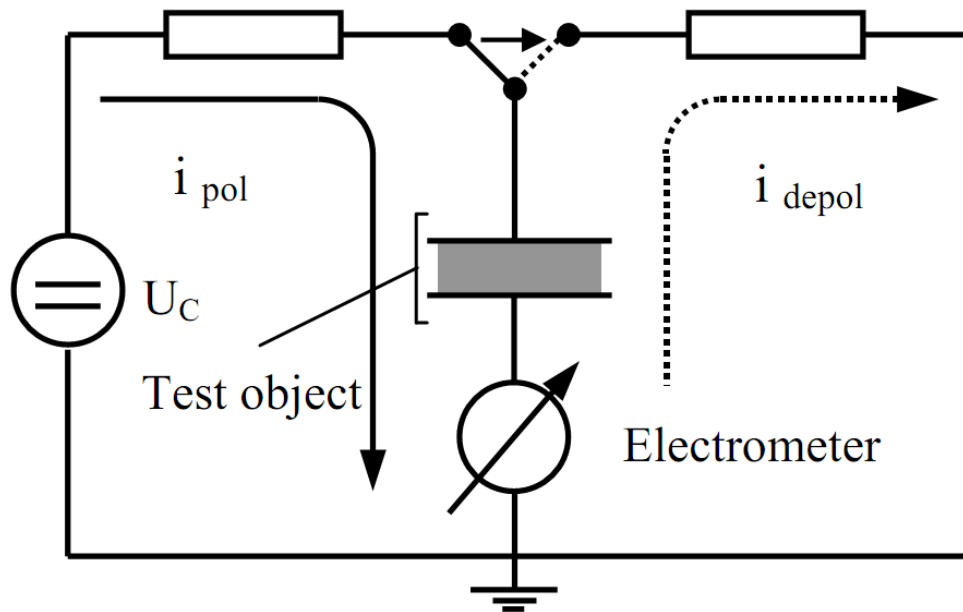


Figure 5.3 Principle of test scheme for the PDC measuring technique

The measured currents are then defined by the selected electrode arrangement and can be sensed at virtual earth potential. The complex insulation system of a power transformer is a typical example for such an application. Finally, an example of recently performed relaxation current measurements is shown in figure 5.4.

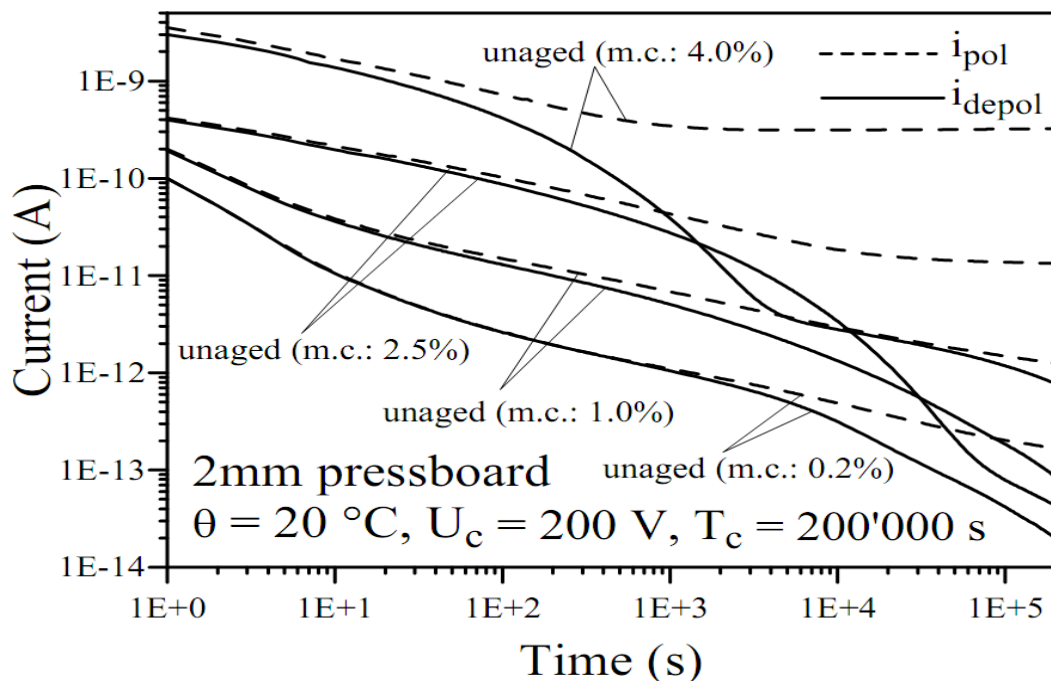


Figure 5.4 Relaxation currents of unaged samples with different moisture contents

It is taken from investigations concerning the dielectric response of oil-impregnated pressboard with the *moisture content (m.c.)* as a parameter. Here, all measurements started 1s after voltage application (i_{pol}) and after short circuit (i_{depol}). From the selected results it can be recognised, that only for the higher moisture content the final value of the polarisation current could be reached, though the measurements lasted up to 200000 s, which is about 56 hours. Representation of these results in log-log scale is paramount due to the large dynamic of the process.

This is shown y means of equations (5.7) and (5.10) in which an ideal step response for the total current density of an ideal dielectric response function $f(t)$ considering also instantaneous polarisation processes are assumed:

$$j(t) = \sigma_0 E(t) + \varepsilon_0 \frac{dE(t)}{dt} + \varepsilon_0 \frac{d}{dt} \int_0^t f(t-\tau) E(\tau) d\tau \quad (5.13)$$

Taking into account $j(t) \Rightarrow j(p)$; $E(t) \Rightarrow E(p)$; $E'(t) \Rightarrow p E(p)$; $f(t) \Rightarrow F(p)$; and considering the convolution of the last term in this equation we get with p being the Laplace Operator:

$$j(p) = \sigma_0 E(p) + \varepsilon_0 p E(p) + \varepsilon_0 p F(p) E(p) \quad (5.14)$$

As p is nothing else than the *complex frequency $i\omega$* , we can reduce the equation to:

$$\bar{j}(\omega) = E(\omega) [\sigma_0 + i\omega\varepsilon_0(1 + F(\omega))] \quad (5.15)$$

Thus it becomes obvious, that $F(\omega)$ is the Fourier Transform of the dielectric response function $f(t)$ or the complex susceptibility $\chi(\omega)$:

$$\chi(\omega) = F(\omega) = \chi'(\omega) - i\chi''(\omega) = \int_0^{\infty} f(t) \exp(-i\omega t) dt \quad (5.16)$$

Combining equations (5.15) and (5.16) shows the well known relationship:

$$\bar{j}(\omega) = \{\sigma_0 + \varepsilon_0 \omega \chi''(\omega) + i\omega\varepsilon_0[1 + \chi'(\omega)]\} E(\omega) \quad (5.17)$$

The complex electric displacement $D(\omega)$ can now be expressed by the *relative, but complex dielectric permittivity*, $\varepsilon(\omega)$, with the relation:

$$D(\omega) = \varepsilon_0 \varepsilon(\omega) E(\omega) = \varepsilon_0 [1 + \chi'(\omega) - i\chi''(\omega)] E\omega \quad (5.18)$$

where:

$$\varepsilon(\omega) = \varepsilon'(\omega) - i\varepsilon''(\omega) = (1 + \chi'(\omega)) - i\chi''(\omega) \quad (5.19)$$

Actual measurements of this dielectric response in frequency domain is difficult to perform if the frequency range become large. Usually such measurement is applied for a single power frequency. New approach can cover some decades in frequency range. Note, that according to equation (5.17) such instruments can not distinguish between the current contribution of the “pure” DC conductivity σ_0 and that of the dielectric loss $\varepsilon''(\omega)$. This means that the effective measured relative dielectric permittivity $\varepsilon_r(\omega)$ is different from the relative permittivity $\varepsilon(\omega)$ as defined in equations (5.18) and (5.19). Then the effective relative dielectric permittivity $\varepsilon_r(\omega)$ is defined from the following relations:

$$\varepsilon_r(\omega) = \varepsilon'(\omega) - i \left[\varepsilon''(\omega) + \frac{\sigma_0}{\varepsilon_0 \omega} \right] = 1 + \chi'(\omega) - i \left[\chi''(\omega) + \frac{\sigma_0}{\varepsilon_0 \omega} \right], \quad (5.20)$$

and the “dielectric dissipation factor” $\tan \delta$ can be written as:

$$\tan \delta(\omega) = \frac{\varepsilon''(\omega) + \frac{\sigma_0}{\varepsilon_0 \omega}}{\varepsilon'(\omega)}. \quad (5.21)$$

The real part of equation (5.20) represents the capacitance of a test object, whereas the imaginary part represents the losses. Both quantities will depend on frequency. Often, this fact is not appreciated, if only one single frequency is applied for the measurement. As ageing effects will change these magnitudes in quite different and specific frequency ranges, new diagnostic tools have to take care for this effect. Measurements in the frequency domain need voltage sources of variable frequencies. So, these measurements become very lengthy if low frequencies are considered. At least 3 cycles of an AC voltage are in general necessary to determine of amplitude and phase shift between voltage and current. Therefore, up to 3 000 s can be necessary to get a single value only of C and $\tan \delta$ for a frequency 1 mHz. Figures 5.5 and 5.6 display the frequency range for the (real part of the) capacitance $C' = \varepsilon' C_0$ and dissipation factor of the pressboard samples as used in figure 5.4. The measurements have been made with a special “dielectric spectrometer” [5, 6] for selected individual frequencies, which can be identified

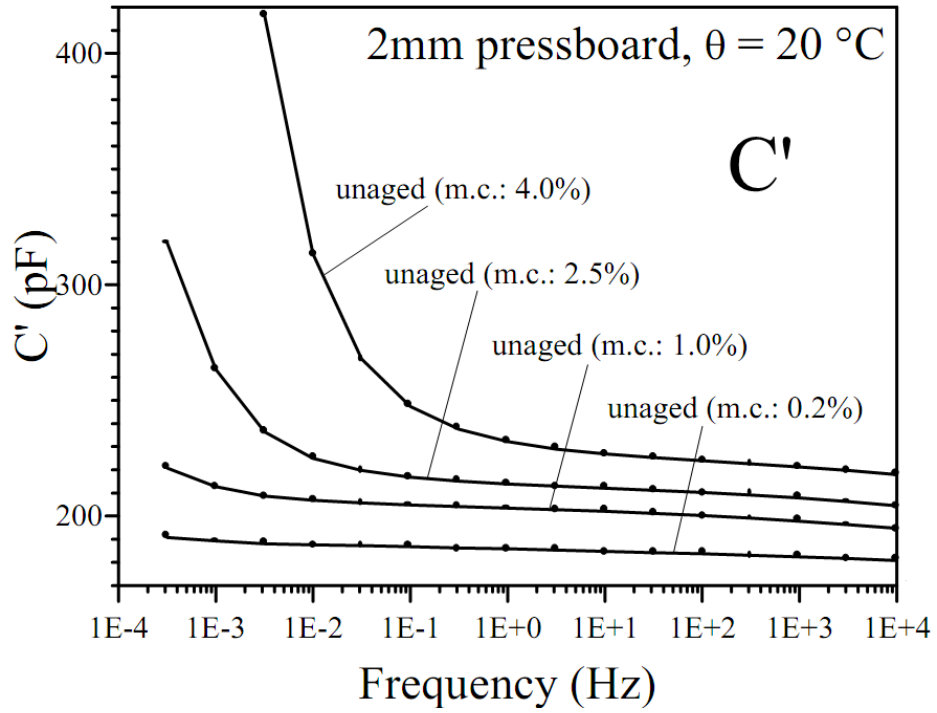


Figure 5.5 Real part of the complex capacitance of the pressboard sample

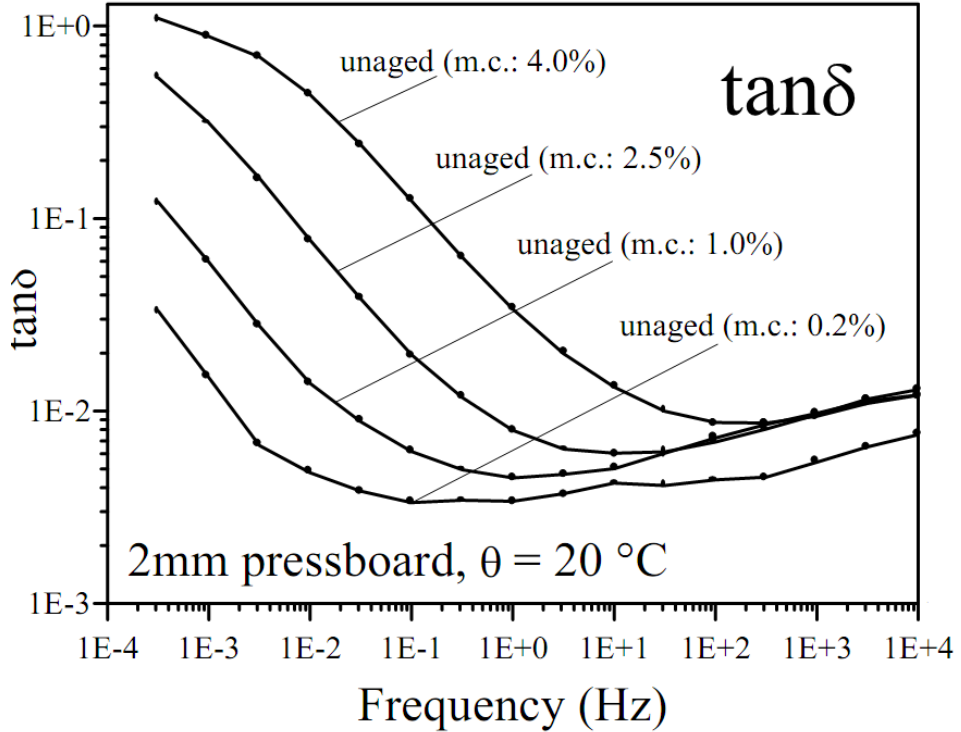


Figure 5.6 Dissipation factor $\tan\delta$ of the pressboard sample

by the straight lines between measuring points. The results show, that the m.c. of the pressboard affects the low and very low frequencies much more than the power frequency, this for the dissipation factor as well as for the capacitance, C' ; this increase is obviously caused by the conductivity of water and thus increased interfacial polarisation inside the board.

Ageing of insulation materials can be detected by its dielectric response in any of the two domains. But also many other methods exist as based on other physical reactions, as e.g. changes in chemical, mechanical or optical behaviour. Since many years such methods are applied to power transformer diagnostics, as e.g. by oil parameter analysis including DGA or HPLC, or Carl Fischer tests for detecting moisture in oil and paper, for which a very large amount of publications does exist. This paper, however, is completely restricted to dielectric response techniques, which can be applied to any kind of equipment. The test objects are treated as “black boxes” accessible only by their terminals. *The disadvantage of dielectric response measurements in either of the two domains is their “off-line” character, i.e. the equipment must be switched off from the power transmission voltage.*

A single *Return or Recovery Voltage (RVM)* measurement is the oldest method to qualify dielectric properties (permittivity and losses) of “anomalous” dielectrics, defined by not only a single relaxation time, see e.g. [7, 8]. Only the principle is shown in figure 5.7.

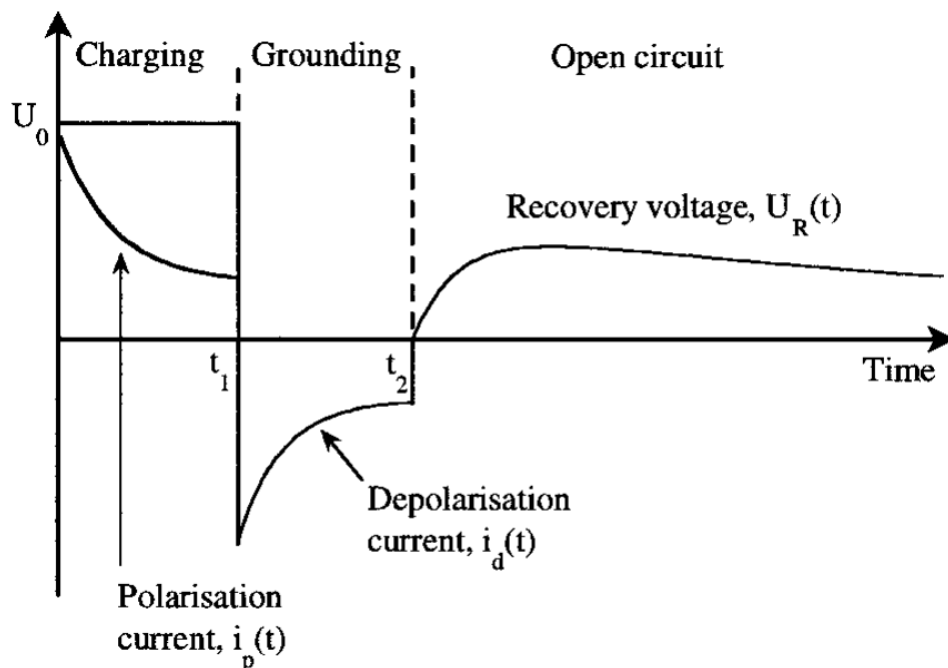


Figure 5.7 Principle of a Return Voltage Measurement

To get complete information, similar to fig. 5.1 a step voltage U_0 is applied across the electrodes of the completely discharged object. After a short grounding (short-circuiting) period, a recovery voltage, $U_R(t)$, can then be measured under open circuit conditions, if the input impedance of the voltmeter is very high. The source of the recovery voltage are the relaxation processes inside the dielectric material, i.e. the depolarisation current, $i_{\text{depol}}(t)$, which a voltage builds up on the electrodes of the test object. The grounding period shall be much less than 1 second so that only the “instantaneous” polarisation processes disappear. $U_R(t)$ can be calculated numerically if the dielectric response $f(t)$ of the test object has been measured and if the duration of the grounding period, $(t_2 - t_1)$, together with other boundary conditions are taken into account. The phenomena, however, can easiest be explained if we represent the dielectric by an *equivalent circuit* which is able to explain all measurements in time domain: As already shown earlier, for “slow” polarisation processes the function $f(t)$ and thus the relaxation currents are monotonically decreasing, see fig. 5.4. These currents can be simulated by a sum of exponential functions as shown in [9] and elsewhere. This sum is, together with the power (high) frequency capacitance $C_\infty = \epsilon_\infty C_0$ as determined by conventional methods and the final value of the insulation resistance R_0 (equivalent to σ_0), the origin of this well known and general equivalent circuit, see figure 5.8.

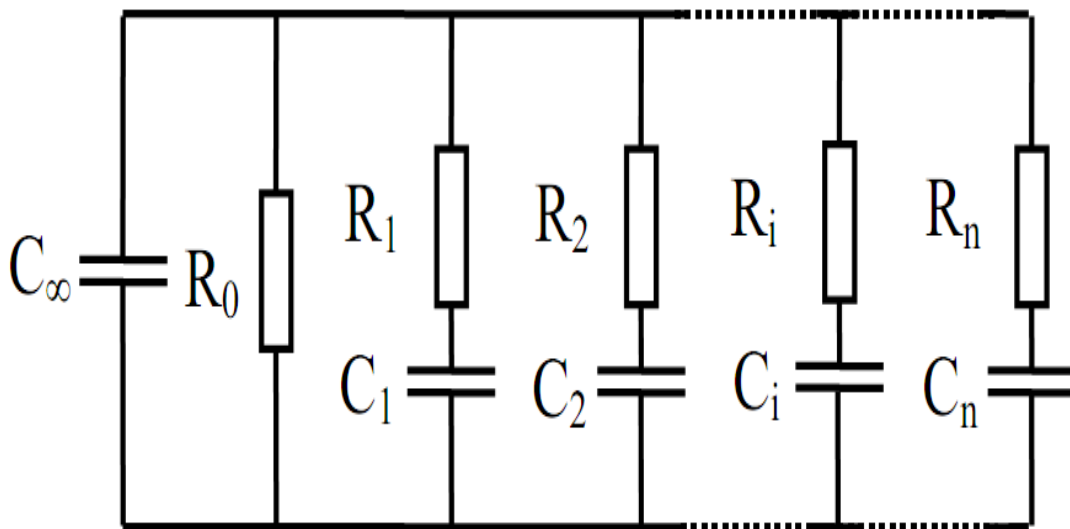


Figure 5.8 Equivalent circuit to model any linear dielectric

If this circuit is charged with a voltage source U_0 during $0 \leq t \leq t_1$, the individ-

ual polarisation currents including the constant current through R_0 will flow into the circuit, charging instantaneously C_∞ and, with some delay, the RC -elements according to their time constants. Depending on how long (t_1) the object is charged, the different polarisation processes as represented by the RC elements become either fully or only partly activated. A short grounding period from $t_1 < t \leq t_2$ will only discharge C_∞ but if this period is larger, also the slower polarisation processes start to relax. As soon as this short circuit is opened for $t > t_2$, the recovery voltage is measured at open circuit conditions, as the polarisation processes (or RC elements), which either not or only partly relaxed during the short circuit period, will partly discharge into C_∞ and R_0 . The magnitude of the return voltage is thus always proportional to U_0 . This method can be traced back to the beginning of the last century and was originally applied due to the difficulties in measuring small (depolarisation) currents. It was, however, always possible to measure voltages with electrostatic voltmeters, the input impedance of which is extremely large. The application of this method is of advantage if the “ground” terminal of the test object is not accessible. In Germany, at least one measuring system based on this method is available [3].

If this ancient method is nowadays again applied, it was triggered by the appearance of a similar, but specialised method called simply “**RVM-technique**”. The method, originally proposed in [5] and somewhat later commercialized [6], became attractive for diagnosing transformer insulation as it was claimed that the moisture content in the pressboard of the complete insulation system can be quantified by analysing a so-called “**polarisation spectrum**” resulting from the measurement. This “spectrum” is performed by applying a series of charging voltages U_0 to the test object, followed by the short circuiting as explained before, at each step increasing the charging time $t_1 = t_c$ and the short circuiting time $(t_2 - t_1) = t_g$ and using a fixed ratio of $(t_c/t_g) = 2$. During these periods, nothing is measured. After t_g has elapsed, the recovery voltage is recorded and from its peak value, the amplitude U_{Rmax} is quantified and plotted as a function of t_c . This dependency is called “polarisation spectrum” as its maximum appears indeed at a t_c -value, which agrees with a single time constant RC of our equivalent circuit, fig. 8. The method, however, is very lengthy as after each measuring cycle (the longest of which is 10 000 s the insulation system must be discharged to prepare the next cycle. The method is thus fully based on *depolarisation* currents only which are, depending on the charging period, incomplete as only a part of these currents is used to build up the individual return voltages. Instead of performing such a measurement, it is possible to compute the “polarisation

spectrum” and its parameters if the dielectric response function $f(t)$ is known. A quite new instrument, the *PDC Analyser*, as described recently in [3] and manufactured by a Swiss company, measures a complete set of polarisation and depolarisation currents and thus also the response function $f(t)$, examples of which have already been shown. The default software of this instruments calculates all other quantities as e.g. insulation resistance in function of time, all kinds of “Polarisation Indexes”, single Return Voltages or “polarisation spectra” as applied by the *RVM-technique*, and complex capacitance including loss factor in the frequency domain. Some examples of application and evaluation are shown below. This is basic fundamentals of *Principles in Frequency Domain*. The measurement of “ $C-tan \delta$ ” at power frequency (i.e. at one single value in the frequency domain) by means of bridge circuits, which are based on “standard capacitors”, is well known. Since some years this quantity is sometimes measured at 0.1 Hz in combination with a low frequency HV test equipment as used for diagnostic tests of medium– voltage PE cables, the loss factors of which are sensitive to chemical treeing. A quite large frequency range is now covered by a new instrument called “*IDA 200*” manufactured by a Swedish company. This “Insulation Diagnostic Tool” measures $C-tan \delta$ from 0.0001 Hz – 1000 Hz and covers thus also the low and very low frequency range which is most prone to ageing effects. Below, an example for the application of one of the new diagnostic tools is presented based on *time domain (PDC) measurements*. The example is taken from very recent investigations in the *CIGRE Task Force 15.01.09*. In the course of the investigations, a test object modelling power transformer insulation systems was designed, constructed and used. The measurements as performed on this model are based on the 3 methods as explained in chapter 5 (RVM–technique, PDC Analyser and IDA 200). The design of the test object and the goal of the investigations was already published in [6].

The model can be characterised as follows: metal tank (ca. 490x1040x1560 mm) with bushings to connect the inside flat electrodes between which different insulation configurations have been sandwiched. Each insulation configuration consisted from flat plates of pressboard (“Kraft Thermo 70”) with or without oil gaps between the electrodes. Pressboard plates have been fixed in the middle of the whole gap between electrodes by means of pressboard spacers.

In the following figures, the curves are marked by codes indicating the insulation configurations. The effective area of the electrodes is about 1 m^2 . The “instantaneous” capacitance as measured with 50 Hz ranges from about 4.8 nF to 2.35 nF . Figure 5.9 shows all 4 sets of relaxation currents as

measured on the either “pure board” – configuration 01 or the multi-layer configurations of code 02 to 04.

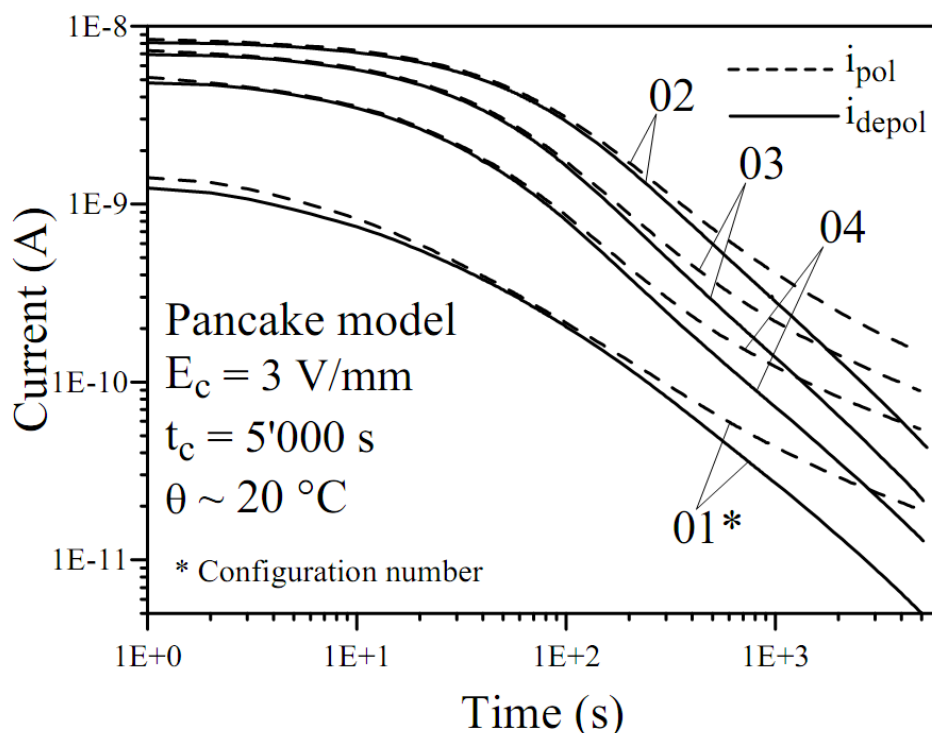


Figure 5.9 Relaxation currents measured on four different configurations of the “pancake” model. The electrode spacing ratio is 3 V/mm for all measurements.

The currents have been recorded just 1 s after voltage application or short-circuiting, and measurement periods have been 5 000 s each. The shapes of the currents for these 4 configurations can be subdivided into 2 groups: The multi-layer configurations 02 to 04 are characterised by their *pronounced exponential shape* at short times of less than about 200 s. **This kind of shape is typical for PDC measurements on all kinds of HV power transformers.** They are essentially produced by the formation of the *interfacial polarisation* between oil gaps and pressboard barriers. It can well be identified from these shapes in log-log-scales that their dominating time constants increase with the thickness ratios of oil gaps to pressboard barriers. The dielectric response of the pressboard becomes more apparent at long times, at which the depolarisation currents are quite well in parallel indicating the identity of the dielectric response function of the pressboard material as used to reach different thickness (from 2 to 10 mm) of the barriers. The (nearly) homogeneous gap of configuration 01 behaves quite different, as the initial shape of the currents is not pronounced exponential. A comparison with e.g. the relaxation current shapes in figure 4 (unaged, 1% m.c.) shows

that still some small oil gaps exist in series to the pressboard, confirmed by not ideal electrode systems not further discussed here.

Figure 5.10 presents the calculated “*polarisation spectra*” for all 4 configurations 01 to 04 of the model and for a charging voltage of 1 V.

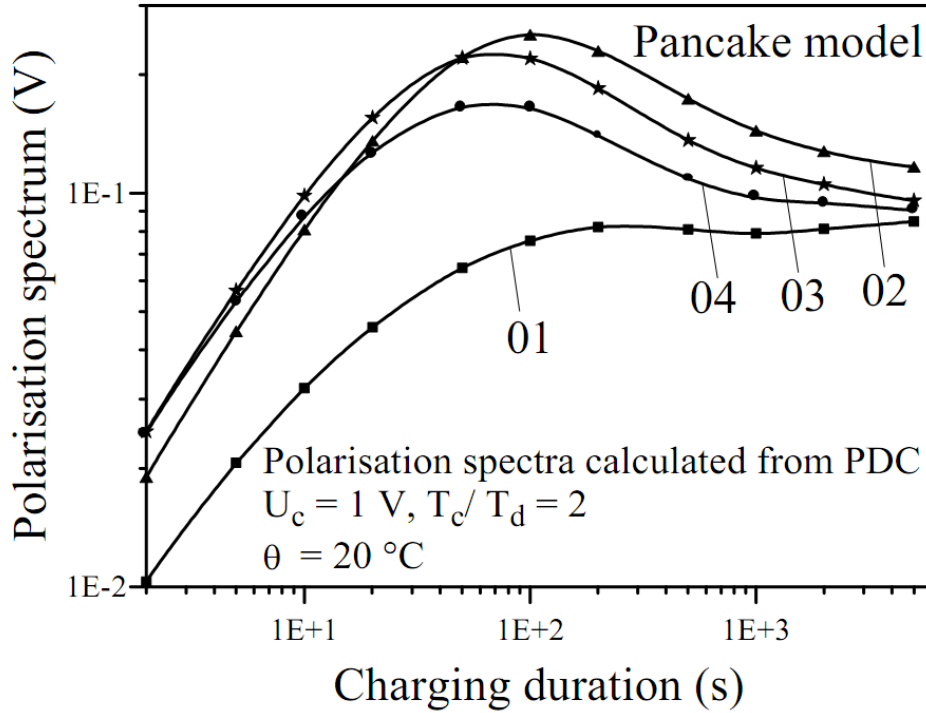


Figure 5.10 Calculated polarisation spectra of all configurations.

The results show that the position of the peak value in “*polarisation spectrum*” does change in dependence of geometry. For the configurations 02 to 04, this maximum is due to the “macroscopic” interfacial polarisation and its geometric position at the interface between oil gaps and pressboard. This fact can also be calculated by assuming a simple Maxwell–Wagner interfacial polarisation process. In this model, 2 series–connected dielectrics with losses are assumed. Each dielectric can then be modelled by – for our example – the conductivity and relative permittivity of the oil (σ_{oil} , ϵ_{roil}) and of the pressboard (σ_{Board} , ϵ_{rBoard}). Then the time constant τ of the interfacial polarisation is given quantitatively by the following equation, where d_{oil} and d_{Board} are the thickness of oil gap and pressboard barrier [13].

$$\tau = \epsilon_0 \times \frac{d_{Board} \epsilon_{rOil} + d_{Oil} \epsilon_{rBoard}}{d_{Board} \sigma_{Oil} + d_{Oil} \sigma_{Board}} \quad (5.22)$$

Though in equation (5.22) the much more complex dielectric properties of the pressboard are not taken into account and only simulated by a single time constant, a numerical evaluation with approximate values for both components would already show quite good agreement with the results as measured. This equation can not simulate the spacers as applied to fasten the board within the gaps, but it shows already for the different ratios of oil gaps to board thickness the change of the “dominant” time constants, which decrease in magnitude if this relationship decreases. The default software of the “PDC Analyser” calculates for all measured currents (see Fig. 5.9) the specific equivalent circuits (see fig. 5.8) so that the transition to frequency domain is easy to perform. In figure 5.11 the results of such calculations are displayed for the most interesting configurations 02 to 04 and compared with the measured values of capacitance $C'(\omega)$ and dissipation factor $\tan \delta(\omega)$ as registered by the dielectric spectrometer “IDA 200”.

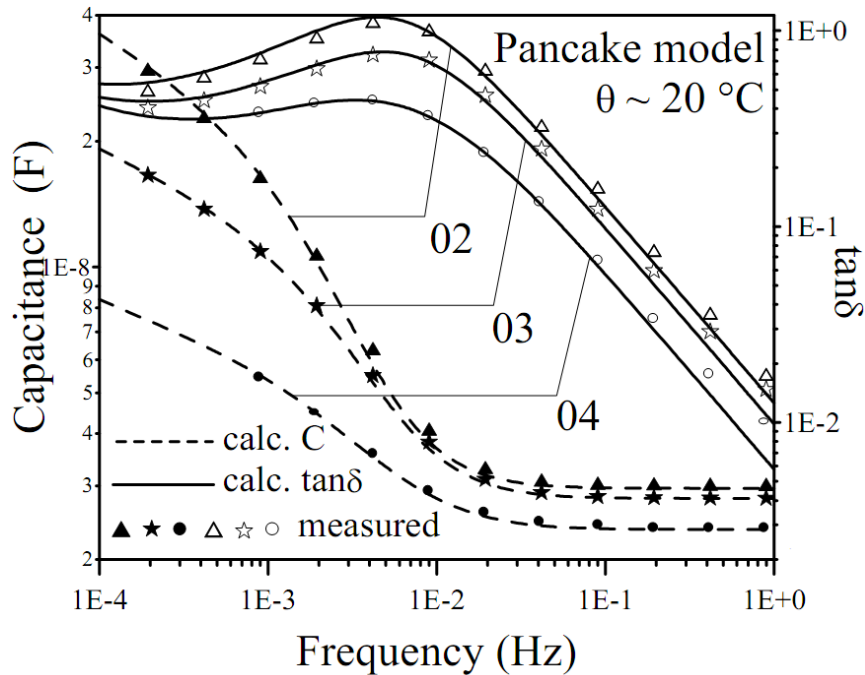


Figure 5.11 Comparison between calculated and measured capacitance and dissipation factor $\tan \delta$.

The comparison shows the good agreement of measured and calculated values down to very low frequencies. The maxima in the $\tan \delta$ curves and the significant increase of capacitance at low frequencies confirm again the predominant influence of interfacial polarisation on the total dielectric response of multi-layer arrangements. All measurements as shown in figures 5.9 and 5.11 have been made with the original new oil of type “Nynas Nytro 10GBN” with a conductivity of about 2 pS/m (20°C). As also the influence of the oil and its conductivity should have been investigated, it was decided

to replace it by an oil of different origin with lower conductivity. The new type was “*Shell Diala D*” with $\sigma = 0.24$ pS/m (21°C). For configuration “02” figure 5.12 shows now the measured relaxation currents before and after oil exchange.

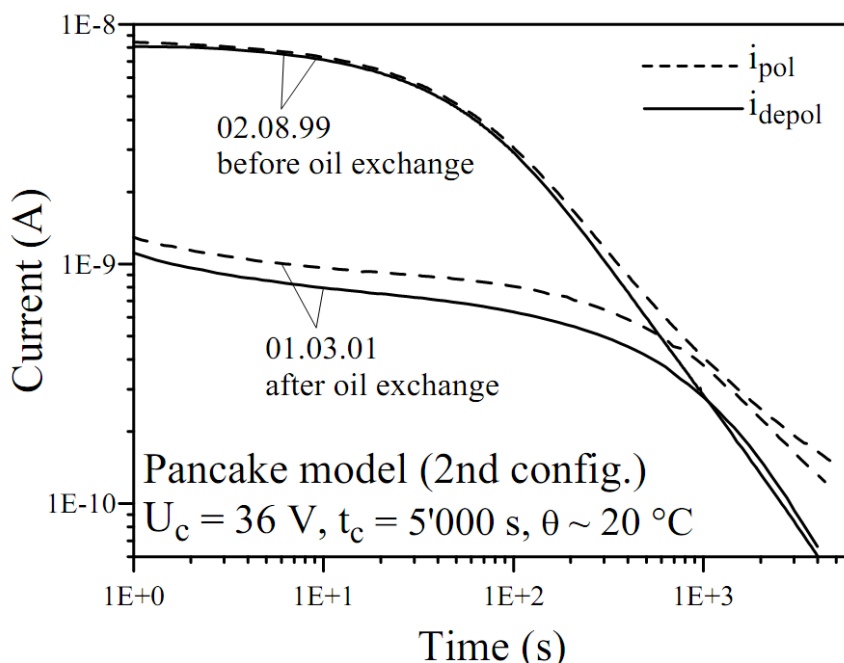


Figure 5.12 Measured relaxation currents on configuration 02 before and after oil exchange.

Now, the initial amplitudes dropped by a factor of about 9 and the duration of the nearly exponential decay of the currents is heavily prolonged. This decrease of the initial current amplitude and the shift of the time constant of interfacial polarisation to long times is thus only due to the decrease of oil conductivity.

The significant changes must also appear in the frequency domain. Figure 5.13 shows the calculated and partly measured dependencies of capacitance $C'(\omega)$ and dissipation factors $\tan \delta(\omega)$.

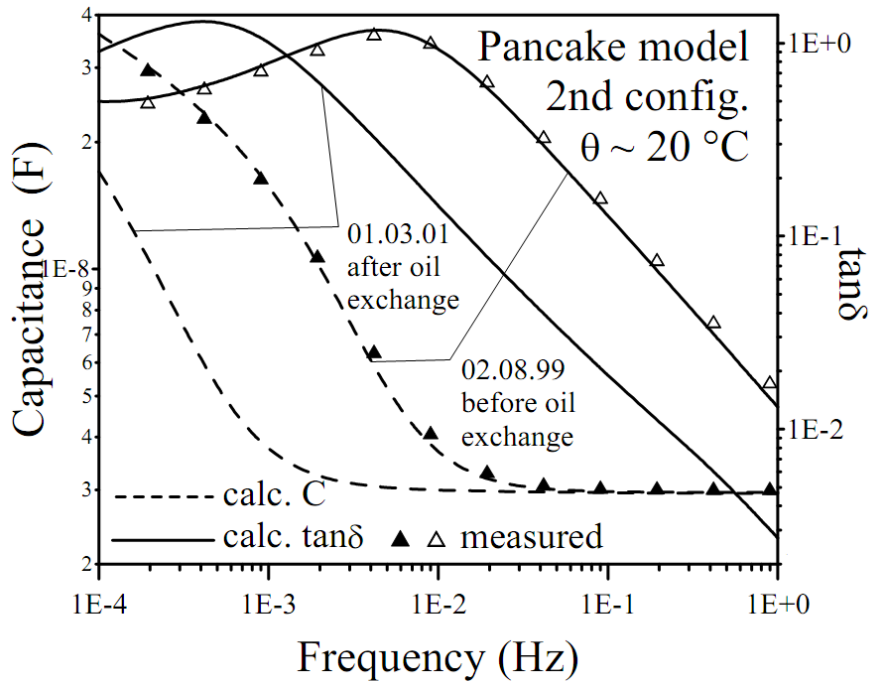


Figure 5.13 Comparison of calculated capacitance and $\tan \delta$ curves before and after oil change

The calculated values are determined from the relaxation currents as displayed in fig. 5.12. In the low frequency domain, the increase of the capacitance takes now place for much lower frequencies for the low conductivity oil as the process of interfacial polarisation between oil and pressboard needs much more time. This increase in capacitance is due to the simple fact that the electric field in the oil gap will more or less vanish with time; therefore, for extremely low frequencies, the capacitance of the pressboard alone will appear.

Finally, figure 5.14 displays the two polarisation spectra as calculated by the *PDC* Analyser from the measured relaxation currents (fig. 5.11). For this calculation the charging voltage was set to 500 V permitting the direct comparison with measured values as performed by the *RVM* technique, marked by triangles and stars.

This figure shows again the significant influence of oil conductivity on the time position of the first maximum in the polarisation spectrum and the good agreement between calculated and measured values, although the *RVM* meter quantifies a somewhat different insulation system than the *PDC* Analyser (1-terminal against 2-terminal measurement).

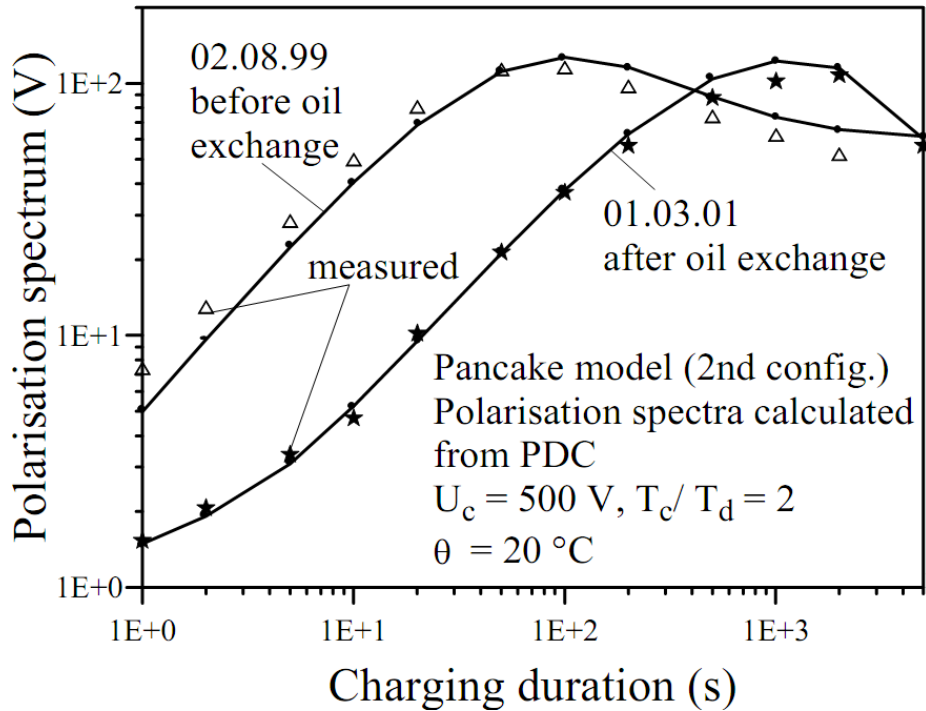


Figure 5.14 Comparison of calculated and measured polarisation spectra of configuration 02 before and after oil change

These investigations confirm that the main (or first) maximum in the “polarisation spectrum” of the RVM technique for multi-layer arrangements is due to the interfacial polarisation and that its time position is dependent on the geometrical layout (thickness ratio of oil gap to pressboard barrier) and conductivity of oil. Therefore, the time position of the first maximum cannot be correlated with the moisture content of the pressboard material.

The results as presented confirm already the possibility to distinguish between oil and impregnated pressboard as applied for insulation systems in power transformers. Much more quantitative data can be evaluated if the geometry of the insulation system including spacers is quantitatively taken into account. This can be done by a specific software for the PDC Analyser which is based on dielectric response functions $f(t)$ of otherwise investigated materials and its comparison with measured data. As an example, the actual oil conductivity of the test object can immediately be determined as the first part of the polarisation current is completely governed by this conductivity. Similar evaluations are possible if frequency domain measurements have been made.

So, principally new technologies for power transformer insulation state control have been developed. Examples of this technologies application with

detailed explanations are shown below.

Measurements of resistance, the dielectric loss factor $tg\delta$ at power frequency, and calculation of the absorption coefficient R_{60}/R_{15} have been used for many years to assess the condition of paper-oil insulation. Capacitance between two windings has also been measured at 2Hz and at 50Hz, to derive C_2/C_{50} ratio that reveals the moisture content in transformer main insulation. Recently, usefulness of these parameters to transformer diagnostics was contested [5]. New methods, based on dielectric polarization relaxation in a broad frequency range have been proposed. Moisture content cellulose and its thermal degradation can be assessed using these methods. In consequence, the remaining technical life of the transformer can be assessed. Polarization RVM and PDC records are taken in the time domain, whereas frequency characteristics of the insulation capacitance and dielectric loss factor $tg\delta$ are recorded in the range from 0.1 mHz to 100 Hz.

PDC method may be perceived as a modification of traditional insulation resistance measurement and calculation of R_{60}/R_{15} quotient. A direct voltage is applied to the transformer insulation, and the resulting current charges capacitance of the examined insulation. This current is composed of polarization current i_{pol} that decays, and the constant current determined the insulation conductivity. Subsequently, the charged insulation is short-circuited and an opposite-polarity depolarization-current i_{dep} decays to zero. The rate of current decay depends on polarization relaxation of the paper-oil insulation, and contains several exponential components [5, 6]. Test scheme is shown on the figure 5.15.

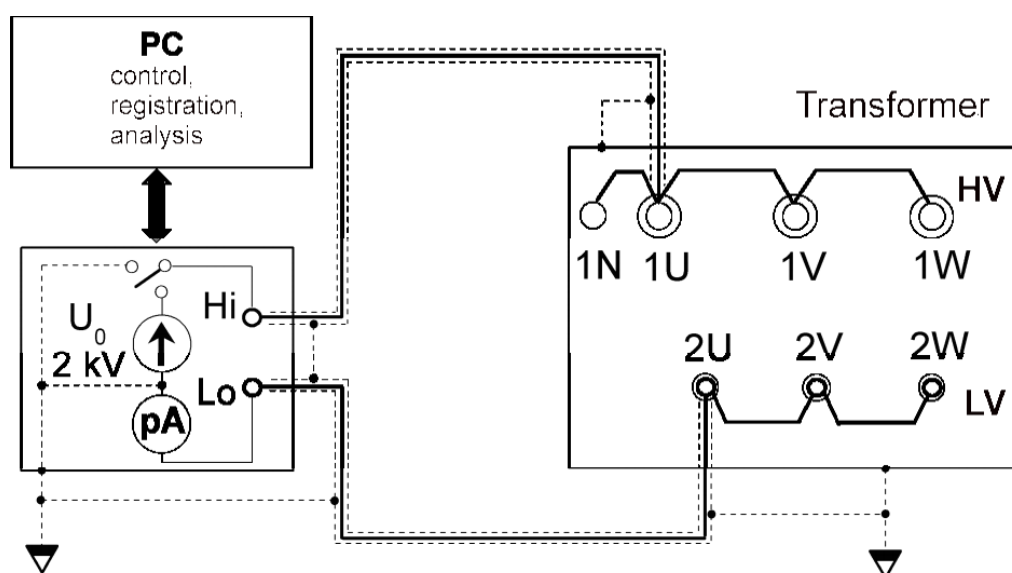


Figure 5.15 Test scheme for PDC measurements on real transformer

The transformer oil conductivity determines the polarization current magnitude during first 100 s. This conductivity depends on the water content in oil, its acid number, contamination and temperature. The polarization current intensity is proportional to oil conductivity that can be derived from the initial value of i_{pol} . Water content in cellulose (barriers, spacers) can be derived from the i_{pol} and i_{dep} characteristic after 100 s. **Increased water content in cellulose accelerates depolarization and results in a faster decay of i_{dep}** , as well as in an increase of i_{pol} after 100 s (Fig.5.16).

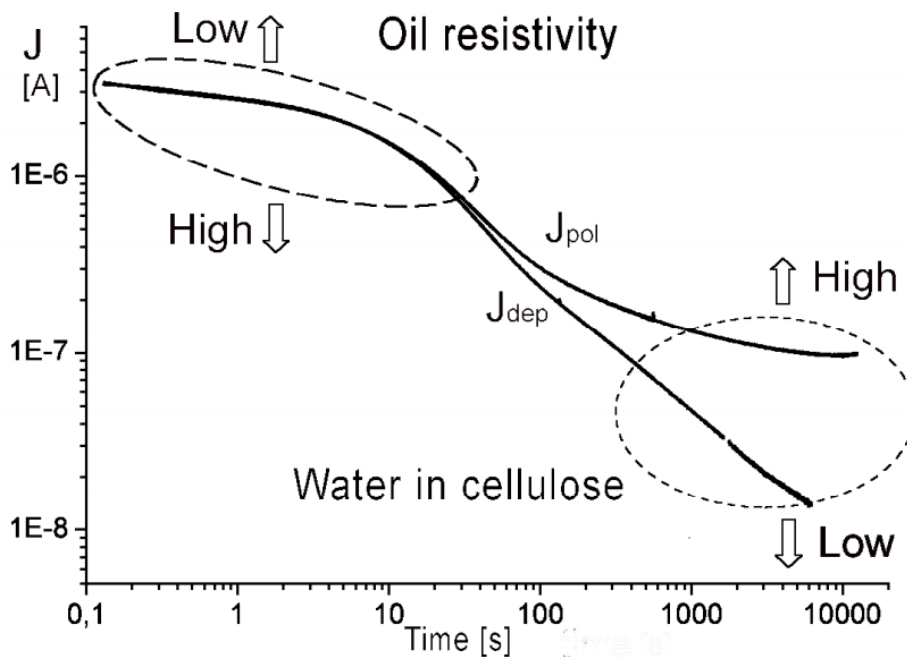


Figure 5.16 Polarization and depolarization current plotted against time, with the water content in oil and in cellulose as parameter

Specialized expert programs compare the i_{pol} and i_{dep} characteristics taken on an examined transformer to the respective curves obtained on pre-conditioned Transformerboard samples with a known water content and cellulose degradation. Transformer diagnostics in service often relies on a comparison of the characteristics taken on similar transformers, or at subsequent inspections of the same unit. Such procedure allows for identification of transformers that represent a higher operational risk, and scheduling their repairs or decommissioning.

An example of 270 MVA, 220/15kV transformer is shown in Fig.5.17, where the measured i_{dep} characteristic was analyzed and water content in cellulose determined by comparison to reference data from Transformerboard

samples.

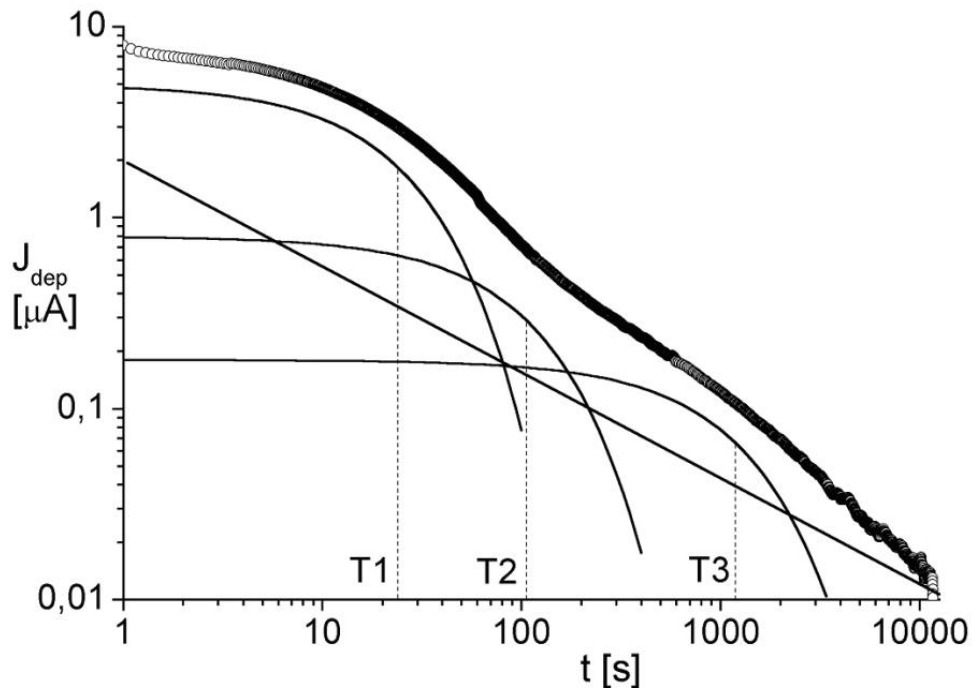


Figure 5.17 Identification of the exponential components and their time constants

Frequency Time Domain (FDS) measuring procedure and the test circuit are the same as used for the time domain measurements, and shown in Fig. 5.15. An examined insulation capacitance C and $tg\delta$ low-frequency characteristics depend on temperature, insulation degradation and water content. This relation has been determined and an effect of increased water-content in cellulose and oil on C and $tg\delta$ was associated with certain frequency ranges (Fig.5.18). Reference frequency characteristics of capacitance and $tg\delta$ have been determined in laboratory conditions for different insulation samples with controlled ageing and water content. They are built-in the software provided by manufacturers of the FDS measuring instrument to facilitate interpretation of recorded curves. Geometry of the examined winding has to be input together with the transformer nameplate data, and the program assesses the insulation condition in terms of ageing and water content. A database of the reference characteristics should preferably be developed for a given type and make of the paper-oil insulation, since the material characteristics do differ, and there are no universal reference curves.

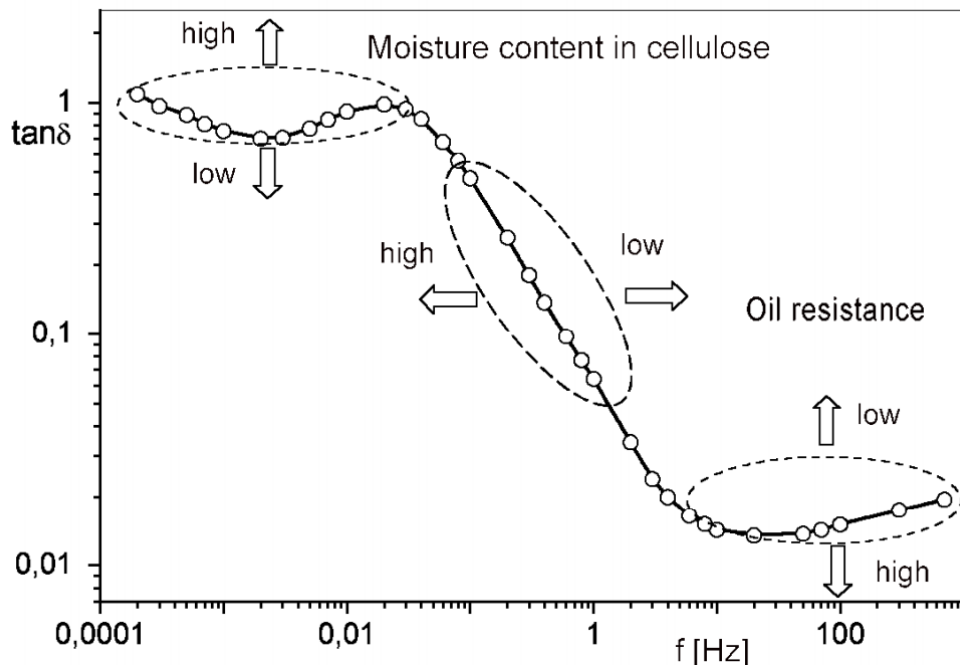


Figure 5.18 Frequency characteristic of $tg\delta$ reveals water content and oil resistance in different frequency ranges

Another approach consists in using the Havriliak–Negami equation and examining the relaxation characteristic of the examined insulation. Havriliak–Negami equation (5.23) describes dielectric relaxation in polymers. This equation is used to analyse examined insulation.

$$\varepsilon(\omega) = \varepsilon' + j\varepsilon'' = \frac{\Delta\varepsilon}{(1 + (\omega\tau)^\alpha)^\beta} + \varepsilon_\infty - j\left(\frac{\sigma}{\omega\varepsilon_0}\right)^N \quad (5.23)$$

where: $\Delta\varepsilon$ – polarization, $\omega = 2\pi f$ – pulsation, τ – relaxation time constant, σ – conductivity, α , β , N – coefficients, $\varepsilon(\omega)$, ε_∞ , ε_0 – complex, optical and static dielectric permittivity respectively. **It is necessary to note that dielectric constant is used in engineering texts, but in reality ε is variable.**

Such analysis is presented on an example of 75 MVA, 110/10.5 kV transformer manufactured in 1988 by Siemens. Two relaxation time constants $\tau_1 = 12.1$ s and $\tau_2 = 294$ s were identified from C and $tg\delta$ characteristics (Fig. 5.19 and 5.20) taken on the main insulation at 20°C. The faster relaxation occurs at the oil–cellulose interface, and the slower one reflects properties of Transformerboard with a high water content.

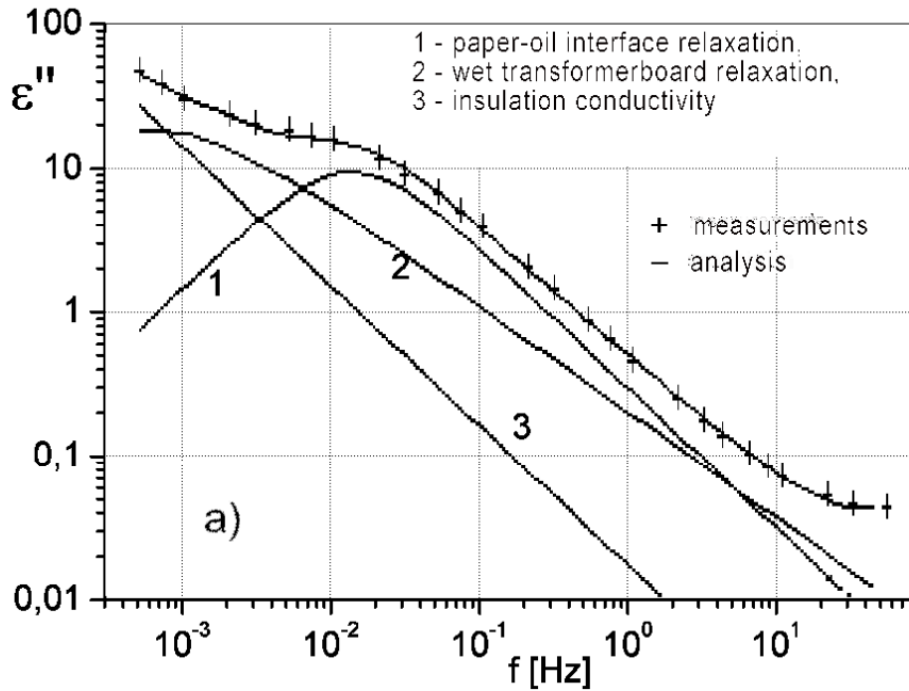


Figure 5.19 Identification of time constants from $\tan \delta$ frequency characteristics

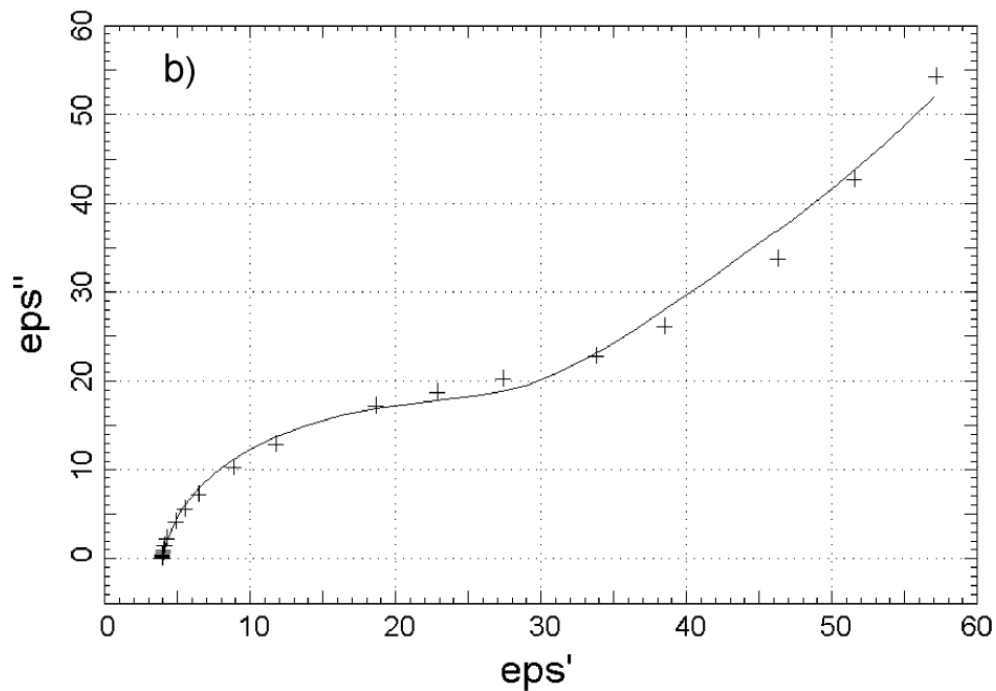


Figure 5.20 Cole-Cole graph derived from measurements taken on 75 MVA, 110/10.5 kV transformer

Water content in cellulose can be assessed using nomograms used by the recovery voltage measurement (RVM) method, since it is based on the time constant of interfacial relaxation. The relaxation time—constant of solid in-

insulating materials, such as Transformerboard, have to be obtained from the material samples examined in the laboratory.

Additional parameters derived from these characteristics are given in Table 5.1. Water content in the examined insulation was assessed at 3.2% from the time-constant of the interfacial relaxation, and at 3.3% from the relaxation time-constant measured on the Transformerboard samples, taking into account the temperature corrections.

Table 5.1 Dielectric relaxation parameters from measurements taken on 75 MVA, 110/10.5 kV transformer

Parameter	σ_0 S/cm]	$\Delta\epsilon_1$	τ_1 [s]	α_1	$\Delta\epsilon_2$	τ_2 [s]	α_2
Value	8,4· e-15	20,9	12,1	1,00	61,7	294	0,76

An important advantage of the FSD methods lies in finding the insulation water-content even if the water-content in cellulose and in oil are not in equilibrium.

This method can separate the two polarization structures: at the paper-oil interface and in solid insulation, i.e. Transformerboard. It should be emphasized that the polarization behaviour of wet cellulose is relatively stable, but the properties of paper-oil interface depend on the water-content equilibrium and on products of oil decomposition [5, 7].

The same transformer was also examined using *RVM method* and the main time-constant $T_p = 9.7$ s is comparable to $\tau_1 = 12.1$ s that corresponds to 3.3% water-content at 20°C. In this case the moisture content in paper and oil are in equilibrium, as it is indicated by the well-defined, single peak of Ur and its slope Sr characteristics, as well as by the similar moisture-content obtained using *FDS method*. This situation is shown on figure 5.21. Apparently no oil-decomposition products are deposited on the Transformerboard surface.

So, new technologies of high voltage insulation diagnostic are very prospect. They will substitute all “typical” insulation diagnostic methods. RVM, PDS and FDS are based on dielectric spectroscopy phenomena. Basic fundamentals are detailed described in this paragraph.

One of the last tendencies in this direction is FDM using only.

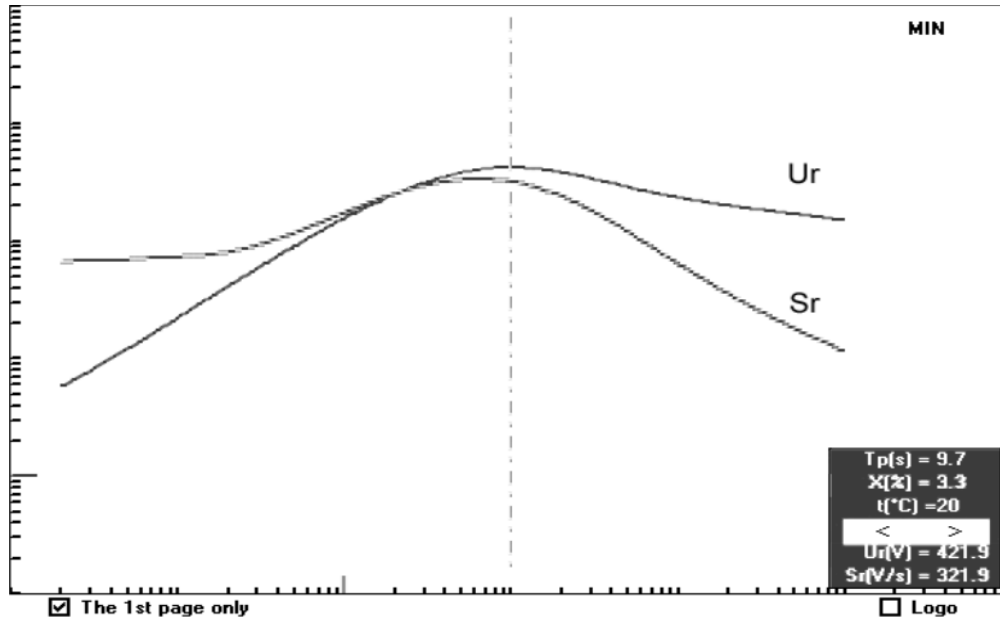


Figure 5.21 Time-domain RVM characteristics measured on 75 MVA, 110/10.5 kV transformer insulation:
 U_r – the polarization recovery voltage, S_r – initial steepness of U_r characteristic

5.1.2 New technologies of active part of transformer diagnostics

This is very important task in high voltage technology – to make state control of active parts of power transformers. One of the new and prospect technology here is *Sweep Frequency Response Analysis (SFRA)*. Most widespread term is *FRA*.

The FRA method is used to check the eventual change in the internal geometry of the active part of the transformer: displacements or deformations. The main causes of such defects may be linked with the transportation or with the working conditions of the machine, such as the presence of external short-circuits with the consequent development of important mechanical stresses linked with electrodynamic forces (radial or axial depending on the constructive technology of the machine), affecting the tightness of the relative connections in the core and/or in the windings. Once the transformer has been damaged, even if not extensively, its capability to withstand further stresses may be heavily jeopardized. Defects of this nature evolve generally towards the complete destruction of the machine in a dielectric breakdown as a consequence of a mechanical collapse during electrodynamic stresses or in a progressive deterioration of the insulation leading to a dielectric breakdown of internal solid insulation (partial discharges). In such a context it is important to check that the windings are not

affected by incipient mechanical deformations.

The classical method adopted for checking the presence of such internal defects is the measurement of the leakage inductance; however, practical experience has shown that only radial deformations can be seen using this method, while axial deformations linked with localised mechanical stresses on the winding extremities may not be detected. The FRA method was developed to cope with this lack of sensitivity. It is based on the assumption that any mechanical deformation may be associated with a change in the capacitive- inductive equivalent circuit and therefore detectable through a transfer function. In essence, the method consists in applying on one end of machine winding a low voltage sinusoidal signal made of a sweep of frequencies covering a range between 10Hz and 2MHz and measuring on the other end of the winding the corresponding response in terms of amplitude ratio with respect to the input signal. The applied sweep maintains the same level of energy for each frequency analysed in such a way as to obtain accurate and reproducible results. Little influence from the test set-up is evidenced: the same testing accuracy can therefore be obtained in the laboratory and in the field. This method being essentially based on a comparison approach it is useful to have reference data: in particular it would be advisable to have reference tests on the machine when new, so to compare data in different stages of the machine life. The test is carried out typically considering two configurations for the winding opposite to the tested one: i.e. winding open and floating and winding short-circuited. These testing conditions allow the selective evaluation of the presence of defects: in fact, in the conditions in which the winding opposite to the tested one is open and floating, the effect of the mutual coupling between the *HV* and *LV* windings can be seen in addition to the effect of the magnetic circuit; in the other testing configurations (short-circuited winding) the effects of the mutual coupling and of the magnetic circuit are masked and the effect of the single winding is to be seen.

The experience has shown that in the evaluation of the test results, the behaviour in three different ranges of frequencies must be considered:

Frequency < 10 kHz: in this range phenomena linked with the transformer core and magnetic circuits are evidenced: the analysis in this range must take into consideration the residual magnetisation which can slightly modify the obtained response from one test to the other. In this range coil faults, winding interruptions, magnetic circuit problems are brought to light;

Frequency in the range 5 kHz to 500 kHz: in this range phenomena linked with radial relative geometrical movements between windings are evidenced;

Frequency > 200 kHz: in this range axial deformations of each single

winding are evidenced.

The power transformer subjected to the test had tripped on differential protection without any Buchholtz tripping. An additional check on the on-line DGA system showed an important increase in the hydrogen equivalent total gases and the machine was removed from service and planned for an off-line thorough check. As no reference data existed for that specific machine, the *FRA test*, carried out after disconnection of the transformer was elaborated through comparison among different circuit configurations.

Measurements carried out on the high voltage windings (400kV) star connection. The result of the measurements carried out on the high voltage (*HV*) windings are reported in Figure 5.22 and Figure 5.23 for the configurations with the low voltage (*LV*) windings open and floating and with the low voltage windings short-circuited respectively.

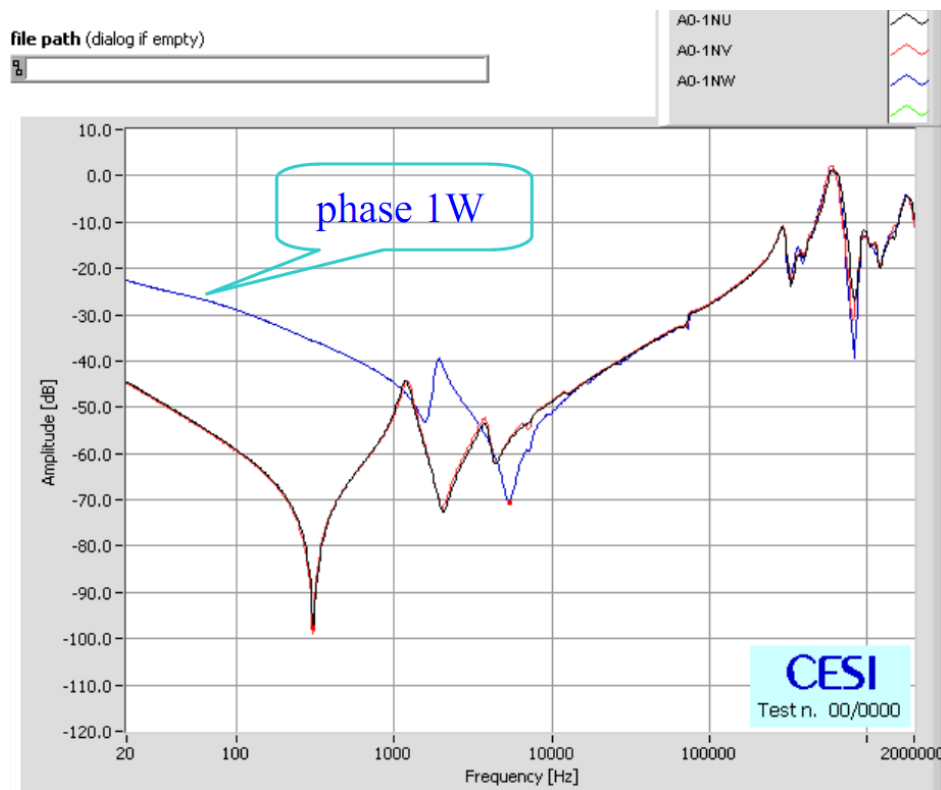


Figure 5.22 Measurements carried out on the HV winding with the LV winding open and floating

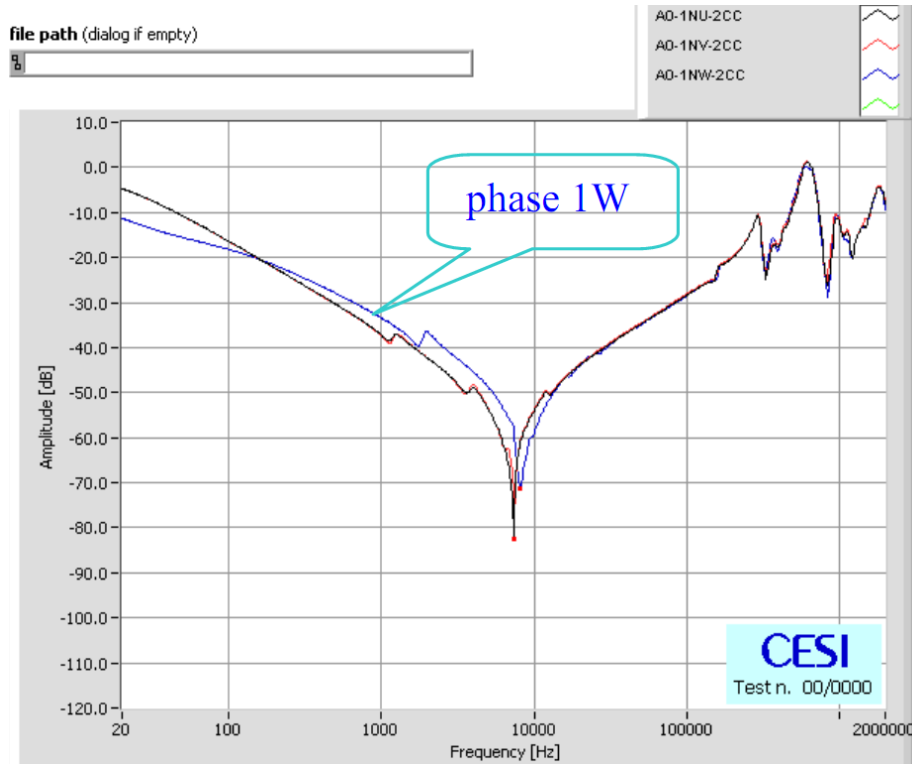


Figure 5.23 Measurements carried out on the HV winding with the LV winding short-circuit

It can be seen in Figure 5.22 that the shape of the frequency response corresponding to phase W deviates substantially from that of the other two phases of the machine, especially in the open-circuit configuration and for a frequency range under 20 kHz. The response to higher frequencies is not substantially affected, thus excluding the possibility of geometrical deformations of the faulted winding. Such huge deviations in the low frequency range, as shown in Figure 5.22 can only be linked with a variation of the turns ratio of one phase (possibly due to an internal partial short circuit of one winding and/or to the opening and separation of part of the winding, affecting the magnetic coupling). This electrical change is also visible in the low frequency range in Figure 5.23: however, the deviation appears much lower: in fact, when the winding opposite to the tested one is short circuited, inductive coupling is very much affected and the sensitivity at low frequencies becomes much less; moreover, being the short-circuit reactance much smaller than the no-load reactance, the signal attenuation in the low voltage range is much smaller.

Measurements carried out on the low voltage windings (15 kV) delta connection. The SFRA measurements were repeated on the low voltage windings opening the delta connection and keeping the high voltage wind-

ings open and floating or short-circuited. The respective diagrams obtained are shown in the Figure 5.24 and Figure 5.25. Waveshapes confirmed that the fault was confined on phase W. The check carried out with the opposite winding short-circuited, showing a perfect superposition of all tracks, confirmed the idea of a problem on the HV winding.

No further elaboration of the SFRA data was deemed necessary (e.g. numerical evaluation of the shape differences of the damaged phase with respect to the sound phases, etc.) because a major fault was detected and it was unavoidable to open the machine and carry out the necessary repair operations. A series of traditional checks were carried out after the SFRA, such as the turn ratio, the winding resistance and the leakage inductance: all the checks confirmed the hypothesis.

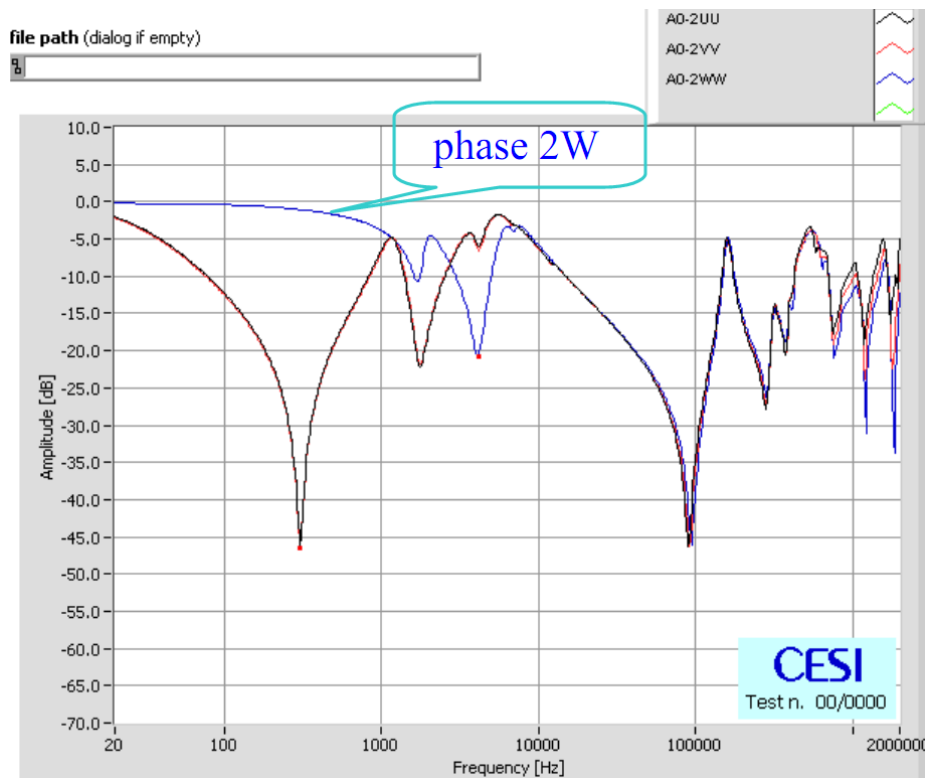


Figure 5.24 Measurements carried out on the LV winding with the HV winding open and floating

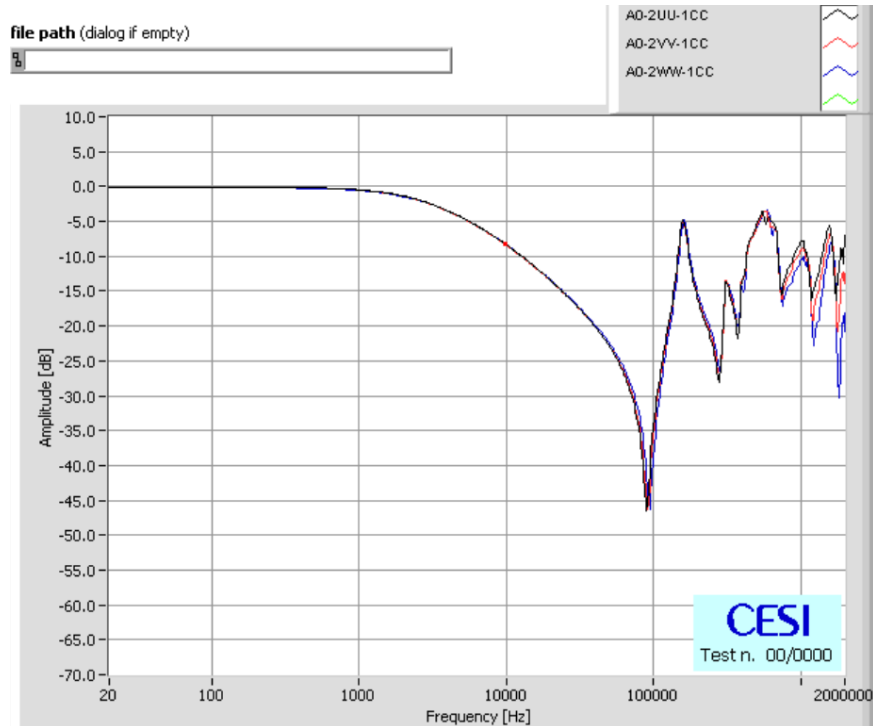


Figure 5.25 Measurements carried out on the LV winding with the HV short-circuit

The opening of the machine, with the visual inspection of the windings has confirmed the hypothesis, as shown in Figure 5.26 a short-circuit between two coils of the *HV* winding of the phase W was noticed, with the interruption of part of the *HV* winding. No mechanical deformation was seen on the windings. The transformer was repaired on site through the replacement of the *HV* winding of phase W.

SFRA results Case 2: single-phase transformer during a short circuit withstand test, 60/30-30 MVA 400/27.5-27.5 kV.

A single phase transformer with two secondary windings (*LV1* and *LV2*) positioned on separate columns was subjected to short circuit withstand test and the *SFRA* method was used, in addition to the leakage inductance measurement to check the effects of the power test. On the low voltage winding *LV2*, after the last current application, an anomalous behaviour was noticed, confirmed by a variation of 6% in the leakage inductance measurements. In particular, the following *SFRA* traces were found testing the low voltage windings *LV1* and *LV2*, shown in Figure 5.27 and Figure 5.28 respectively:



Figure 5.26 Damage to the HV winding of phase W as seen after opening of the transformer

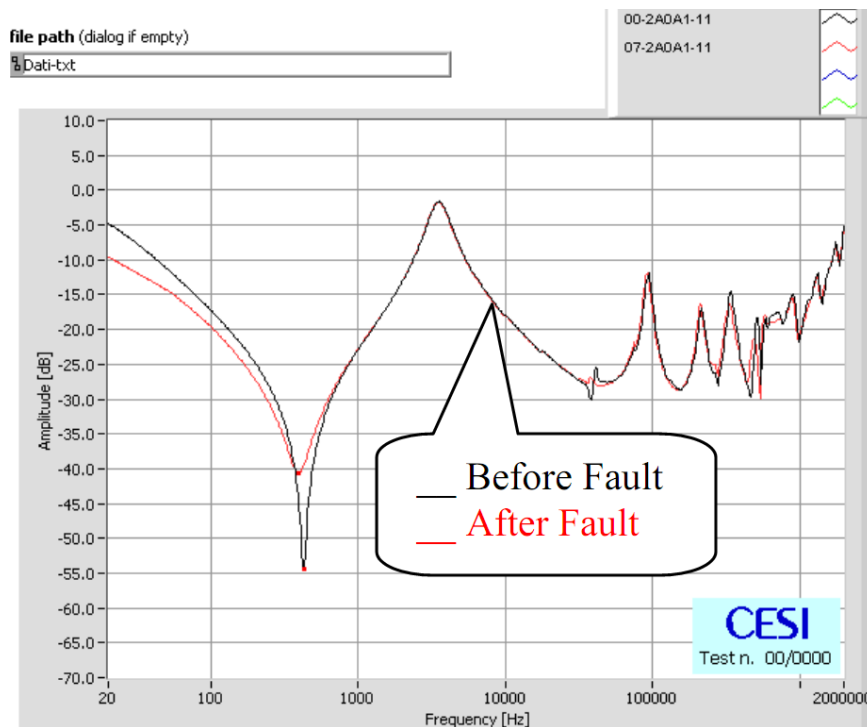


Figure 5.27 Measurements carried out on the LV winding LV1 with the HV windings open

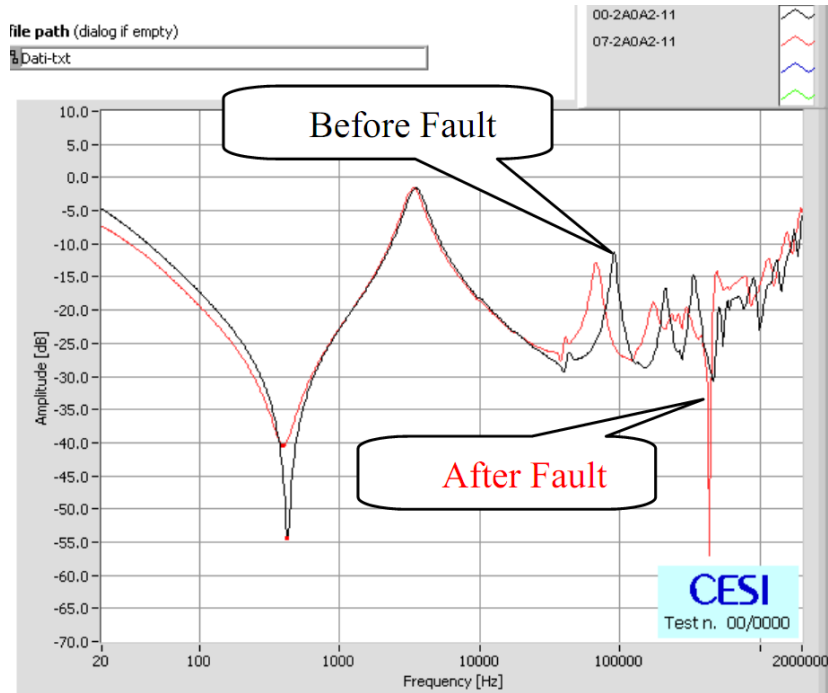


Figure 5.28 Measurements carried out on the LV winding LV2 with the HV windings open

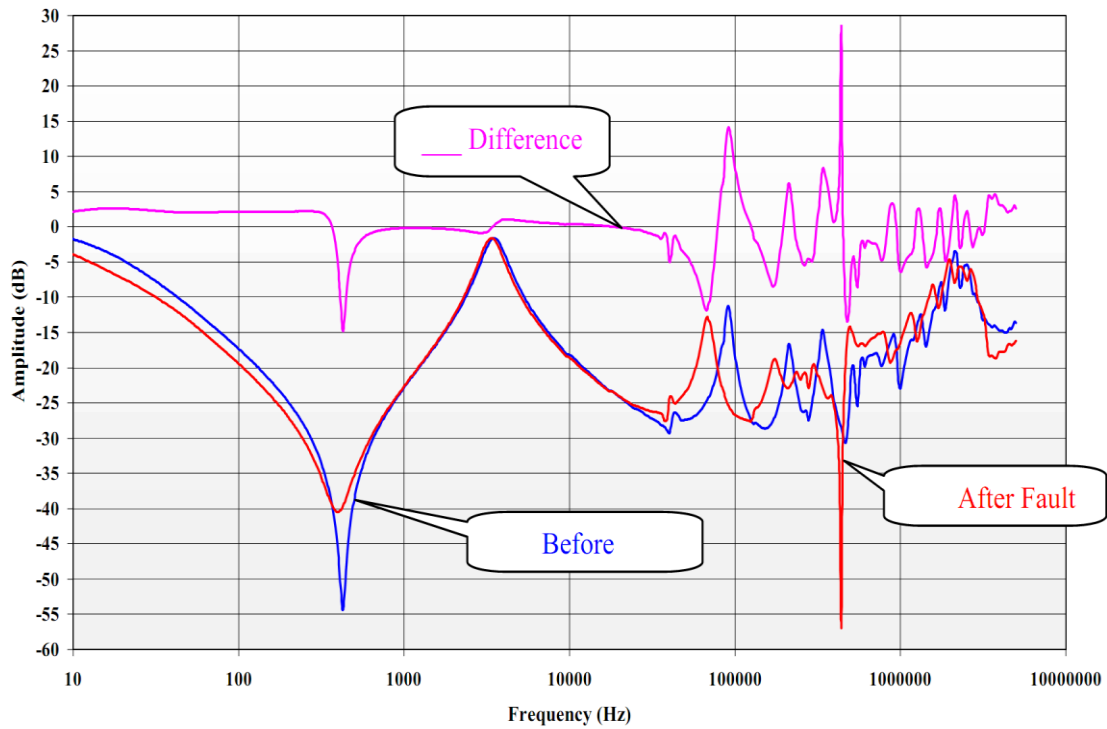


Figure 5.29 Measurements carried out on the LV winding LV2 with the HV windings open; trace of difference is shown

Another approach to transformer winding diagnostic is advanced pulsed technology. It is based on low-voltage pulsed method (LVPM). This technology was researched and engineered by Polish electrical engineers V. Lekh and L. Tyminskiy in 1966. The method is recognized in transformer's world as reliable and sensitive technology to determine an mechanical deformations more than 45 years. In many countries, including Russia, LVPM is included in national standards of power transformer test methods to electrodynamic firmness of winding control. It is good alternative to FRA technology.

The crux of matter is in rectangular pulse of low-voltage supply to one of winding of transformer; at the same time transient current is registered on the other. Transient current is reaction of the winding to rectangular probe pulse. Comparative analysis of differences in pulsed transient current curves before and after electrodynamic impact is basic fundamentals. Analysis is comparison of normogram (signal from "healthy" winding) and defectogram (signal from damaged winding). It is necessary to note that, many types of power transformers have no normograms at all. This fact makes diagnostics procedure very difficult and impossible in some cases. In such cases analogical phase normograms of similar transformer types are used, but diagnostics accuracy are not reliable at such approach. It is done to advance abovementioned pulsed method and extend it for electrical machine winding control. Duration of rectangular pulse in standard method is 1 microsecond. We propose to use probe pulse duration no more than 500 nanosecond and less. Pulse front is several units of nanosecond. Decrease of pulse and front duration up to nanosecond range leads to much more exact fixing of transient process in comparison with standard LVPM. Diminished probe pulse duration allows to increase a sensitivity method due to response signal formation in capacitive elements only. As result oscillations are excited with bigger intrinsic frequency than in LVPM. Any changes of winding geometry changes, even most negligible are caused by radial or axial deformations, impressing, lodging conductors, turn to turn short circuit and other factors lead to considerable changes of longitudinal and cross winding capacities. Reaction of windings is changed seriously at the same time and provides more exact measurement result.

Winding diagnostics of power transformer 110/10 kV, 63 MVA

Nanosecond pulsed method was applied to control mechanical state of winding transformers in real electric energy system. Type of transformer is TRDTSN – 63000/110 – U1 (Russian Federation Government Standard 12965 – 74). There are four transformers of the same type, produced by Tol'yatti transformer's plant in 1980. Diagnostics procedure is following: probe pulse has been put in one of winding, response signal have been fixed

at the windings. Oscillogram on the entrance of high voltage winding 110 kV is showed on the Figure 5.30. Analogical signal was fixed on the entrance of low voltage winding 6kV. This fact is evidence that input resistances of both windings are practically the same and have capacitive character for frequency range of probe pulse. This signal is not enough to make conclusion about winding element state. Response signals from other windings are more sensitive to different geometrical changes of turns.

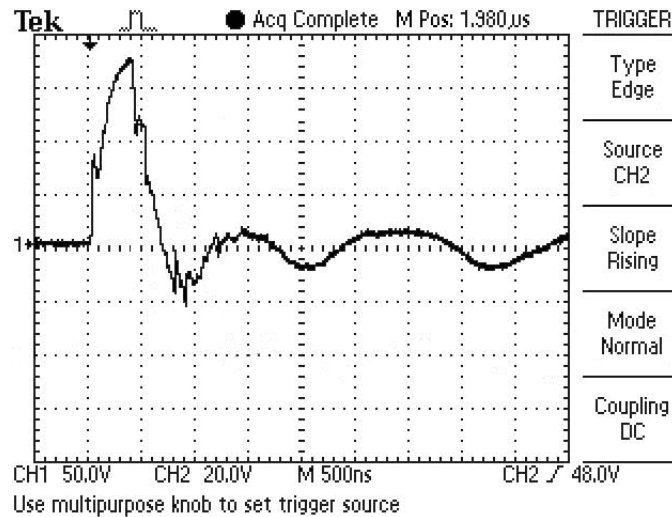


Figure 5.30 Signal view at the entrance of transformer winding

Responses from all windings have individual character at the probe pulse putting in the one of those. This is confirmation of high sensitivity of “nanosecond pulse diagnostics”. Signals from high voltage windings of phases A and C at the probe pulse putting on high voltage winding B are shown on the Fig. 5.31.

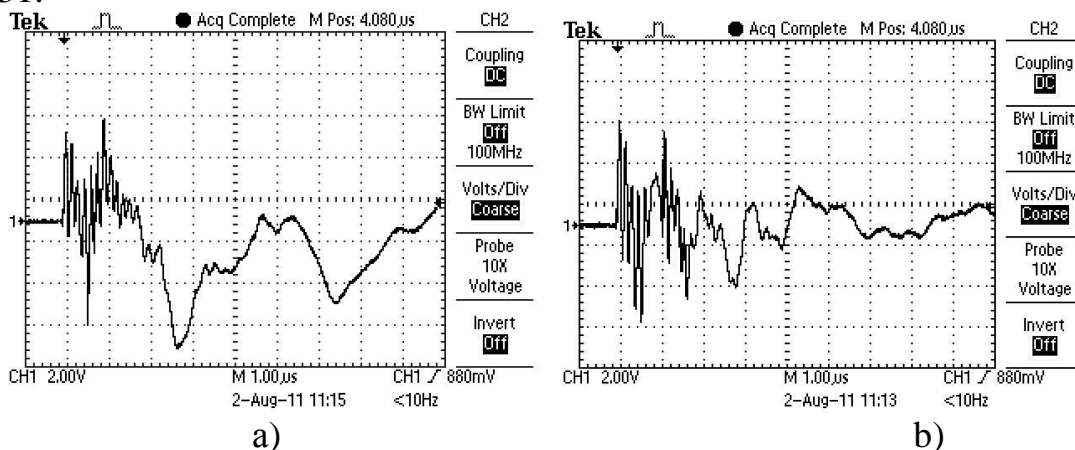


Figure 5.31 Pulsed responses from high voltage windings A and C at the probe pulse putting on the phase B:
a – response signal from winding A, b – response signal from winding C

Winding similarity is confirmed by signal forms when probe pulse and response-pulse are changed by places. Figure 5.32, a illustrates response-pulse from at the high voltage winding A at the probe pulse putting on the high voltage winding B. In turn, Fig. 5.32, b demonstrates response-pulse from the winding B at the probe pulse putting on the high voltage winding A. It is seen that, response-pulse forms are equal. This is evidence of good correspondence of mutual geometrical placement of windings A and B between each other.

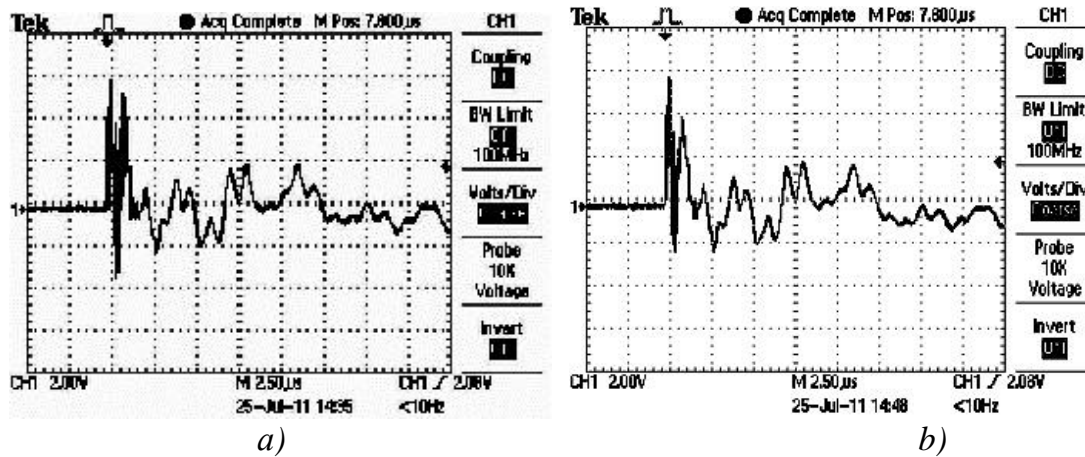


Figure 5.32 Response oscillograms:
 a – at the winding A, probe pulse on the winding B;
 b – at the winding B, probe pulse at the winding A

The same way is used to check how identical windings are made which are placed on different transformer rods. On the Fig. 5.33 are shown the response-pulses from winding a_2B_2 at the probe pulses putting to windings a_1B_1 and, $B_2C_2 - B_1C_1$ respectively. It is seen that, all response forms are equal. So, this is good evidence of good geometrical correspondence of windings, placed on the different rods between each other.

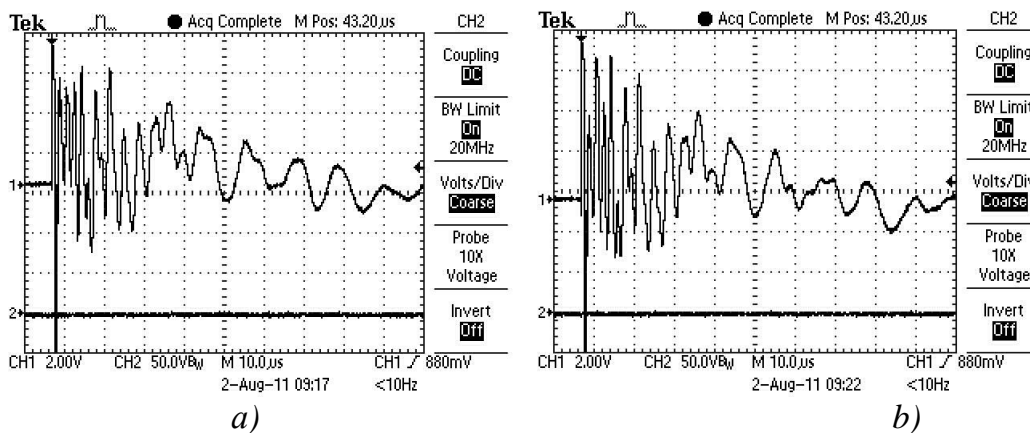


Figure 5.33 Response pulses from the low voltage windings:
 a – a_2B_2 at the probe pulse putting to the a_1B_1 ,
 b – B_2C_2 at the probe pulse putting to the winding B_1C_1

Showned results confirm high sensitivity of nanosecond pulse technology (NNPT). In this connection proposed approach could be prospect and successful at the mechanical state control of transformer winding.

This method is one of the sensitive, exact and prospective for state control of transformer windings.

5.2 Synthetic test circuit and vacuum circuit breaker improvement

One of main goal of modern high voltage engineering is development and manufacturing of new high voltage equipment. One of the advanced modern high voltage technique is vacuum circuit breaker (VCB). General view of VCB is shown on Fig.5.34. VCB has to provide nominal current flow in switch-on position and interrupt current flow in commutation regime or case of emergency. To improve this kind of high voltage apparatus it is necessary to fulfill VCB research and testing. To make this special facility is used. It is called “synthetic test circuit” and corresponded two high voltage generators in one facility – high current and high voltage sources. Such kind of circuit is used in high voltage laboratories and World-famous electric engineering concerns. On Fig. 5.35 advanced synthetic test circuit is shown. It has been developed and designed in ABB research laboratory in Germany.



Figure 5.34 General view of circuit breaker

Circuit diagram of the synthetic test circuit with the high current source at the left hand side and the high voltage source on the right. At the high current source side the DC power supply is 600 V and at the high voltage side the

DC power supply is 20 kV.

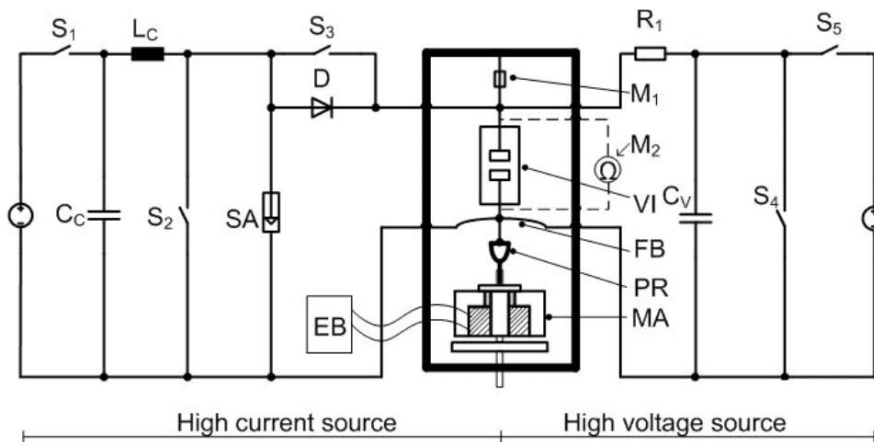


Figure 5.35 Synthetic test circuit:

VI – vacuum interrupter, FB – flexible band, PR – push rod, MA – magnetic actuator, S₁ – S₅ – switch device, M₁ – M₂ – measuring devices

The vacuum interrupter (VI), installed at the center, is driven by the magnetic actuator (MA) and the control unit (EB). The forces are transferred by the push rod (PR). The current flow is established by providing a flexible band (FB) to the movable side of the VI. The weld formation during the closing process is measured by opening in a “static” or “dynamic” mode by the gauge M₁. After each closing operation the resistance of the VI is measured by the M₂ device. This circuit provides high current (1–35 kA) and recovery voltage (6–36 kV) on the contacts of VCB in vacuum chamber. Contacts of VCB are most sensitive elements. Most of them consist of CuCr alloy in ratio 50/50 or 75/25. Typical view of these after 180 hours under 31.5 kA is shown on Fig. 5.36.



Figure 5.36 Contacts of VCB

REFERENCES

1. Walter S. Zaengl. Dielectric spectroscopy in time and frequency domain for HV power equipment. – Proceedings of 12th International. Symposium on High Voltage Engineering – ISH 2001, Bangalore, India, 20 – 24 August 2001.
2. Electric Systems Issues at the turn of the 21st Century. Cigre ELECTRA, Special Issue 2000.
3. von Hippel, A. R. Dielectric Materials and Applications. The Technology Press of M.I.T. and J. Wiley & Sons, New York, 1958
4. Jonscher, A.K. "Dielectric relaxation in solids", Chelsea Dielectrics Press, 1983.
5. Maxwell, J.C.: "A Treatise on Electricity and Magnetism", vol. 1. Clarendon Press, Oxford, third edition, reprint by Dover, 1981, pp. 450–464.
6. Der Houhanessian, V.: "Measurement and Analysis of Dielectric Response in Oil–Paper Insulation Systems". Ph.D. dissertation, ETH No. 12832, Zurich, 1998.
7. Pugh, J. "Dielectric measurements using frequency response analysers". Fourth International Conference on Dielectric Materials, Measurements and Applications, IEE Conference Publication 239, IEE London, 1984, pp. 247–250.
8. Whitehead, J.B.: "Lectures on Dielectric Theory and Insulation". McGraw–Hill, New York.
9. A. Bogнар, L. Kalocsai, G. Csepes, E. Nemeth, J. Schmidt: "Diagnostic tests of high voltage oil–paper insulating systems (in particular transformer insulation) using DC dielectrometrics". CIGRE 1990 Session, paper 15/33–08.
10. J. Alff, V. Der Houhanessian, W.S. Zaengl and A.J. Kachler: "A novel, compact instrument for the evaluation of relaxation currents conceived for on–site diagnosis of electric power apparatus". Conference Record of the 2000 IEEE Int. Symposium on Electrical Insulation (ISEI), Anaheim, CA, USA, April 2–5, 2000, pp.161–167.
11. Uno Gufvert: "Condition Assessment of Insulation Systems – Analysis of Dielectric Response Methods". Proc. Nordic Insulation Symposium (Nord IS 96), June 10–12, 1996, Bergen, Norway, pp.1–20.
12. Proceedings of XIV International Symposium on Discharges and Electrical Insulation in Vacuum. – Braunschweig, Germany, August, 30 – September, 3, 2010, V.1.
13. Proceedings of XV International Symposium on Discharges and Electrical Insulation in Vacuum. – Tomsk, Russia, September, 2 – 7, 2012, V.1.
14. Proceeding of 8th International Conference on "Technical and Physical Problems of Power Engineering". – Ostfold University College, Fredrikstad, Norway 5–7 September 2012, V.1.

Summary

This textbook is for students, who study Bachelor's course in Electrical Engineering of Tomsk Polytechnical University. It contains 5 chapters and encloses main parts of high voltage engineering. Chapter 1 deals with the fundamental phenomena in gaseous media at the strong electric field application. This chapter contains main knowledge about kinetic gas theory, of ionization, emission and recombination of charge particles. Description of main forms and kinds of electrical discharges in gases is given.

Chapter 2 discusses main mechanisms of breakdown in condensed dielectric materials. Reasons and ways of plasma channel formation are discussed here.

Chapter 3 tells about the techniques of generation of all kinds of high voltages. Measurement techniques of high voltages are discussed in this chapter also.

Chapter 4 deals with overvoltages. Lightning phenomena, switching overvoltages, insulation coordination problem are discussed. Design and engineering of protection devices are shown and described.

Chapter 5 devoted to new technologies of modern high voltage engineering. New approaches to power transformer diagnostics are covered and discussed. High current synthetic test circuit is shown. This chapter deals with new information which is in special scientific papers only. These are advanced scientific directions which are developed in High voltage laboratory of Power engineering institute of Tomsk polytechnical university.

It is necessary to note that successful studying of this discipline is possible in combination with special laboratory workshop course.

Contents

Preface	3
Introduction	4
Chapter 1. Electrophysical processes in gases	5
1.1 Basic fundamentals of kinetic gas theory	5
1.2 Charge particles generation, movement and recombination	19
1.2.1 Ionization processes	19
1.2.2 Recombination processes	28
1.2.3 Charged particle movement in electric field	34
1.2.4 Emission processes	39
1.3 Forms of electrical discharge	44
1.4 Discharge in non–uniform electric fields. Main discharge processes	50
Chapter 2. Electrophysical processes in condensed dielectric materials	64
2.1 Electrophysical processes in solid dielectrics	64
2.1.1 Intrinsic breakdown	66
2.1.2 Streamer breakdown	67
2.1.3 Electromechanical breakdown	68
2.1.4 Edge breakdown	68
2.1.5 Thermal breakdown	69
2.1.6 Partial discharges	72
2.2 Electrophysical processes in liquid dielectrics	76
2.2.1 Electronic breakdown	76
2.2.2 Suspended solid particle breakdown mechanism	77
2.2.3 Cavity breakdown	78
Chapter 3. Generation and measurement of high voltages	80
3.1. Generation of high voltages	80
3.1.1 Alternating voltages	80
3.1.2 Direct voltages	84
3.1.3 Impulse voltages	87
3.2. Measurement of high voltages	91
Chapter 4. Overvoltages: nature and protection	98
4.1 General characteristic of overvoltages	98
4.2 Nature of overvoltages	98
4.3 Insulation coordination	104
4.4 Protection devices	107
Chapter 5. Advanced high voltage technologies	117
5.1 New approaches to high voltage equipment diagnostics	117
5.1.1 Dielectric spectroscopy technology	117
5.1.2 New technologies of active part of transformer diagnostics	145
5.2 Synthetic test circuit and vacuum circuit breaker improvement	156
Summary	159
Contents	160

Alexey Mytnikov Author was born 2 June 1966. He received Ph. D. degree in 2001. He is Associate Professor of Electrical Power System Department, Power Engineering Institute of Tomsk Polytechnical University. Area of scientific interests: power transformer diagnostics, high voltage technologies.



Textbook

MYTNIKOV Alexey Vladimirovich

HIGH VOLTAGE ENGINEERING

Textbook

Computer design A.V. Mytnikov
Cover design A.V. Mytnikov

Подписано к печати 05.11.2012. Формат 60x84/16. Бумага «Снегурочка».

Печать XEROX. Усл.печ.л. 9,01. Уч.-изд.л. 8,16.

Заказ . Тираж 100 экз.


Национальный исследовательский Томский политехнический
университет

Система менеджмента качества

Издательства Томского политехнического университета сертифицирована

NATIONAL QUALITY ASSURANCE по стандарту BS EN ISO
9001:2008



ИЗДАТЕЛЬСТВО  ТПУ. 634050, г. Томск, пр. Ленина, 30
Тел./факс: 8(3822)56-35-35, www.tpu.ru